Terms and Conditions of Use of Digitised Theses from Trinity College Library Dublin

Copyright statement

All material supplied by Trinity College Library is protected by copyright (under the Copyright and Related Rights Act, 2000 as amended) and other relevant Intellectual Property Rights. By accessing and using a Digitised Thesis from Trinity College Library you acknowledge that all Intellectual Property Rights in any Works supplied are the sole and exclusive property of the copyright and/or other IPR holder. Specific copyright holders may not be explicitly identified. Use of materials from other sources within a thesis should not be construed as a claim over them.

A non-exclusive, non-transferable licence is hereby granted to those using or reproducing, in whole or in part, the material for valid purposes, providing the copyright owners are acknowledged using the normal conventions. Where specific permission to use material is required, this is identified and such permission must be sought from the copyright holder or agency cited.

Liability statement

By using a Digitised Thesis, I accept that Trinity College Dublin bears no legal responsibility for the accuracy, legality or comprehensiveness of materials contained within the thesis, and that Trinity College Dublin accepts no liability for indirect, consequential, or incidental, damages or losses arising from use of the thesis for whatever reason. Information located in a thesis may be subject to specific use constraints, details of which may not be explicitly described. It is the responsibility of potential and actual users to be aware of such constraints and to abide by them. By making use of material from a digitised thesis, you accept these copyright and disclaimer provisions. Where it is brought to the attention of Trinity College Library that there may be a breach of copyright or other restraint, it is the policy to withdraw or take down access to a thesis while the issue is being resolved.

Access Agreement

By using a Digitised Thesis from Trinity College Library you are bound by the following Terms & Conditions. Please read them carefully.

I have read and I understand the following statement: All material supplied via a Digitised Thesis from Trinity College Library is protected by copyright and other intellectual property rights, and duplication or sale of all or part of any of a thesis is not permitted, except that material may be duplicated by you for your research use or for educational purposes in electronic or print form providing the copyright owners are acknowledged using the normal conventions. You must obtain permission for any other use. Electronic or print copies may not be offered, whether for sale or otherwise to anyone. This copy has been supplied on the understanding that it is copyright material and that no quotation from the thesis may be published without proper acknowledgement.

Mathematical processing of *in-vivo* electrophysiological data with applications to implanted electrode recordings

A dissertation submitted to the University of Dublin

for the degree of Doctor of Philosophy

Ehsan Chah

Trinity College Dublin

2012

Department of Electronic and Electrical Engineering
Trinity College Dublin

I declare that this thesis has not been submitted as an exercise for a degree at this or any other university and it is entirely my own work.

I agree to deposit this thesis in the University's open access institutional repository or allow the library to do so on my behalf, subject to Irish Copyright Legislation and Trinity College Library conditions of use and acknowledgement.

Thesis summary

Neurons are the principal cellular elements that underlie the function of the nervous system, which includes the brain, spinal cord, and peripheral ganglia. These electrically excitable cells process and transmit information primarily via electrical signalling through the generation of action potentials. These action potentials can be recorded

in-vivo by placing electrodes in the vicinity of the neuron's membrane within the extracellular space.

Electrodes measure electric potential fluctuations in the extracellular space. These fluctuations generally contain two types of activity, low frequency content, also known as Local Field Potentials (LFPs) and extracellular action potentials (spikes) which contribute to the higher frequency content.

The advancement of neural recording techniques allows for the simultaneous recording of many neurons. It has been estimated that the ability to record simultaneously from several neurons has been growing exponentially since the 1950s and it has been predicted that this number doubles every 7 years (Stevenson and Kording, 2011). The technological advance in neural recording systems demands the parallel advancement of neural decoding algorithms to analyse and extract information from these signals automatically and objectively.

In this thesis, methods to extract information from extracellular recordings are presented; the first step in this process is called spike sorting. Spike sorting is defined as the process of isolating spikes generated by each neuron in the vicinity of the

recording electrode. This thesis presents a new method of automated spike sorting based on Laplacian eigenmaps and *k*-means clustering. Using simulated and *in-vivo* recordings this method was compared to previously reported algorithms and improvement in unit isolation is achieved.

The variability of *in-vivo* spike recordings is examined over short and long recording periods. This was achieved by identifying cells across successive sessions using the information carried by the cells. This method allows the identification of cells across different sessions using markers independent of the waveform, which permits identification of the cell even during large waveform variability. The result shows that a *t*-distribution would be a better fit to the residues of the spikes. Understanding the variability of spike waveforms is important in many applications such as spike sorting and neural prostheses.

The information transmitted by these neurons is also examined in closer detail. In this thesis a subset of cells in the brain's thalamic nuclei is examined. Specifically the relation between spikes in head-directional cells and theta rhythms in the thalamic anteroventral nucleus are closely studied. This thesis shows evidence that there is a substantial population of head-direction cells in the thalamic anteroventral nucleus that spike rhythmically in the theta frequency range, further demonstrating the importance of theta oscillation in spatial learning.

This thesis provides a platform to extract information from *in-vivo* recordings and presents insights into the information transmitted by these neurons, in order to contribute to research into the brain function.

Acknowledgement

I would like to acknowledge and thank a number of people without whom this thesis would not be a reality. First and foremost, I wish to express my sincere gratitude and appreciation to my supervisor Prof. Richard Reilly who has patiently supported and encouraged me since my time as an undergraduate student and has accompanied me through my journey as a PhD student. I would also like to thank Prof. Shane O'Mara for his invaluable input, time and assistance with the research presented in this thesis and also scholarship funding. In addition, I would also like to thank Prof. Michael Rowan for his experimental research support and assistance with scholarship funding.

To Dr. Vincent Hok and Dr. Marian Tsanov, a big thank you for their assistance, advice and suggestions especially with regards to the neuro-biological aspects of my research during the course of my PhD.

I cannot complete my acknowledgements without mentioning all the members of both the Reilly and O'Mara laboratory groups. Thank you all for making my time as a PhD student so memorable and enjoyable. I will always look back on my time with you all with a big smile especially when I think of all the laughter and entertainment during our numerous social events together.

Finally I would like to thank my family. To Neysan and Sahar for their patience while reading this long thesis, Rohieh and Mum for cheering me on when I needed it the most and Dad for his unconditional support in my life, thank you. Their love, support and backing made this PhD a possibility and a reality.

This thesis is lovingly dedicated to the memory of my father Gholam-Hassan Chah who always taught me to strive for excellence in education whilst never faltering in his unconditional support and love. In addition, I wish to dedicate this thesis to the thousands of young Baha'i students in Iran who are unable to achieve their academic goals and denied access to higher education solely because of their religious beliefs.

Table of Contents

Abbreviations

ACC: Accuracy

AD: Thalamic Anterodorsal Nucleus

AIC: Akaike Information Criterion

AV: Thalamic Anteroventral Nucleus

BIC: Bayesian Information Criterion

CEM: Classification Expectation-Maximization

CM: Classification Matrix

DBS: Deep Brain Stimulation

DBVI: Davies-Bouldin validation index

DD: Discrete Derivatives

DR: Distributive Ratio

DWT: Discrete Wavelet Transform

ECoG: Electrocorticography

EEG: Electroencephalography

EM: Expectation Maximization

EML: Extreme Machine Learning

FFT: Fast Fourier Transform

fMRI: Functional Magnetic Resonance Imaging

HD: Head-direction

HMMs: hidden Markov models

ICA: Independent Component Analysis

ICBV: Independent Component Basis Vector

ISI: Inter-Spike Intervals

KS: Kolmogorov-Smirnov test

LE: Laplacian eigenmaps

LFP: Local Field Potentials

MEG: Magnetoencephalography

MLM: Maximum Likelihood Model

NEO: Nonlinear Energy Operator

PCA: Principal component analysis

RVB: Robust Variational Bayes

SA: Sorting Accuracy

SE: Sorting Error

SENS: Sensitivity

SEM: Standard Error of the Mean

SIC: Spatial Information Content

SPEC: Specificity

SVM: Support Vector Machine Classifier

TPD: Theta-modulated Place-by-direction

UWT: Undecimated Wavelet Transform

WT: Wavelet Transform

List of figures

Chapter 1. Introduction

1.1 Introduction:

The brain is a complex system; brain disorders include a wide spectrum of mental and neurological diseases (e.g. addictive disorders, dementia, epilepsy, multiple sclerosis, Parkinson's disease, etc.). It is estimated that 38% of the European Union (EU) population suffer from mental disorders every year (Wittchen et al., 2011). Hence the economic and social burdens of brain disorders are enormous. With a recent report estimating the total cost of brain disorders in Europe in 2010 to be €789 billion, it is suggested that brain disorders are "likely to constitute the number one economic challenge for European health care" (Gustavsson et al., 2011). The report recommends actions to increase funding for brain research; it also urges the pharmaceutical industry to reverse their policy of moving away from neuroscience research.

The report predicts that the cost of brain illness to increase in future as a natural consequence of an increased life expectancy. Thus today's research in understanding the brain and brain disorders is vital in addressing future health challenges.

1.2 Importance of understanding the neural code:

Neural sciences intend to decode how neural circuits give individuals their perception of the world around them. Traditionally there are two approaches that neural scientists have adopted in researching these circuits. The bottom up approach involves the study of the nervous system in terms of elementary components (molecules, cells, etc.), whereby the changes of connection and signalling properties of nerve cells are studied. The second approach, the top-down approach, involves examining the mental functions of intact human beings, where the relationship between these activities and population of neurons are researched (Albright et al., 2000).

The first discovery of neuroscience starts with the idea by Ramon y Cajal that neurons serve as the basis for signal transmission in the nervous system (Albright et al., 2000). Subsequent research, described these neurons and their anatomy consisting of dendrites that serve as inputs to receive information, and the axons that allow for the propagation of the signal to other neurons (outputs). Later Alan Hodgkin and Andrew Huxley detailed how these cells transmit information via a process referred to as the action potential, The process underpinning the action potential was quantitatively described by Hodgkin and Huxley (1952). Who outlined how ionic flow into and out of neurons can lead to potential differences associated with the generation of an action potential.

Additional studies sought to link these action potentials and behaviour in the intact brain. To this end, advances have been made in reporting cells that correlate with specific behaviours, for example, hippocampal cells (place cells) have been shown to fire when animal is in a specific location within its environment (O'Keefe and

Dostrovsky, 1971), and are thought to provide the animal with an internal sense of it's location in space (Moser et al., 2008). An example of place cell activity is shown in Figure 1.1. The place field (the location where the cell is active) can be examined in more detail using firing frequency plots (Figure 1.1B).

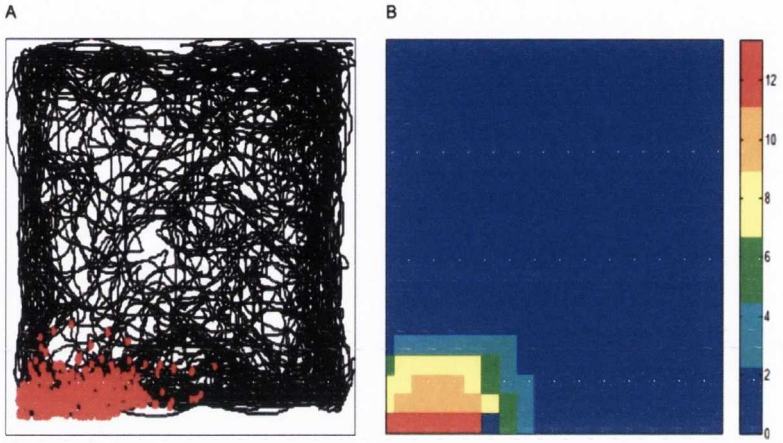

Figure 1.1. Example of a place cell recorded in the hippocampal CA1 subregion (A) black line indicates the trajectory of the animal in the environment (square box) red dots correspond to the location of the animal when the cell fired a spike (B) firing frequency plot of the same place cell; the environment is divided by a set of squares (bins) (3x3 cm) and the number of spikes in each bin is divided by the time spent by the rat in that bin. The firing rate in each bin was smoothed using a 5 X 5 kernel, meaning that the firing rate for each bin was calculated as the average of the 5 X 5 bin square centred on that bin. The six colours of firing-rate maps were autoscaled to represent 20% of the peak rate (red to dark blue).

Other cells have been shown to correlate with the head direction of the animal (Taube et al., 1990), head-directional cells are accepted to act as an internal compass providing an innate sense of direction (Knierim et al., 1998). The firing of these cells is determined by the animal's head direction, and is independent of other factors such as behaviour, location in the environment and trunk position (Taube, 1995). Figure 1.2 shows an example of a head-directional cell. With the firing rate that is maximal in the preferred head direction, as the animal head moves away from this direction the firing rate decreases.

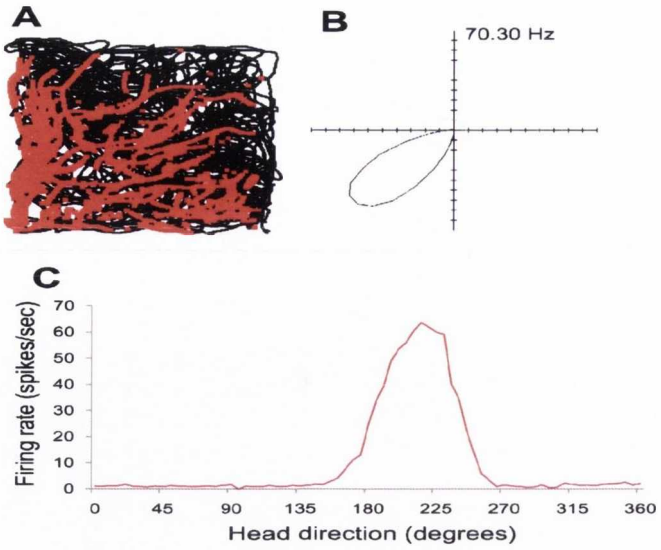

Figure 1.2: Example of a head-directional cell. (A) Shows the trajectory of the animal (black line), coloured dots represent the location of the animal when a spike was emitted. (B-C) shows head directional preference of the cell.

A third type of cells (grid cells) are reported that are thought to be important for spatial navigation, these cells are similar to place cells however they differ in having multiple place fields arranged in periodic triangular grids (Fyhn et al., 2004, Hafting et al., 2005). An example of grid cell is shown in Figure 1.3. These cells are thought to provide metric system in spatial navigation (Moser et al., 2008).

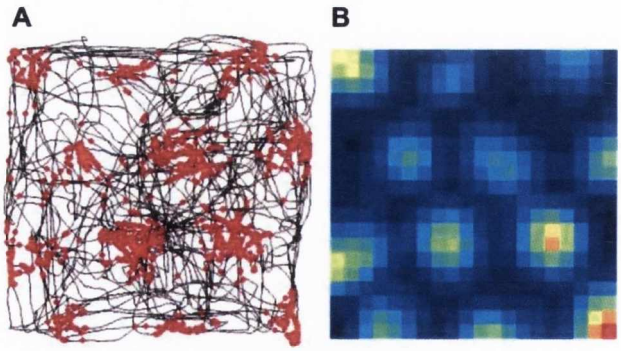

Figure 1.3: Grid cell example (Moser, 2007) (A) Shows the trajectory of the animal (black line), coloured dots represent the location of the animal when a spike was emitted. (B) Firing frequency plot of the same grid cell.

These cells population are thought to interact with each other to support the cognitive function of navigation within an environment (Moser et al., 2008, Burgess, 2008b). These are some examples of how the brain encodes information. Discoveries have also been made into how the brain encodes sensory information, for example how the brain encodes different visual stimuli (bar, rectangles, squares, etc.) (Albright et al., 2000). The field of neuroscience have advanced vastly in the past century (Albright et al., 2000). This introduction is focused on discoveries related to subsequent chapters of the thesis.

With regards to clinical implication of neural research, an exploration of the brain's encoding methods allows for the design and development of better diagnostic and treatment methods to find ways of repairing and/or replacing dysfunctions within the brain. One method of treating brain disorders involves administering medications to alleviate symptoms of the disease. Hence a better understanding how the brain functions can aid finding the most effective pharmaceutical intervention. A lack of success in pharmaceutical treatments is thought to be one of the reasons for the reluctance of investment from the pharmaceutical industry in brain diseases (Gustavsson et al., 2011).

An alternative treatment option is the use of active implants which constitute one of the emerging areas in neuroscience (neural prostheses). These devices link the nervous system with passive or active electronic systems. Such systems can replace or supplement a function which is impaired or completely lost due disease or injury (Akay, 2007). Examples of neural implanted devices include Deep Brain Stimulation (DBS), where symptoms of movement disorder disease (such Parkinson's disease, dystonia) are alleviated by delivering electrical pulses (Holtzheimer and Mayberg, 2011). Cochlear implant technology is an example of a sensory neural device. This

type of implant transfers sounds to neural inputs with the aim of restoring hearing in subjects with hearing impairment (Zhou and Greenbaum, 2009). Similarly, visual prostheses aim to restore eyesight for the visually impaired (Weiland and Humayun, 2008). Further examples of neural prostheses include prosthetic limbs (Schwartz et al., 2006). While many of these devices are still in need of further research and development, success has been achieved in producing FDA approved neural devices, most notably in the area of cochlear implants (Dilorenzo and Dronzino, 2008).

Implanted devices generally consist of four components:

- Recording neural activity
- Extraction of intended action
- Generation of action
- Feedback

An example of a neural prosthesis with the four components described above is shown in Figure 1.4. As shown the first step in the neural prosthesis is recording neural activity and extracting the relevant information to generate action.

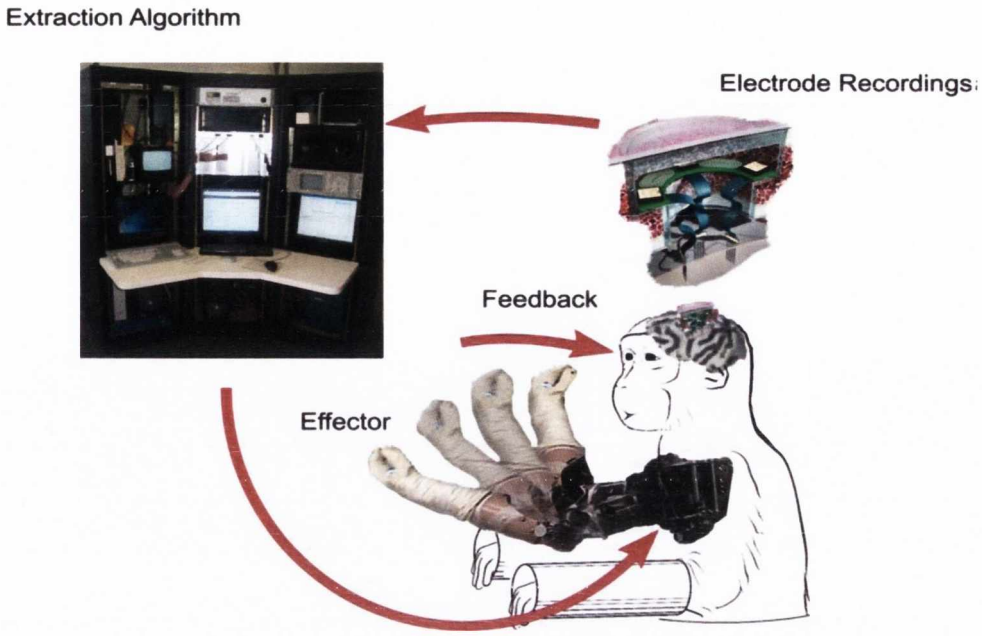

Figure 1.4: Example of a neural prosthetic limb. Neural activity is recorded from the brain using microelectrode arrays with implanted microprocessors sampling and transmitting the neural activity. An extraction algorithm decodes the information transmitted by these neurons. The information is fed to a robot controller to move the prosthetic arm, which generates feedback to close the control loop (Schwartz et al., 2006).

The main focus of this thesis is to build this framework of extracting and understanding the basic brain information, more specifically information recorded and carried by these implanted electrodes.

1.3 Neural recording methods:

Electrical signals of the brain can be recorded using several invasive and non-invasive methods. Electroencephalography (EEG) is an example of a non-invasive technique that measures electrical activity of the brain on the surface of the scalp. The electrocorticography (ECoG) is an invasive method that measures the electrical potential on the cortical surface of the brain. Epidural or subdural arrays of electrodes are used to record the signal from the surface of the brain (Waldert et al., 2009). This provides a higher noise to signal ratio and a higher bandwidth than EEG. The local

field potentials (LFP) are recorded from deeper regions within the brain structure. The LFP signal reflects the local cell activity around the electrode tip (Waldert et al., 2009). The single unit recording method is used to record potential from a single cell (neurons). Single cell recordings or "spikes" provide the best spatial resolution. However the disadvantage of this method is that it is invasive and the stability of the recordings can change over long terms, due to electrode deterioration or other factors such as the brain's inflammatory response. A summary of the electrophysiological recording methods and their corresponding spatial resolution is provided in Figure 1.5. Magnetic approaches to record brain activity are also available. These methods include functional magnetic resonance imaging (fMRI), and magnetoencephalography (MEG).

In an analogy given by Buzsaki (2004), if the brain is considered to be an orchestra, and the goal is understanding the function of the orchestra, then EEG and MEG can be thought of as tools recording the overall activity, without the ability of distinguishing individual instruments strings, woodwind, etc. fMRI can be considered as taking infrared snapshots of the orchestra; it can reveal spots of dominant activity within the orchestra. However it fails to capture the essence of the music. Spikes can be thought of as pressure sensors close to individual instruments; when the pressure exceeds certain value a pulse is sent. By monitoring a large number of instruments and using these pressure sensors, one can reconstruct the essential features of the orchestra.

The focus of this thesis is on electrophysiological recording using implanted electrodes, hence in subsequent chapters, only local field potentials and spike recordings are described.

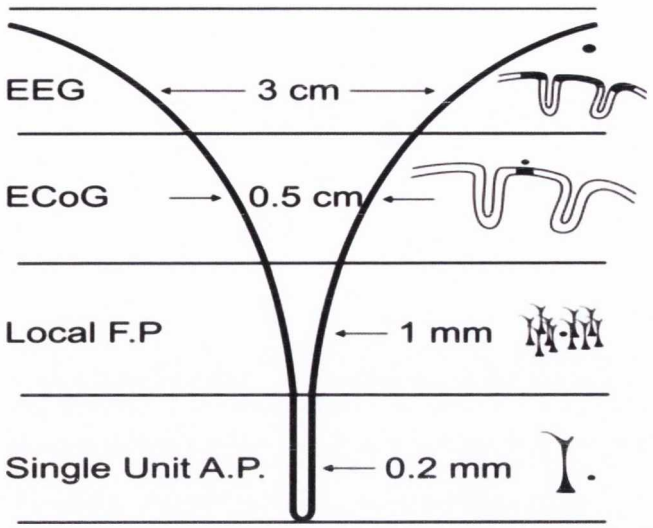

Figure 1.5: Electrophysiological recording (Schwartz et al., 2006)

1.4 Neurons:

Nerve cells (neurons) constitute the basic units of the brain, with the human brain exhibiting approximately 10^{11} neurons. These cells can be categorized into many different types, although the basic architecture is shared among all the different types. The neuron morphology as shown in Figure 1.6 consists of four regions, namely the cell body, dendrites, the axon and the presynaptic terminals. The dendrites are short terminals responsible for receiving incoming signals from other nerve cells. The axon can range from 0.1mm up to 3m and has the role of transmitting electrical signals to other neurons. These electrical signals are called action potentials and are the means by which the brain transmits, receives and analyses information (Kandel et al., 2000).

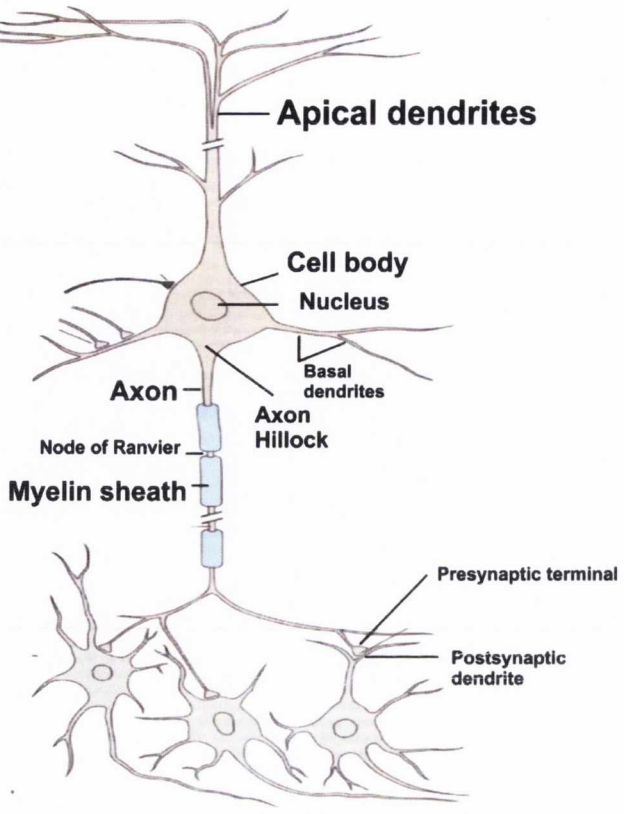

Figure 1.6: Morphology of the neuron (Kandel et al., 2000)

1.5 Chronic electrode implants:

One of the most widely used recording electrode is the microwire electrodes (Polikov et al., 2005). The conducting material used in these electrodes can range from gold, platinum, tungsten, iridium or stainless steel. With the exception of the tip of the electrodes, the wires are coated with an insulator (non-cytotoxic). Microelectrodes can be arranged in several configurations stereotrode (two wires), tetrode (four wires Figure 1.7A). These wires are spaced closely to each other and offer advantages in the analysis process (Gray et al., 1995). Larger arrangements are also available, where electrodes are arranged in a grid. An example of 128 electrodes is shown in (Figure 1.7B).

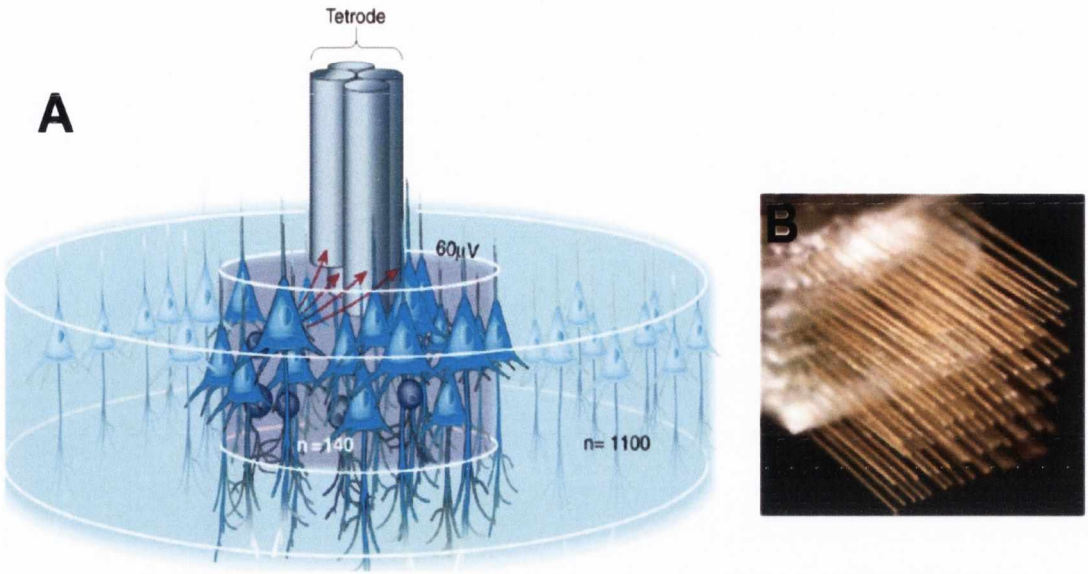

Figure 1.7: microwires (A) schematic of tetrode configuration (Buzsaki, 2004) (B) microelectrode arrays (Nicolelis et al., 2003)

The advantages of microelectrodes include easier fabrication and hence lower costs (Polikov et al., 2005). However among their disadvantages are that the wire could bend during insertion, hence the precise location of the electrode within the brain tissue can be difficult to determine.

To overcome the short-comings of wire electrodes, most recently silicon electrodes are manufactured, where the distance between recording sites can be controlled during fabrication. The silicon probes have also the advantage that more dense recording sites can be achieved with less tissue damage, the size of recording area can be controlled and in general offers more flexibility in their design (Polikov et al., 2005).

The disadvantages of silicon probes are the high cost, reliability in chronic implantations (Polikov et al., 2005), and mechanical stability. Examples of silicon probe designs are provided in Figure 1.8.

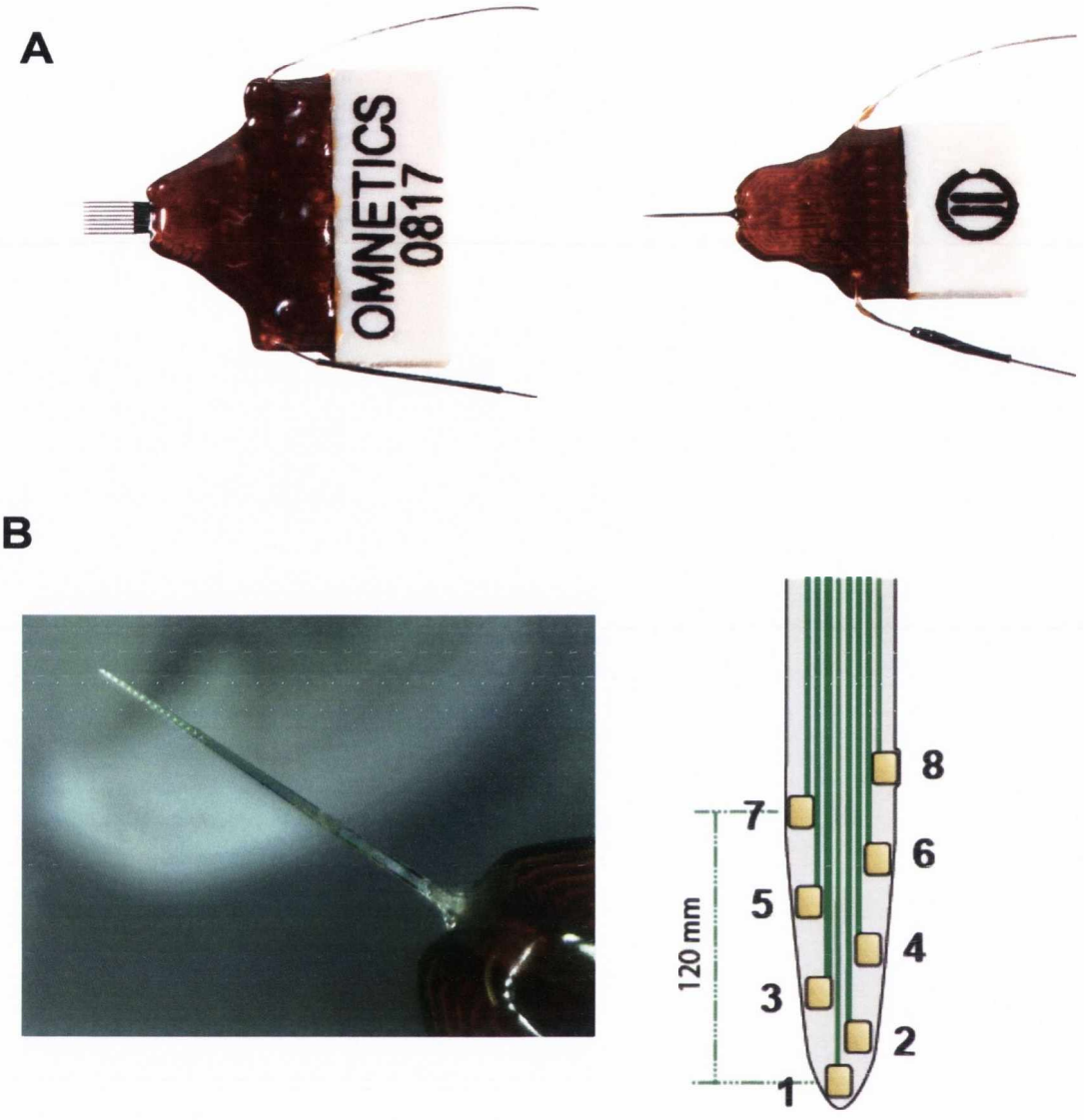

Figure 1.8: NeuroNexus silicon probe designs (A). Two electrodes multi shank and single shank electrodes. (B) Close up of view of the shank, each shank can have several recording sites.

1.6 Challenges of implanted electrophysiology recordings:

The challenges of decoding neural recordings can be summarised (Buzsaki, 2004) in to three components:

1. Neuron-electrode interface
2. Spike sorting/identification
3. Methods for analysis of multiple spike trains

The first challenge of implanted recording is the ability to sample a large number of neurons in order to gain sufficient information to decode the function of the brain. As in the orchestra analogy described in the previous section, examining one instrument will not be sufficient to analyse the complete orchestra.

It has been estimated that the progress in sampling from a number of neurons simultaneous recordings doubles every seven years (Stevenson and Kording, 2011). Several factors dictate the design of the electrodes, biocompatibility, minimisation of tissue damage during insertion and long term stability of the electrode (Polikov et al., 2005).

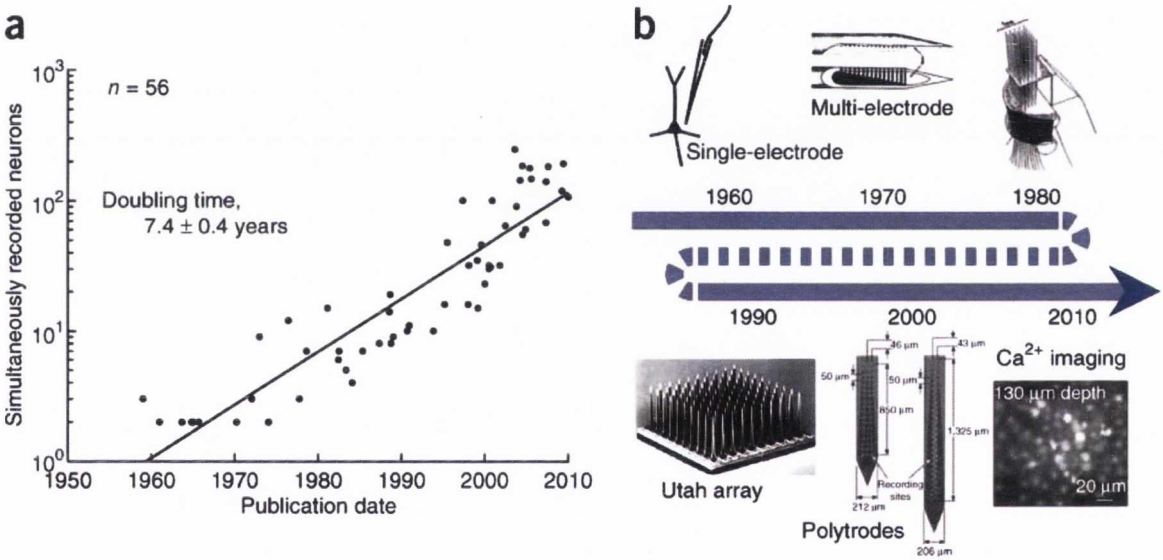

Figure 1.9: Recent advances in neural recording techniques (Stevenson and Kording, 2011) (A) 56 studies were examined by the authors and the number of simultaneous neurons recordings plotted against publication date, indicating doubling every 7 years. (B) Timeline of electrode designs starting with single microwire and to mulitprobes and electrode arrays.

The second challenge is the capability of processing and storing large number of recordings sampled at high frequencies. The processing power has been doubling every two years obeying Moore's law. Hence substantial progress is being made in this area.

The third challenge is to develop tools to decode the information carried by these large numbers of neurons (Quian Quiroga and Panzeri, 2009). It has to be noted that this thesis contributes in addressing the third challenge. Therefore the third challenge is explored next in greater details.

The first step in analysing spike recordings (neurons activity) is called spike sorting. In the orchestra and pressure pulse analogy this can be thought of as each pressure sensor picks ups pressure from more than one instrument. The sorting step is therefore to separate the pulses from each instrument so that roles of each instrument can be examined. The second step is extracting the information from these spikes and identifying their roles. The third step is then to explore the interaction between these neuron populations.

1.7 Thesis outline:

Chapter 2 outlines the progress reported in the literature in one of the major and oldest challenges of neural recordings, namely the problem of spike sorting. There after within the chapter, an automatic method to sort spikes is introduced; this method is tested and compared to other algorithms in the literature and an improvement in performance is reported.

Chapter 3 builds on the findings of chapter 2, and examines the variability of spike waveforms during short and long terms recording, with the aim of aiding the design of spike sorting methods and neuron-electrode interfaces. In the chapter the information carried by place cells are used as markers to identify these cells across subsequent recording sessions.

Chapter 4 focuses on the step after spike sorting which is examining the information carried by spike recordings. This is the main aim of any neural recording. The chapter explicitly explores the relationship between theta oscillations of the limbic system and head-direction cells in the thalamic anteroventral nucleus.

Chapter 5 provides a summary of the major contributions of this thesis. It also provides a discussion on future trends and possible advancements.

1.8 Contributions of the thesis:

- New method addressing some of the challenges of spike sorting is introduced.
- Validation of the spike sorting method by comparing it against other popular methods employed in the literature. Improvement in spike sorting is achieved using the proposed method in the thesis.
- Quantifying the residue distribution of *in-vivo* spike recordings which has important implications in the assumptions made by spike sorting algorithms.
- Investigating amplitude variability of *in-vivo* spike recording between successive sessions.
- Investigating a method of identifying a cell across successive sessions.
- Exploring a population of cells in thalamic anteroventral nucleus which integrate both head-direction and theta oscillations.
- Investigating directional modulation of theta cells in the anteroventral nucleus.
- Exploring the coherence between the anterventral nucleus and hippocampus oscillations.

- Examining the possible relation between theta cells of anterventral nucleus and sniffing behaviour of rodents.

1.9 Publications related to this thesis:

1.9.1 Journals:

Chah, E., Hok, V., Della-chiesa, A., Miller, J. J., O'Mara, S. M. & Reilly, R. B. 2011. Automated spike sorting algorithm based on Laplacian eigenmaps and k-means clustering. *J Neural Eng,* 8, 016006.

Tsanov, M., **Chah, E.,** Vann, S. D., Reilly, R. B., Erichsen, J. T., Aggleton, J. P. & O'Mara, S. M. 2011. Theta-modulated head direction cells in the rat anterior thalamus. *J Neurosci,* 31, 9489-502.

Tsanov, M., **Chah, E.,** Wright, N., Vann, S. D., Reilly, R., Erichsen, J. T., Aggleton, J. P. & O'mara, S. M. 2011. Oscillatory entrainment of thalamic neurons by theta rhythm in freely moving rats. *J Neurophysiol,* 105, 4-17.

Tsanov, M., **Chah, E.,** Wright, N., Vann, S. D., Reilly, R., Erichsen, J. T., Aggleton, J. P. & O'mara, S. M. (submitted). Thalamic head-direction processing is sustained during sleep and correlates with theta power.

Hok V., **Chah E.**, Reilly R. B., O'Mara S. M. (In preparation). Hippocampal Dynamics Predict Inter-Individual Cognitive Differences in Rats

1.9.2 International peer-reviewed Conferences:

Chah, E., Hok, V., O'Mara, S. M. & Reilly R. B., A Waveform Independent Cell Identification Method to Study Long-Term Variability of Spike Recordings. *Conference Proceedings of Annual International IEEE EMBS Conference*, Boston, USA. Aug 2011.

1.9.3 Poster presentations:

M. Tsanov, **E. Chah**, N. Wright, S. D. Vann, R. B. Reilly, J. T. Erichsen, J. P. Aggleton, S. M. O'Mara. Theta unit-induced thalamic oscillations are conditioned by descending hippocampal inputs. San Diego, CA: Society for Neuroscience, 2010. Online.

V. Hok, **E. Chah**, R. B. Reilly, S. M. O'Mara. Late-onset hippocampal place cells activity in aged rats. San Diego, CA: Society for Neuroscience, 2010. Online.

Chapter 2. Spike sorting method

2.1 Introduction:

Neurons are the principal cellular elements that underlie the function of the nervous system, which includes the brain, spinal cord, and peripheral ganglia. These electrically-excitable cells process and transmit information mainly by electrical signalling through the generation of action potentials (Kandel et al., 2000). These action potentials can be recorded *in-vivo* by placing electrodes in the vicinity of the neuron's membrane within the extracellular space. The design of the electrodes used in extracellular recordings may vary from single wire, tetrode (four wires twisted together) to microelectrode array configurations.

Although the electrodes' configuration can differ from one experiment to another, the basic principle behind action potential sampling remains the same. Electrodes measure electric potential fluctuations in the extracellular space. These fluctuations generally contain two types of activity, low frequency content, also known as local field potentials (LFPs) and extracellular action potentials (spikes) which contribute to the higher frequency content (Mitra and Bokil, 2009). The spikes recorded by the electrodes represent spike events generated by an unknown number of neurons. The role of spike sorting is therefore to assign each spike to the neuron that produced it (Brown et al., 2004). As the technology progresses multi-electrode arrays are increasingly being employed (Rizk et al., 2009, Csicsvari et al., 2003). Increasing the

number of recording electrodes augments the need for automatic sorting, as manual sorting or human supervised sorting becomes a time consuming and tedious task.

The complexity of spike sorting can be attributed to several factors. It has been reported that spike waveforms for a given neuron can vary (Fee et al., 1996b); for example, during a complex spike burst, the amplitude of the spike can decrease by up to 80% (Buzsaki, 2004). Overlapping spikes create another complication when it comes to spike sorting; this phenomenon occurs when two or more closely spaced neurons fire action potentials simultaneously. Moreover, in the course of the recording session, the electrode may move slightly within the brain tissue due to external physical constraints, causing the spike waveform to vary in time (Lewicki, 1998).

Spike sorting algorithms are typically composed of four steps in total (illustrated in Figure 2.1). The first step involves detecting spike segments. The second step consists of extracting features that best discriminate the spikes produced by the different neurons. In the third step the number of neurons is estimated and often this step is carried in conjunction with final step. In the final step each spike is assigned to the neuron that generated it.

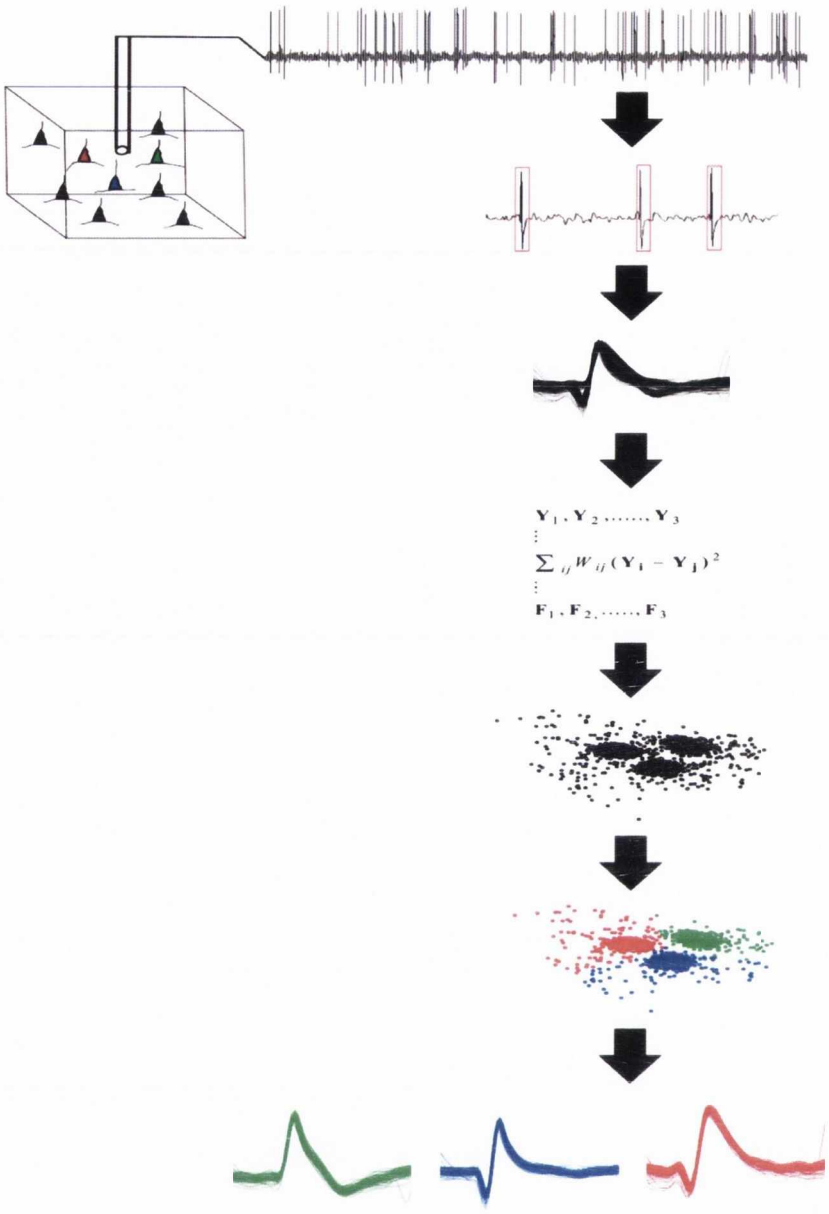

Figure 2.1 Spike Sorting Process, Spike detection, feature extraction, identifying the number of neurons and clustering

In this chapter a review of the spike sorting algorithms reported in the literature is presented. Lewicki (1998) reported a review of spike sorting methods in 1998, hence this chapter reports findings that were published in that review paper, and focus the rest of the chapter on methods reported subsequently (A summary is provided in Table 2.1).

The earlier spike sorting methods were based on temporal features of the spikes (Dinning and Sanderson, 1981); Features such as amplitude and spike width were used to discriminate spikes generated by different neurons. While these methods are simple to implement they do not offer the best results since spikes of distinct neurons can have similar spike amplitudes; also during complex burst spikes the amplitude of spike can vary largely.

Principal Component Analysis (PCA) was proposed for spike sorting by (Abeles and Goldstein, 1977, Glaser and Marks, 1968), the principle behind this method is that a set of orthogonal basis vectors are chosen that explain the largest variation within the data set (Lewicki, 1998). This method became popular and is widely used in the literature. An alternative approach employed in the literature is template matching (Yang and Shamma, 1988, Gerstein and Clark, 1964, D'Hollander and Orban, 1979), where sample spikes are chosen as templates, and spikes are assigned to the template that best matches it. Templates can be selected manually or automatically (Lewicki, 1998). A different approach reported earlier was to find a set of filters that separates the spikes of different neurons (Roberts and Hartline, 1975, Andreassen et al., 1979, Stein et al., 1979, Gozani and Miller, 1994). The principle behind these methods is to find a set of optimal filters that will yield high response to a specific spike waveform while suppressing others. In order to find these filters spike templates estimations are required. This method also requires that noise power spectrum and spikes shapes are accurately estimated. However these methods were reported to perform poorly when compared to PCA methods (Wheeler and Heetderks, 1982).

More recently spike sorting algorithms can be divided into three main categories namely, Wavelet, Dimension reduction, and probability based measures.

2.1.1 Wavelet based methods:

Wavelet Transform was proposed by Zouridakis and Tam (1997) as a feature for spike sorting. This method relies on shift-invariant wavelet transform and, the performance of the method is highly dependent on spike templates, hence the fuzzy clustering was used initially on a portion of the recordings to determine the spike templates. It is reported that the method has advantage of sorting overlapped spikes.

A method based on Discrete Wavelet Transform (DWT) was proposed by Letelier and Weber (2000). The method is based on Daubechies wavelet basis, which is computed by the fast pyramidal algorithm. The relative variability of the DWT coefficients are calculated using mean and standard deviation, these coefficients are then judged for their differentiating potential visually, which corresponds to a large standard deviation, mean and a bimodal or multimodal distribution. Then m most differentiating coefficients were then selected and spikes were sorted manually. The results show that the method proposed preforms better than PCA however this method requires manual clustering.

An algorithm based on Wavelet Packet Decomposition is proposed by (Hulata et al., 2002, Hulata et al., 2000), This method is reliant on Wavelet transform with a 3^{rd} order Coiflet mother wavelet, spikes were also detected using this method, a simple *k*-means clustering method was used to cluster the spikes, however the number of neurons in the recording was manually set. This method was compared to PCA and Wavelet transform spike sorting methods. The main advantage of this method was in the ability to cluster overlapping spikes, hence this method yielded in improved results since 25% of data set used in the study were overlapping spikes.

Quiroga et al. (2004) propose a method based wavelet transform and the superparamagnetic clustering. Haar wavelets were chosen in wavelet transform decomposition. The first 10 wavelet coefficients with the largest deviation from normality were used as features. This method was compared against PCA and *k*-means clustering in most cases the proposed method performed better.

Takekawa et al. (2010) report a sorting algorithm based on WT feature extraction and Robust Variational Bayes (RVB) classification. Haar and Cohen-Daubechies-Feauveau were used in obtaining the wavelet transform. Wavelet coefficients that yielded multi-modal distribution were selected. These coefficients were further reduced using PCA. In the clustering step RVB is used which employs a mixture model of Student *t*-distribution model. Then the number of clusters is determined by applying a minimum message length criterion. It was reported that Cohen-Daubechies-Feauveau wavelets with combination of RVB provides "excellent performance"; however, no specific classification results were reported in this study.

A real-time spike sorting algorithm is proposed by Aghagolzadeh et al. (2010). The method calculates discrete wavelet transform (DWT), with symlet4 wavelet basis. The coefficients of DWT are compared to a pre-set threshold, each time this threshold is exceeded a binary event is recorded. At the classification step, spikes are separated using the probability of each neuron producing those spikes where DWT coefficients would exceed the thresholds. The result was compared to PCA/EM algorithm and a similar performance was obtained using both methods.

Lai et al. (2011) propose an automatic spike sorting method based on Haar wavelet transform and single linkage clustering. The Kolmogorov-Smirnov (KS) test was then used to select the wavelet, and six coefficients which displayed largest divergence

from Gaussian distribution were extracted. In the final step single linkage clustering method is then used to sort the spikes. Performance was measured in terms of percentage of correctly classified spikes and percentage of correctly identified neurons. Comparison to PCA method was also carried out, similar to the WT method, PCA components were selected using KS tests. Classification procedures were also compared such as superparamagnetic clustering, *k*-means. The results presented showed that the proposed method yielded an average accuracy of 95% compared to PCA-KS with *k*-means 85%. It also showed that while single linkage clustering is more appropriate for WT-KS, *k*-means with PCA-MV yielded higher results.

Farashi et al. (2010) report a feature extraction method for spike sorting. DWT with symlet5 basis was chosen in the spike detection procedure. In the feature extraction phase, spikes are first clustered using PCA, and then templates are constructed from the average waveform in each cluster. For each template the undecimated wavelet transform UWT coefficients are calculated. The differences between the coefficients of these templates are then used to find the coefficients that separate the clusters the most. Then the most informative coefficients were used to reconstruct each spike, and finally the PCA of the reconstructed waveform are used as features in spike sorting. Visual plots are provided comparing the feature space of this method, and similar methods based on WT (Quiroga et al., 2004).

A wavelet approach is proposed by Pavlov et al. (2007), in this algorithm. First PCA is used to extract spike templates, in the second step a search is applied to find wavelet parameters that maximizes the differences between templates. These wavelet parameters are then used in the feature extraction algorithm and clustering is carried out using superparamagnetic clustering. The result of this method was compared to PCA and wavelet based methods (Letelier and Weber, 2000) and (Quiroga et al.,

2004). Over three data sets the proposed method performed better than other methods. it was reported that (Letelier and Weber, 2000) and (Quiroga et al., 2004) performed worse than PCA, due to the choice of wavelet basis employed in the methods.

2.1.2 Dimension reduction methods

Harris et al. (2000) recorded simultaneously from neurons intracellularly and extracellularly using a tetrode. They then quantified the error committed by human operators and by semi-automated spike sorting methods. Errors were classified into two types, type I false positives where spikes from different neurons are grouped together, and type II false negatives where spikes generated by a neuron are not all grouped together. Spikes were detected using amplitude thresholding method, two feature extraction methods were employed PCA and peak-to-peak amplitudes. Human operators were instructed to use graphical clustering program to sort the spikes. Semi-automatic clustering were carried out using AutoClass (Cheeseman and Stutz, 1996), the output of the clustering method was then examined by human operator to merge spike clusters deemed to contain spikes from the same neuron. The results showed that there was a large variation between human operators sorting performance, and that semi-automated sorting performed better than human operated sorting.

A method based on Independent Component Analysis (ICA) and *k*-means clustering is reported by (Takahashi et al., 2003a, Takahashi et al., 2003b) whereby, the waveforms are initially sorted based on their temporal features and the number of clusters is set to twice the expected number of clusters. Utilising this technique the clustering problem is reduced to a set of clusters rather than individual spikes. ICA is then used on each cluster to decompose and reconstruct the spikes of the cluster. Each decomposed waveform has an independent component basis vector ICBV and spikes generated by the same neuron will yield a similar ICBV. The distance between ICBVs is then used

to combine clusters using a pre-set threshold. This procedure was followed for "stable waveform", i.e. waveforms with Gaussian variability. Spikes that were not sorted in the previous step are then assumed to contain overlapping spikes and hence the non-Gaussian variability, these data are then divided in large number of clusters (four times the expected number) and then ICBV are compared and combined to the appropriate cluster if the distance was in line with the threshold set. A real-time implementation of the ICA spike sorting algorithm was reported later (Takahashi and Sakurai, 2005).

A spike sorting method relying on multivariate *t*-distribution of the spike waveform was reported Shoham et al. (2003). Where the parameters of the distribution are estimated using Expectation Maximization (EM) algorithm; in this case the spikes complete waveform and principal component analysis were used as feature sets for the algorithm and the EM algorithm was used to estimate the parameter of each cluster. Although it was reported that *t*-distribution would be a better fit to spike waveform, the result of the effectiveness of the algorithm in sorting the spikes were not reported.

Atiya (1992) proposed a sorting method with the specific aim of resolving overlapping spikes. First the number of neurons is determined by extracting peak-to-peak features, using this feature space the spikes are clustered several times by incrementing the number of clusters. This procedure was then stopped when the minimum distance between the clusters was lower than a pre-set threshold. Then templates were constructed from the average waveform within each cluster. Then all possible combinations of the templates are considered, and overlapping spikes are resolved by estimating the highest likelihood combination.

A method to address the problem of overlapping spike is proposed by Zhang et al. (2004). The method uses PCA and subtractive clustering to determine the number of clusters. Then templates are constructed from the results of PCA and subtractive clustering; the final step spikes are then sorted using template matching technique. If any spike did not match the templates then it is assumed that the spike corresponds to an overlapping waveform. Then template matching step is repeated with combination of two or more templates. The noise in spike waveform is assumed to be Gaussian noise, and this principle is applied in the template matching procedure. This method was compared to a method that resolves overlapping spikes (Atiya, 1992), while the performance of proposed method by Zhang et al. was worse than Atiya, the computation complexity was less. An improvement of this method was reported by (Wang et al., 2006, Wang and Liang, 2005) where Fast Fourier Transform (FFT) method is used to decompose and sort overlapped spikes. The method compared all possible combination of templates to decompose overlapped spikes, a cost function was calculated for each combination, and the minimum cost value then corresponds to the best solution for sorting the overlapped spike. The author reports that the performance of this method was superior when compared against (Atiya, 1992).

Vargas-Irwin and Donoghue (2007) propose a method using density grids of two dimensional PCA feature space to determine the number of neurons (i.e. number of clusters) in a recording, the feature space is divided into bins where the complete space is represented by 100x100 grid. The grid is then smoothed with a Gaussian kernel. The local maxima are then assumed to belong to centre of clusters. Templates are then constructed from the detected clusters. Overlapping spikes are resolved by subtracting templates from the spike waveform, if the difference between the template and spike is lower than predefined threshold, the spike is clustered to the matched

template; otherwise other templates are used to resolve the overlapped spike. And the spike is assigned to the combination of templates that produces the best fit. The method yielded improved results compared to (Zhang et al., 2004) and (Quiroga et al., 2004) algorithms.

Sato et al. (2007) propose a template matching spike sorting algorithm, the initial segment of recordings were used to construct the template. PCA are extracted from the spikes then *k*-means clustering is used to find the templates. The number of the neurons is then determined by calculating the Davies-Bouldin validation index (DBVI). The templates are then constructed from the average waveform in each cluster. After this step template matching procedure was used to sort the spikes.

Peng et al. (2008) propose a spike sorting method with low power requirements. The method is similar in principle to template matching sorting algorithms. Initially a template matching method is carried out where the first detected spikes are assumed to be the cluster templates, or spikes belonging to the same neuron if the difference between the template and spikes is lower than a pre-set threshold. Then the memory and power requirement are reduced by storing only relevant information rather than complete information about each spike clusters. This method was compared with PCA/*k*-means sorting method. Both methods yield similar performance however the method proposed by (Peng et al., 2008) has the advantage of having less power requirement.

A method based on feature extraction of the minimax feature set based is reported by Yen et al. (2009). Graphical representation of the feature space is then used to select the number of clusters. Following this fuzzy C-means clustering algorithm is used to cluster the spikes.

Linear filters are introduced to the problem of spike sorting by Franke et al. (2010), the first step is to estimate the templates of the spikes. The templates were estimated using a combination of PCA and EM algorithms. The authors argue that accurate estimation of templates is not required for their algorithm. The principle of the method is to find a set of linear filters (finite impulse filters); these filters should yield a high response to one of the templates and should provide a minimal response to the other templates. To overcome the problem of tissue drift, templates are re-estimated at fixed-time intervals. Templates are then constructed as the mean of the last 350 spikes. This method was compared to (Harris et al., 2000) and (Pouzat et al., 2002); the results show that this method performs better in resolving overlapping spikes and under low signal to noise ratios.

Graph-Laplacian was proposed as feature in spike sorting (Ghanbari et al., 2009, Ghanbari et al., 2010, Ghanbari et al., 2011). This method is a dimension reduction, where spike waveforms are transformed in lower set of dimension conveying most of the spike waveform information. This feature extraction method is compared to PCA and a wavelet features based on Haar wavelet. The result showed that Graph-Laplacian provides better cluster separation than PCA and Haar wavelet.

A human supervised method is reported by Adamos et al. (2010). A dimension reduction method ISOMAP is implemented in the feature extraction phase, then the number of clusters are selected manually with the aid of feature space plots. Fuzzy *C*-means is then used to cluster the spikes; spikes exceeding a set threshold were assigned to the clusters, while spikes not fulfilling these criteria were further processed. Unclassified spikes from the previous step were then processed using Extreme Machine Learning (EML) algorithm. The EML method is trained using data obtained from the previous step. The EML algorithm is then used to sort noisy and

overlapped spikes. The performance of this method was compared against PCA/EM and WaveClus, the result showed an improved performance in spike classification.

A frequency shaping filter is proposed for spike sorting algorithms by Yang et al. (2009b), in the study the first derivate of the spike was chosen as the shaping filter. Clustering was carried out using evolving mean shift algorithm (Yang et al., 2009a). This algorithm was compared to PCA and simple amplitude features. It was reported that the addition of spike derivate can improve spike sorting, however in this study overlapping spikes were excluded from the data set.

A template matching method is reported by Thakur et al. (2007), the templates are generated using PCA and hierarchical agglomerative clustering, the noise statistic within the recording is also estimated, where it is assumed that noise in neurophysiological recording is Gaussian. A lower dimensional space is then constructed using the templates and the first few PCA components. This lower dimensional space was designed to maintain spike energy while reducing the noise energy. And spikes were sorted by applying template matching and taking into account the background noise.

The feature extraction for spike sorting method proposed by Horton et al. (2007) is based on curvature features of the spike waveform. A set of scores is calculated for each point of the waveform, where each score quantifies the curve shape, and the amount of curvature. These scores are then averaged within time segments to obtain a reduced set of scores. For the clustering step Kohonen network is used to identify the number of neurons, in this process training data should be allocated for the clustering method to calculate decision boundaries and carry out clustering subsequently.

The spike sorting method reported by Yang et al. (2011) relies on extracting spike samples that show a multimodal distribution. The method starts by estimating the probability of each sample being partitioned into several clusters, and then sample information is quantified using Shannon entropy, using this probability waveform samples yielding highest information are then selected for feature extraction. The results show that this method yields higher accuracy in spike sorting, however details about clustering method and detection of the number of neurons are not provided.

A method based on projection pursuit is proposed by (Kim and Kim, 2003, Kim, 2006), where projection pursuit based on negentropy entropy is used to find projections with maximum separation. These projections are then examined to find the number of Gaussian distribution within the feature space. Finally the parameters of Gaussian distribution are estimated and spikes are clustered accordingly. The result showed better separation of clusters compared to PCA.

Balasubramanian and Obeid (2011) propose a method based on fuzzy logic, the method extracts temporal features of spikes, such as spike power, spike amplitude range slope of the spike. Then features are converts categories for example spike power is divided into low, medium and high. In the classification step, Fuzzy rules are evaluated and score is assigned to the spike. The scores were then clustered using Fuzzy *C*-mean algorithm. The performance was compared with PCA algorithm and no significant difference between these methods was found. The advantage of proposed method however lies in the computational complexity.

2.1.3 Probability based methods:

A Bayesian classification for neural signals is proposed by Lewicki (1994). The noise is modelled as Gaussian noise, and then the probability of each spike belonging to

each cluster is calculated using Bayes rule. Overlapping spikes are decomposed by determining the most probable sequence using *k*-dimensional search trees.

Fee et al. (1996a) propose a method to overcome the limitations of Gaussian isotropic assumption. As a first step a subset of spike waveform are clustered into a large number of clusters. Secondly these clusters are combined by taking into account waveform similarities and inter-spike intervals of combined clusters.

A method of spike sorting based on the modelling of spikes' noise was proposed by Pouzat et al. (2002). The Bayesian Information Criterion (BIC) was used to determine the number of clusters, and then probabilistic data generation model was computed for each cluster. Each spike was then assigned to the cluster with highest probability of generating the spike.

A neural network method is presented by Chandra and Optican (1997), the method requires a training phase. During the training phase templates are constructed, and then these templates are used to train the neural network. It was shown that this method yields better separation of overlapping spikes than matched filter method. The main disadvantage of this method is that it requires training, and initial estimation of clusters (Lewicki, 1998).

Aksenova et al. (2003) propose a method relying on self-oscillating model with perturbations, the method is based on assumption that the spike waveform can be represented by a solution of differential equations, and that a set of similar "cycles" are generated by spikes from of the same neuron. The classification process is carried out first on a subsection of the recording to estimate the number of clusters and then spikes are clustered based on Gaussian distribution.

A semi-automated method is proposed by Delescluse and Pouzat (2006) an advancement of a previous algorithm reported (Pouzat et al., 2004), the method is based on modelling the firing statistics of neurons, such as inter-spike intervals ISI using Markov chain Monte Carlo. The model also takes into account amplitude dynamics of the spikes, where the amplitude is modelled with exponential decay at short ISI. In the sorting algorithm the number of neurons recorded must be set by the user. This method was tested on real data recorded from Purkinje cells, where the amplitude of these cells decreases within short ISI. The result showed good separation of spikes 98% compared to (Pouzat et al., 2002) 85%.

A method based on neuron localization is proposed by Chelaru and Jog (2005), the method depends on multichannel spike recording electrodes (tetrodes). The assumption is that the amplitude of the spikes recorded decreases linearly with respect to the distance between the electrode and neuron. This assumption is then used to estimate the origin of the spike in 3D space. Self-organizing map (a modification of *k*-means) is used then to cluster the spikes. The number of clusters is determined using Davies-Bouldin validity Index.

An online spike sorting method is proposed by Rutishauser et al. (2006), the number of neurons and the spike sorting is based on the estimation of noise properties of the signal. Noise standard deviation is calculated with sliding window, and then the threshold is set as the average noise standard deviation squared. Each spike is compared to the average waveform of the sorted clusters, if the distance between the spike and the average waveform was smaller than the threshold this spike is assigned to the cluster, otherwise if no match was found the spike was declared as a new cluster. This method was compared to two other common methods PCA/KlustaKwik

(Harris et al., 2000) and WaveClus (Quiroga et al., 2004), all three methods compared had similar performance.

Bar-Hillel et al. (2006) reported a method of spike sorting to address the non-stationary spike recordings. In the proposed method the recording is divided in non-overlapping time frames, within each time frame PCA was extracted and a "local solution" is found where it is assumed that the spike clusters follow a mixture of Gaussian distributions. Then a transition score is calculated between successive time frames. In the final step a "global solution" is found by calculating the maximum-a-posteriori using Viterbi algorithm. This method was compared against other methods reported where it is shown that the algorithm outperform previous spike sorting method when non-stationary clusters were present.

A method of spike clustering was reported in (Wood and Black, 2008, Wood et al., 2006). The method extracts PCA features and applies infinite mixture modelling in the clustering phase. This approach was compared with traditional EM algorithm combined with Bayesian information criteria. The comparison was carried on a data set recorded from behaving monkey and ground truth was determined using human sorting. It was reported that the author "believe that cluster found" using this approach resembles human sorting more than EM algorithm. However no specific results were reported.

Nguyen et al. (2003) propose reversible-jump Markov chain to estimate the number of neurons and to cluster the spikes. The feature vector is modelled as an anisotropic mixture of Gaussians. The method is then used to estimate the number of clusters and model parameter in order to classify the spikes. In simulation the algorithm performed

well, however in real data set the algorithm achieved worse results due to presence of outliers and violation of Gaussian assumption.

Support vector machine classifier (SVM) was used in sorting spikes by Ding and Yuan (2008), multi-class "one against all" SVM was used since it yielded in higher performance. One tenth of the recorded spikes were assigned to train the classifier. Once the training procedure is completed the spikes are classified. If the SVM output for a particular cell is less than a pre-set threshold, the spike is regarded as overlapped spike and further processing are carried out where templates are subtracted from the spike to resolve the spike.

Herbst et al. (2008) apply probabilistic hidden Markov models (HMMs) to the spike sorting problem. In the learning stage the parameters of the models (state transition probability, spike templates and noise variance) were estimated using Baum-Welch algorithm. The Viterbi algorithm was then used to compute the most likely state of the hidden variables from the data. The algorithm was compared to WaveClus, and when this algorithm did not find the real number of clusters, this parameter was corrected. The number of false positives in both algorithms was similar. However HMMs method performed better in number of false negatives. This was mainly due to the fact WaveClus does not classify overlapping spikes.

Ventura (2009) propose a method that relies on combining spike waveform and tuning information. The waveform and tuning parameter are estimated from the data using Expectation maximization EM. For simplicity it is assumed that spike waveforms follow a normal distribution. Then linked EM is employed to estimate neurons' tuning function. i.e. given the waveform and firing parameters of the neuron, the tuning parameters of the neuron are estimated. The algorithm was tested on simulated data,

inspired from movement decoding recordings obtained from the motor cortex. The number of neurons is identified by using Akaike Information Criterion (AIC) and Bayesian Information criterion (BIC). Classification error was reduced using this method compared to waveform only classification.

Calabrese and Paninski (2011) introduce a spike sorting algorithm with the aim of tracking changes in spike waveform characteristic during neural acquisition. The method uses PCA the common feature extraction method applied in the literature, then for the clustering step, the method assumes mixture of Gaussian model where the parameters can be estimated using EM algorithm. The authors advance this model a step further to mixture-of-Kalman filters, by allowing the mean voltage waveform to vary across time. Hidden Markov Model was also used to account for refractory period of the spikes. The method was tested on several simulated and real data sets. In these tests the number of clusters was determined manually. In simulations where the mean waveform varied, traditional clustering method (mixture of Gaussian) performed worse than proposed algorithm. In real recordings the difference between the two algorithm was minimal (~ 2%), due to that fact clusters remained well separated in real recordings.

2.1.4 Computation comparison of spike sorting:

An important aspect of real time spike sorting is the computation complexity of spike sorting methods. A comparison of the power requirement of spike detection method is reported by (Gibson et al., 2008, Gibson et al., 2010). The results showed the least computational complexity is a simple amplitude threshold method. In terms of spike detection performance the Nonlinear Energy Operator (NEO) yielded the highest results, although the difference in performance between simple amplitude threshold and NEO was minimal. Complexity of feature extraction methods was also compared

it was shown that PCA, discrete wavelet transform DWT and Discrete Derivatives (DD) had similar sorting performance, although DD had the lowest computational complexity.

Table 2.1 Summary of Spike sorting methods

Author	Spike detection	Feature extraction	Clustering	Automation	Overlapping spikes
(Atiya, 1992)	Peak-to-peak threshold	Peak-to-peak	Template matching	Yes	Yes
(Gozani and Miller, 1994)	--	Templates	Optimal filtering	Yes	No
(Lewicki, 1994)	Amplitude thresholding	Spike waveform	Bayesian clustering	Yes	Yes
(Fee et al., 1996a)	Amplitude thresholding	Spike waveform	Recursive bisection/aggregation step	Yes	No
(Chandra and Optican, 1997)	Amplitude thresholding	Templates	Neural networks	No	Yes
(Letelier and Weber, 2000)	Amplitude thresholding	Wavelet transform	Manual graphical	No	No
(Zouridakis and Tam, 1997)	Unknown	Wavelet transform	Template	No	Yes
(Harris et al., 2000)	Amplitude thresholding	PCA/ peak amplitude	AutoClass	Semi-automated	No
(Hulata et al., 2002)	Wavelet packet	Wavelet packet decomposition	*k*-means	Semi-automated	Yes
(Pouzat et al., 2002)	Threshold	Noise modeling	Gaussian distribution	No	No
(Takahashi et al., 2003a, Takahashi et al., 2003b)	Amplitude thresholding	ICA	Gaussian distribution	Yes	Yes
(Kim and Kim, 2003, Kim, 2006)	Teager energy operator/ discrete wavelet transform	negentropy	Gaussian distribution	Yes	No
(Aksenova et al., 2003)	First derivative	Differential equation phase	Gaussian distribution	Yes	No
(Shoham et al., 2003)	threshold	Waveform/ PC	t-distribution, E-M	No	No
(Nguyen et al., 2003)	--	Spike amplitude	Reversible-jump Markov chain Monte Carlo	Yes	No
(Pouzat et al., 2004)	Markov chain Monte Carlo			No	No
(Zhang et al., 2004, Wang et al., 2006)	Threshold	PCA	Template matching/Gaussian distribution	yes	partial
(Chelaru and Jog,	Threshold	Spike	Self-organizing map	Yes	No

2005)		localization			
(Rutishauser et al., 2006)	Power 38hreshold	Spike residuals	Noise threshold	Yes	No
(Quiroga et al., 2004)	Amplitude threshold	Wavelet transform	Superparamagnetic	Yes	No
(Bar-Hillel et al., 2006)	Amplitude threshold	PCA	Gaussian distribution	Yes	No
(Wood et al., 2006)		PCA	Infinite mixture modeling	Yes	No
(Horton et al., 2007)	Amplitude threshold	Curvature component	Kohonen network	Yes	No
(Vargas-Irwin and Donoghue, 2007)	Amplitude threshold	PCA	template	Yes	Yes
(Pavlov et al., 2007)		WT	Superparamagnetic	Yes	No
(Sato et al., 2007)	Template	PCA	*k*-means/Template	Yes	No
(Thakur et al., 2007)	Matched filter	PCA	Template	Yes	No
(Ding and Yuan, 2008)	--	--	Support vector machine	No	yes
(Herbst et al., 2008)	Amplitude threshold	Automated template	Hidden Markov models	Yes	Yes
(Peng et al., 2008)	Not reported	Template	Preset thresholds	Yes	No
(Yen et al., 2009)	Amplitude threshold	Minimax reduced feature set	Fuzzy C-means	No	No
(Ventura, 2009)	--	Waveform and tuning information	EM	Yes	Yes
(Ghanbari et al., 2009)	Amplitude Threshold	Graph-laplacian	--	--	--
(Yang et al., 2009b)	NEO	Frequency shaping filter	Evolving mean shift clustering.	Yes	No
(Franke et al., 2010)	Optimal filter	Linear filters		Yes	No
(Takekawa et al., 2010)	Amplitude threshold	PCA/ WT	Robust Variational Bayes (RVB)	No	Yes
(Adamos et al., 2010)		ISOMAP	Fuzzy C-means	Yes	No
(Yang et al., 2011)	NEO	Waveform samples	--	--	--
(Aghagolzadeh et al., 2010)	DWT	DWT	Bayesian	Yes	No
(Farashi et al., 2010)	DWT	PCA and UWT	--	No	No
(Calabrese and Paninski, 2011)	Amplitude threshod	PCA	Mixture of Kalman filters	No	No
(Balasubramanian and Obeid, 2011)	--	Temporal features+ Fuzzy logic	Fuzzy C-means	Yes	No
(Lai et al., 2011)	Amplitude threshold	WT	Single linkage clustering		Yes

2.2 Literature review discussion

A summary of the spike sorting algorithms are provided in Table 2.1. Some of these algorithms require human supervision e.g. (Ding and Yuan, 2008, Letelier and Weber, 2000, Harris et al., 2000), to select the number of neurons active during the recordings, or to carry initial training of the classifier. Human supervised methods require time and training and hence are not feasible with large data sets.

The disadvantage of methods relying on firing properties of the neurons is that prior assumptions about the information of firing statistics should be made, while in most applications this information is unknown. Prior assumptions about firing statistics can distort any further analysis carried out.

The method of wavelet transform has been shown to provide a good separation between neural spikes, however depending on the data set the choice of wavelet basis can have profound effect on the performance of spike sorting as shown by (Pavlov et al., 2007). Data sets employed in literature can vary in difficulty of spike sorting, or noise statistical assumptions. For example in some studies (Yang et al., 2009b) overlapping spikes were excluded from the data sets and hence the results report could be biased. Therefore it is important to test the algorithm on public data sets to provide objective comparison between different spike sorting methods in literature.

PCA is a simple algorithm used commonly directly or indirectly in spike sorting, for example in template matching algorithms (Vargas-Irwin and Donoghue, 2007, Zhang et al., 2004). Generating templates is an important step. Some use initial clustering based on PCA to extract these templates. And hence the accuracy of these algorithms

depends on the effectiveness of the initial standard dimension reduction and clustering.

An ideal spike sorting method will be able to address the following challenges:

1. Isolating the spikes of all neurons close to the recording electrode
2. Minimal human intervention
3. Resolving overlapping spikes
4. Taking into account non-stationary recordings
5. Ability to carry spike sorting online i.e. during the recording session
6. Low computational complexity, so it can be implemented on implanted chips

It should be noted that due to complexity of spike sorting challenges, designing an algorithm that can overcome all challenges is a demanding task. Hence depending on the experiment requirement certain algorithms can be more suitable. For example, if it is required to have online sorting, then methods that factor this should be selected. Or if the recording contains a large percentage of overlapping spikes, then algorithm addressing this issue would be more suitable.

In the next section of this thesis, an automated spike sorting algorithm is introduced to address some of the challenges associated with spike sorting, namely the challenges of efficient spike isolation and automation. The method shares the simplicity offered by PCA, hence this method can be used as alternative to generate templates. The proposed method was compared to common applied methods including PCA methods. The test data compromised a publically available data set, where the objectiveness of the comparison can be retained.

2.3 Spike sorting method:

An important aspect of spike sorting is to extract the maximum information available from the neural recordings, hence it is important to develop spike sorting methods that will produce high sorting accuracies.

In this chapter a robust method of automatic spike sorting is proposed. Locality preserving projections (Xiaofei and Partha, 2003), which is linear approach of Laplacian eigenmaps was previously reported for manual spike sorting (Ghanbari et al., 2011), In this chapter a fully automated spike sorting based on nonlinear feature extraction method (Laplacian eigenmaps) and *k*-means clustering is reported. The performance of the proposed method is compared with systems based on simple amplitude features, and on PCA derived features. Two types of classification algorithms were employed in this thesis, namely *k*-means and classification expectation-maximization algorithms (CEM, as implemented in KlustaKwik (Harris)).

The data set used in this chapter included publically available simulated data set, where it allows objective comparison between different algorithms.

Simulated data set has the advantage that the spike origins are known and are free from expert sorting subjectivity (Harris et al., 2000, Wood et al., 2004), however it is important to test the algorithm in practical environment. Hence in this chapter *in-vivo* data recorded from rodents was also used in evaluating the performance of the methods.

The main finding of this chapter was reported in:

Chah, E., Hok, V., Della-chiesa, A., Miller, J. J., O'Mara, S. M. & Reilly, R. B. 2011. Automated spike sorting algorithm based on Laplacian eigenmaps and *k*-means clustering. *J Neural Eng,* **8,** 016006.

2.4 Data set:

Simulated data used in this chapter were obtained from the publicly available data set WaveClus (Quiroga et al., 2004). All simulated recordings 22 in total, named in Table 2.2 according to the convention used by the author of WaveClus (Quiroga et al., 2004), where the number at the end of file indicated the noise level. The data set included simulations of complex spike cells (data set, Burst_Easy2_015) and electrode drift (data set, Drift_Easy2_015). Each file contains spikes from three neurons.

The average number of neural spikes in the files was ~ 2790. In most recordings the standard deviation of noise in the data set varied between 5% - 20% of the spike peak amplitude, the only exception was data set "easy1" where noise level was varied up to 40%. The noise was constructed to simulate background neural activity. This was achieved by adding average spike waveforms at random times and with random amplitudes to form the noise signal. The simulated data spike clusters had a mean firing rate of 20 Hz and a 2 ms refractory period.

Simulated data has the advantage of being objective and it provides an error-free benchmark. However, it has several shortcomings. For example, the simulated data represents a single channel recording. However it has been established that multichannel recording such as tetrodes markedly improve spike sorting (Gray et al.,

1995). Hence, it is vital to consider multichannel recording when assessing the performance of spike sorting algorithms.

The simulated data sets in this study contained spikes from three neurons in each recording; however, when it comes to *in-vivo* studies, more neurons may be recorded by each channel. Theoretical estimations suggest that a tetrode can sense spikes from ~ 140 neurons with sufficient spike amplitude for spike sorting (Henze et al., 2000). In practice, however, the number of neurons sensed will be fewer ~20 (Henze et al., 2000). A higher number of clusters can lead to lower classification accuracy. For example, if there are two clusters, the probability of classifying an object correctly by chance is 50%, while if the number of clusters increase to 10, the probability is reduced to 10%.

To address the shortcomings of the simulated data set, the performance of spike sorting algorithms was also evaluated from *in-vivo* recordings from the hippocampus of a freely-moving rodent. A surgical procedure was followed for the implantation of electrodes; the animal was anaesthetized with isofluorane and mounted on a sterotaxic frame for precise positioning of the electrodes. The animal was allowed to freely explore an enclosure for 20 min during the recording. Experiments were conducted in accordance with European Community directive, 86/609/EC, and the Cruelty to Animals Act, 1876, and followed Bioresources Ethics Committee, Trinity College, Dublin, Ireland, and international guidelines of good practice.

The *in-vivo* data was collected using a commercial spike recording system (Axona, Ltd.). The recording was obtained using a tetrode configuration with one channel set as a reference. In this case, the results of automatic sorting were compared against expert manual sorting. The expert was able to sort and reliably isolate spikes of two

neurons (~3890 spikes). The remaining detected segments were considered as noise event. The total number segments detected (noise and spikes) was ~10400. Manual spike sorting was carried out offline using graphical cluster-cutting software (Axona, Ltd.), where the spikes were sorted based on multiple features including spike amplitude, spike duration, maximum and minimum spike voltage, and the time of occurrence of maximum and minimum spike voltages. The spike sorting performance using *in-vivo* data provides an insight into the performance of the spike sorting algorithms for practical spike sorting by the scientific community.

2.5 Methods:

Spike sorting involves four steps (See Figure 2.2) as follows:

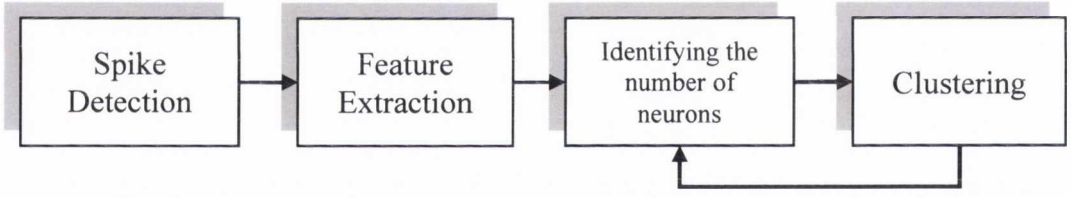

Figure 2.2 Spike sorting steps

2.5.1 Spike detection

The spike detection employed was based on the method reported by (Quiroga et al., 2004). The recordings were high-pass filtered (300 Hz). The background noise standard deviation was estimated using the formula:

$$\sigma_{noise} = \frac{median(|x_f|)}{0.6745} \tag{2.1}$$

Where x_f refers to the sampled filtered signal. For data sets with noise levels between 5% and 20%, the threshold was chosen as in (Quiroga et al., 2004) to be $4 * \sigma_{noise}$, in data sets with higher noise level this threshold was lowered to $2.5 * \sigma_{noise}$, since in these high noise data sets a high threshold would yield in few spikes being detected. Spikes are detected when this threshold is exceeded. Each detected spike is represented by 64 samples when the threshold was exceeded. This corresponds to an interval of ~2.7 ms.

2.5.2 Feature extraction:

Feature sets were divided into three categories:

2.5.2.1 Laplacian eigenmaps:

Laplacian eigenmaps (LE) is a dimension reduction method, that optimally preserves local neighbourhood information in a data set, by preserving these local information in the data set it indirectly emphasizes the natural clusters of a given data set (Belkin and Niyogi, 2003). Thus this method can be utilized to separate spike clusters generated by distinct neurons. As with any data reduction method, the problem is that given a set of $\boldsymbol{x}_1, \ldots, \boldsymbol{x}_M$ of M points in R^l, find a set of point $\boldsymbol{y}_1, \ldots, \boldsymbol{y}_M$ in R^n ($n<<l$) such that y_i represents x_i. The objective of Laplacian eigenmaps is to map points which are found to be similar under a specific definition, to points close together (Chen et al., 2010, Belkin and Niyogi, 2003). Let $\boldsymbol{y} = (\boldsymbol{y}_1, \boldsymbol{y}_2, \boldsymbol{y}_3, \ldots, \boldsymbol{y}_m)^T$ be such a map, this objective is achieved by minimizing the following function:

$$\sum_{ij} W_{ij} (\mathbf{y_i} - \mathbf{y_j})^2 \tag{2.2}$$

Where W_{ij} is defined in Eq. (2.3). This weight function (W_{ij}) ensures that points close to each other assigned a large weight while points further apart assigned a smaller

weight. Since this function decreases exponentially, points mapped further apart incur a heavier penalty (Belkin and Niyogi, 2003). These mappings demonstrate the potential suitability of LE in spike sorting algorithms.

For a detected spike segment $\boldsymbol{x}$ of length M the LE algorithm has the following steps:

First step: The Euclidean distance matrix is computed $||\boldsymbol{x}_i - \boldsymbol{x}_j||^2$. Then n nearest neighbours are connected. i.e. if node j is among the n nearest neighbours of i then nodes i and j are connected.

Second step: Weight matrix is computed according to Eq. (2.3).

$$W_{ij} = \begin{cases} e^{\frac{-\|\mathbf{x}_i - \mathbf{x}_j\|^2}{2\sigma}} & \text{if } i \text{ and } j \text{ are connected} \\ 0 & \text{otherwise} \end{cases} \tag{2.3}$$

Third step: for the connected component the generalized eigenvalues and eigenvectors are computed.

$$L\boldsymbol{f} = \lambda D\boldsymbol{f}$$

Where λ is the eigenvalue and $\boldsymbol{f}$ is the corresponding eigenvector (2.4)

$$\text{With } D_{ii} = \sum_j W_{ij} \tag{2.5}$$

$$\text{Laplacian matrix } L = D - W \tag{2.6}$$

Fourth Step: The eigenvectors are sorted according to their eigenvalues:

$$0 = \lambda_0 \leq \lambda_1 \leq \lambda_2 \leq \ldots \leq \lambda_m \tag{2.7}$$

Final Step: The mapping of x_i into the lower m dimension space is then given by $(f_1(i), \ldots, f_m(i))$. Ignoring the first eigenvector f_0 which corresponds to the eigenvalue 0.

There are two parameters to be determined in the Laplacian eigenmap dimension reduction algorithm, namely n and σ . It is reported in (Ghanbari et al., 2009, Ghanbari et al., 2010) that choosing n values between (*5 - 21*) is sufficient for spike cluster separation. In this study $n = 12$ was chosen which is in the range reported in the literature. σ was determined empirically; higher values than 0.6 were shown to have no effect in improving the cluster separation. In this thesis σ was set to a simple value of 1. The dimension of the features extracted from the spikes using Laplacian eigenmaps dimension reduction was limited to three dimensions, in line with the other feature extraction methods compared in this study.

2.5.2.2 PCA feature:

Principal Component Analysis (PCA) finds a set of orthogonal basis vectors that represent the largest variation of the data. It has been reported for spike sorting that choosing the first three principal components provides good separation (Wheeler and Heetderks, 1982). Choosing a higher number of components would account for higher variation; however, higher components were found to be dominated by background noise (Lewicki, 1998). In this chapter the PCA features consisted of the first three PCA components.

2.5.2.3 Amplitude-Only features:

Amplitude-only features were based on the temporal characteristic of the spike waveform. The distance between the neuron and electrode is an important factor in determining the amplitude sensed by the electrode (Henze et al., 2000, Moffitt and

McIntyre, 2005). In an environment where neurons are not equidistant with respect to the electrode, the amplitude of the spikes can be used to discriminate spikes from different neurons.

The temporal characteristics extracted included:

- The positive peak amplitude of the spike.
- The amplitude of the local minimum before the peak.
- The amplitude of the local minimum after the peak.

2.5.3 Clustering:

Two types of clustering algorithms were used:

2.5.3.1 k-means clustering:

k-means clustering (Theodoridis and Koutroumbas, 1998) is a simple clustering algorithm involving few steps, although the number of clusters k must be predetermined. In spike sorting methods, the number of neurons contributing to the spikes sensed by the electrode is not known, and therefore, it is not possible to pre-set k. To overcome this *k*-means limitation the PBM index (Pakhira et al., 2004) was employed to determine k. The PBM index is a cluster validity index; it measures the "goodness" of clustering using a range of clusters (k).

Below is a short description of the steps in *k*-means combined with PBM index algorithms:

- Step1: number of clusters is initially set to k.
- Step2: k points are chosen randomly in the feature space as the initial cluster centres CC_j where $j = 1, \ldots, k$.

- Step 3: For a feature vector $\boldsymbol{A}$ of length N, find the Euclidean distance between each A_i and CC_j, $j=1,\ldots,k$, where $i=1,\ldots,N$.
- Step 4: Assign A_i to the cluster CC_j which gives the minimum Euclidean distance.
- Step 5: Recalculate cluster centres CC_j using the points in each cluster.
- The steps 2-5 are repeated until no change is obtained, below a certain threshold, in cluster centres CC_j. In practice clustering is repeated a number times with different initial random cluster centres so that a local minimum is not interpreted as the optimum classification result.
- Step 6: Calculate the PBM index for each k:

$$PBM(k) = \left(\frac{1}{k} \times \frac{E_1}{E_k} \times S_k \right)^2 \tag{2.8}$$

- Where k is the number of clusters, S_k is the maximum separation between cluster centres; E_1 is the sum of separation between the points and the cluster centres when number clusters $k=1$. E_k is the sum of separations between the feature points and the k cluster centres.
- Step 7: Choose k that yields the highest PBM index.

2.5.3.2 Classification expectation-maximization:

The software KlustaKwik was used which is based on the Classification Expectation-Maximization algorithm (CEM) (Celeux and Govaert, 1992).

2.6 Performance measure metrics:

Two metrics were used to evaluate the performance of the spike sorting system. Similar to (Yang et al., 2009b) a classification matrix (CM) was computed. However, a modified matrix was developed to include the "noise events" or non-spike events.

$$CM = \begin{array}{c} \\ C_1 \\ C_2 \\ C_3 \\ \vdots \\ C_k \end{array} \begin{array}{c} \begin{array}{cccccc} N_0 & N_1 & N_2 & N_3 & \dots & N_K \end{array} \\ \begin{bmatrix} FP_{10} & TP_1 & FP_{12} & FP_{13} & \dots & FP_{1K} \\ FP_{20} & FP_{21} & TP_2 & FP_{23} & \dots & FP_{2K} \\ FP_{30} & FP_{31} & FP_{32} & TP_3 & \dots & FP_{3K} \\ \vdots & \vdots & \vdots & \vdots & \ddots & \vdots \\ FP_{k0} & FP_{k1} & FP_{k2} & FP_{k3} & \cdots & FP_{kK} \end{bmatrix} \end{array} \tag{2.9}$$

Where N_0 refers to noise events, and N_1 N_2 N_3 ... N_K reflect the spikes produced by each neuron respectively, C_1, C_2 and C_3 ...C_k refer to the clusters identified by the spike sorting method. K refers to the actual number of neurons in the recording, k refers to the number of clusters identified. TP_i is the number of spikes from neuron i in the cluster i (true positives). FP_{ij} is the number of spikes from neuron j in the cluster i (False positives), note that $j = 0$ corresponds to noise events.

The first measure of performance is the Sorting Accuracy (SA) which is the percentage of the detected spikes labelled correctly:

$$SA(\%) = 100 * \frac{\sum_{i=1}^{K} TP_i}{\sum_{i=1}^{K} TP_i + \sum_{i,j=1,i\neq j}^{k} FP_{ij}} \tag{2.10}$$

Sorting Error SE is the ratio between the false positives and the total number of segments (spikes and noise) in identified clusters.

$$SE(\%) = 100 * \frac{\sum_{i=1, j=0, i \neq j}^{K} FP_{ij}}{\sum_{i=1}^{K} TP_i + \sum_{i=1, j=0, i \neq j}^{K} FP_{ij}} \tag{2.11}$$

A perfect spike sorting algorithm will yield a SA of 100% and SE 0% which corresponds to $\sum_{i=0, j=1, i \neq j}^{k} FP_{ij} = 0$.

2.7 Results:

2.7.1 Spike detection:

The performance of the spike detection method was assessed based on the percentage of neural spikes detected correctly. The mean percentage of neural spikes detected was 81% with a standard deviation of 12%. The percentage of noise events is defined as the ratio between noise events and total number of segments detected (noise and neural spikes). The mean noise percentage was 9% and the standard deviation was 16%.

2.7.2 Spike sorting using simulated data set:

The three feature extraction processes mentioned in the previous section were applied to the simulated data set and both types of classifiers were used to cluster the feature data. The results are shown in Table 2.2.

Table 2.2 Simulated data set results.

Data Set	*k*-means classifier						CEM classifier					
	LE features		PCA features		Amplitude -only features		LE features		PCA features		Amplitude -only features	
	SA (%)	SE (%)	SA (%)	SE (%)	SA (%)	SE (%)	SA (%)	SE (%)	SA (%)	SE (%)	SA (%)	SE (%)
Easy1_005	98	1	99	1	66	30	34	68	96	0	63	35
Easy1_01	98	2	67	2	64	20	68	27	97	1	63	17
Easy1_015	72	2	80	3	58	20	75	1	97	2	60	18
Easy1_02	67	4	56	4	60	37	76	2	96	3	68	25
Easy2_005	94	0	82	2	73	25	64	37	93	0	69	21
Easy2_01	93	1	82	4	31	45	67	0	93	3	49	44
Easy2_015	74	3	58	13	30	48	79	3	61	34	47	46
Easy2_02	61	13	61	24	31	53	65	17	34	58	43	54
Difficult1_005	94	0	66	2	40	53	33	64	96	1	32	55
Difficult1_01	89	3	64	10	31	52	70	1	91	9	38	58
Difficult1_015	69	12	38	20	41	59	72	13	34	67	41	62
Difficult1_02	51	34	37	42	30	51	40	41	36	64	40	57
Difficult2_005	93	1	91	6	68	31	79	0	63	27	64	32
Difficult2_01	94	5	64	24	54	47	69	1	65	31	62	23
Difficult2_015	60	27	59	29	38	30	59	28	64	40	51	46
Difficult2_02	63	50	51	50	37	58	57	59	35	67	52	59
Burst_Easy2_01	86	13	48	18	30	50	53	39	59	32	56	57
Drift_Easy2_015	57	6	52	19	36	35	76	5	70	46	46	44
Easy1_025	93	4	92	8	47	41	66	15	93	6	50	41
Easy1_03	86	4	82	25	40	49	80	25	85	32	49	39
Easy1_035	31	45	66	19	27	44	41	37	35	8	39	50
Easy1_04	68	13	44	22	24	54	66	25	47	75	34	51
mean	**77**	**11**	**65**	**16**	**44**	**42**	**66**	**24**	**70**	**28**	**51**	**42**

Comparing the mean performance metrics in the last row of Table 2.2, it is evident that LE combined with *k*-means classification yields higher sorting accuracy and lower sorting error percentages than other methods. By examining the mean performances, it can be concluded that Amplitude-Only features perform poorly when compared to other methods. The mean performance in the Table 2.2 also illustrates that *k*-means classification combined with PCA feature extraction yields lower sorting accuracy than the PCA/CEM algorithm. However PCA/*k*-means provides better sorting error performance than PCA/CEM.

The Friedman test (Friedman, 1937) was employed to assess if the methods produced significant improvements. This test can be used to determine if there is a significant difference between several methods when the different methods were tested on the same data set (Sheldon et al., 1996).

The Friedman test revealed that the sorting accuracies percentages were significantly different with ($p < 0.0001$). Post hoc analysis showed that LE combined with *k*-means yields significant different performance than all other methods compared in this study. Applying the Friedman test to SE percentages showed that the sorting algorithms are significantly different ($p < 0.0001$). Post hoc analysis reveals that LE methods yields significantly lower sorting error than the other methods compared in this study. The test also confirms that PCA combined with *k*-means or the combination of PCA, CEM clustering provides less sorting error than algorithms based on Amplitude-Only features. Figure 2.3 presents a graphical representation of the sorting accuracy of the spike sorting algorithms employed in this study. Figure 2.4 on the other hand compares the sorting error percentages of the algorithms.

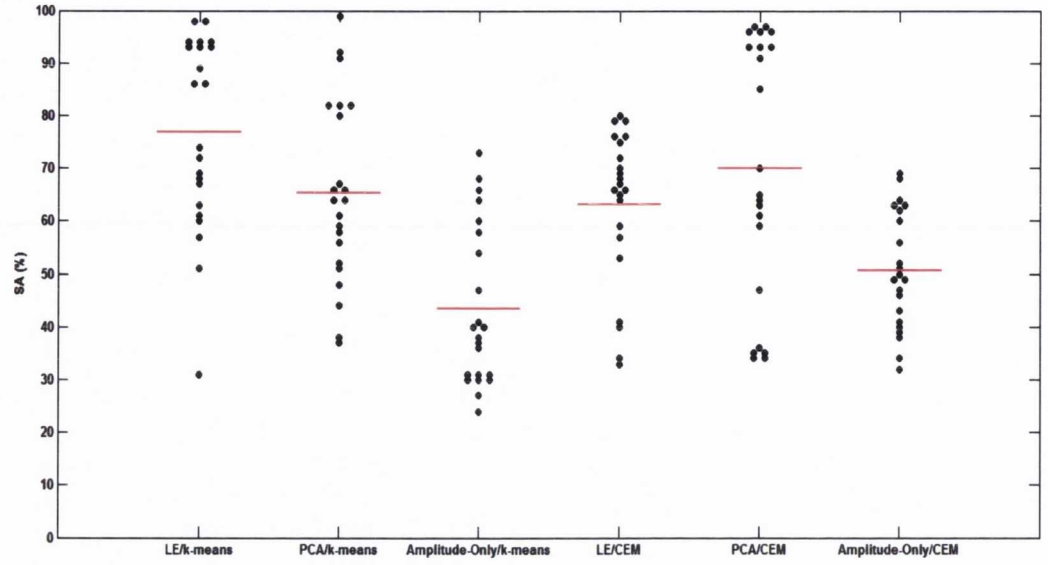

Figure 2.3 Dot plot of the sorting accuracy result obtained using the spike sorting methods. Each dot represents the sorting accuracy of a single simulated data set using the corresponding spike sorting method on the x-axis. Horizontal lines represent the mean sorting accuracy of the spike sorting method.

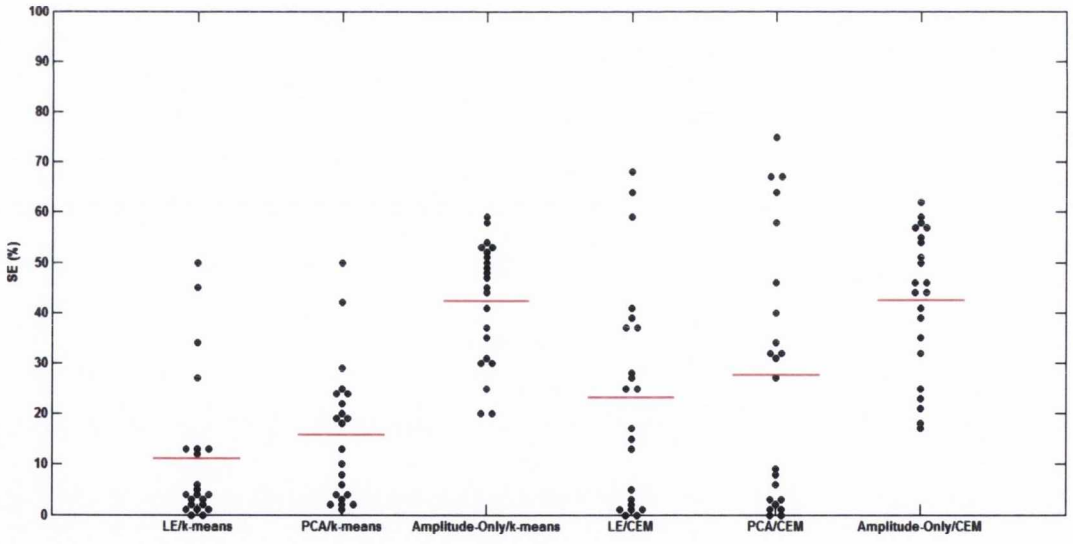

Figure 2.4 Dot plot of the sorting error results obtained using the spike sorting methods. Each dot represents the sorting error of a single simulated data set using the corresponding spike sorting method on the x-axis. Horizontal lines represent the mean sorting error of the spike sorting method.

To further test the effectiveness of LE feature extraction. The ratio between between-cluster and within-cluster distance (cluster validity) was compared to other features extraction methods employed in this chapter (Figure 2.5). Similarly (Ghanbari et al.,

2009) have tested this ratio their results showed that clusters produced by locality preserving projections were better separated than PCA clusters.

$$Cluster\ Validity = \frac{\min_{i=1,2,\ldots,K, j=i+1,\ldots,K}\left(\left\|CC_i - CC_j\right\|^2\right)}{\frac{1}{N_t}\sum_{i=1}^{K}\sum_{A\in N_i}\left\|A - cc_i\right\|^2} \tag{2.12}$$

Where CC_i is the centre of cluster of spikes produced by neuron N_i, N_t is the total number of spikes, K is the number of neurons simulated in the recording, and $\boldsymbol{A}$ is the feature vector. This cluster validity represents the ratio between the between-cluster and within-cluster distance. Higher cluster validity indicates better separation. As shown in Figure 2.5 the mean cluster validity is higher for LE features compared to the other features employed in the study. The differences in cluster validity between all methods are statistically significant ($p < 0.0001$) as indicated by the Friedman test.

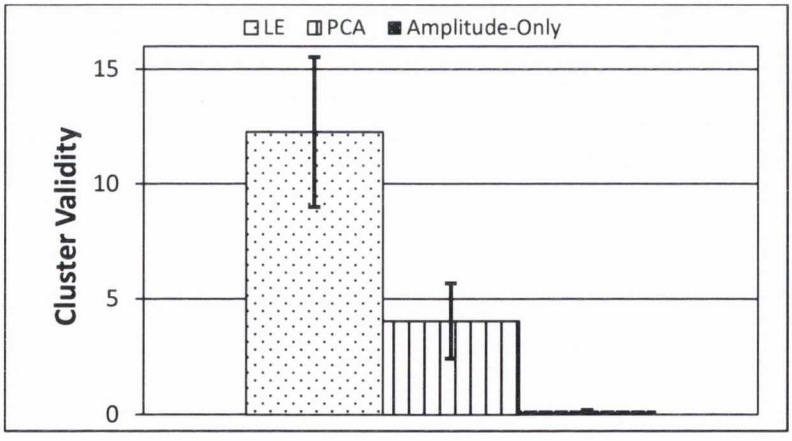

Figure 2.5. Comparison of mean cluster validity index for the feature extraction methods, Vertical lines indicate standard error

Figure 2.6 and Figure 2.7 show the two dimensional feature space for simulated Data set C. Figure 2.6a and Figure 2.7a shows the feature space of the simulated data with three clusters (o , + , .), each point represents the spike produced by the neuron. The markers and colours are used to identify the neuron which the spike belong to. Figure 2.6a shows the PCA feature space and Figure 2.7a shows the feature space

using LE. The separation of the spike clusters is evident in LE feature space on the other hand clusters overlapped in PCA feature space. In some cases, (as shown in Figure 2.7b), over-clustering occurs. The blue cluster (o) in Figure 2.7 is divided into two clusters (o and Δ). The performance of the spike sorting algorithms can be improved by additional step that assess the similarity of the spikes in each cluster and merge the cluster of spikes that belong to a single neuron. Over-clustering is also illustrated in Figure 2.6b.

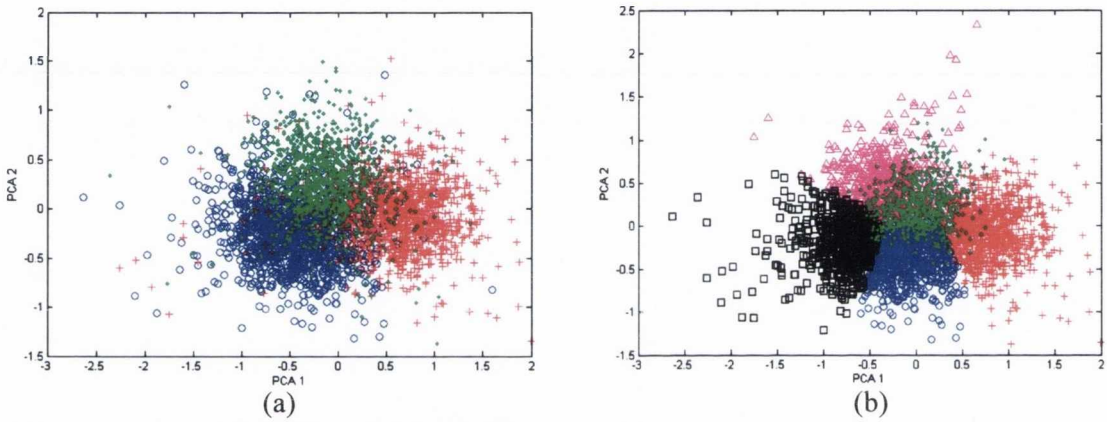

(a) (b)

Figure 2.6. PCA Feature space plots for data set C. Where PCA1 and PCA 2 refers to the first and second principal component respectively (a) PCA feature space of the spikes. (b) PCA feature extraction combined with *k*-means clustering algorithm output where the PBM index has detected five clusters.

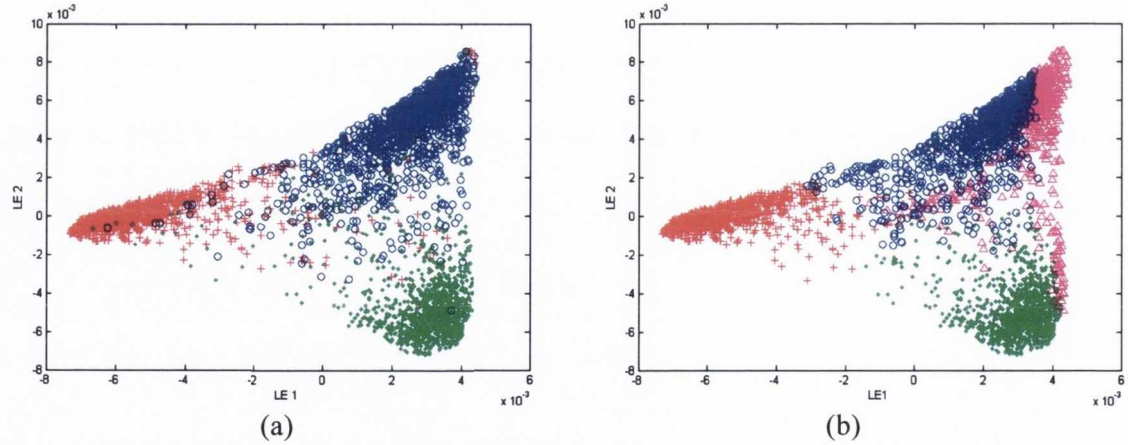

(a) (b)

Figure 2.7. Laplacian eigenmaps feature space plots. Where LE1 and LE2 refer to the first and second eigenvectors (f_1 and f_2) respectively (a) LE feature space of the spikes. (b) LE feature extraction combined with *k*-means clustering algorithm output where the PBM index has detected four clusters.

2.7.3 Spike sorting results using *in-vivo* recordings:

Table 2.3 shows the results obtained from the *in-vivo* recordings. The spike sorting algorithms were initially used to sort data of individual tetrode channels. The last row of the table (multichannel) shows the results obtained when the information is extracted from all three available channels of the tetrode and employed in the sorting algorithms. Features were extracted from each available channel and input to the classifiers. For example, in the PCA feature set the first three components from each channel were computed. Recordings from three channels were available hence the feature space included (3x3 = 9) dimensions.

Table 2.3 *in-vivo* data set results.

Channel	*k*-means classifier						CEM classifier					
	LE features		PCA features		Amplitude-Only features		LE features		PCA features		Amplitude-Only features	
	SA` (%)	SE` (%)	SA` (%)	SE` (%)	SA` (%)	SE` (%)	SA` (%)	SE` (%)	SA` (%)	SE` (%)	SA` (%)	SE` (%)
1	79	32	33	55	79	35	66	55	77	30	61	38
2	98	12	51	8	96	38	74	9	93	12	75	16
3	99	14	51	14	59	37	74	9	96	13	66	18
Multichannel	100	13	74	7	100	35	71	8	82	5	66	5

SA` and SE` refers to the Sorting Accuracy and Sorting Error when the spike sorting algorithm was compared to the experts sorting. The results in Table 2.3 illustrate that the combination of LE features and *k*-means clustering yields best sorting performance. In the combination case most methods yield improved performance this illustrates the advantages of tetrode recording. All the spike sorting algorithms performed relatively poorly while sorting the spikes in the first channel, this is attributed to the low amplitude of the spikes in this channel.

2.8 Discussion:

Recently it was reported that locality preserving projections can aid graphical manual spike sorting (Ghanbari et al., 2009, Ghanbari et al., 2010). In this thesis these findings are extended and propose a fully automated spike sorting algorithm based on LE feature extraction (nonlinear method of locality preserving projection) and *k*-means clustering. The results in Table 2.2 illustrate that there is significant improvement between LE/*k*-means sorting algorithms compared to other automatic sorting algorithms based on PCA and temporal features.

It can be concluded from the results in Table 2.2 that LE provides the best performance in spike sorting when used alongside *k*-means clustering. Table 2.3 shows the results obtained using *in-vivo* recordings confirming the robustness of LE algorithms. The performance difference between CEM and *k*-means algorithms is evident when used with LE features. This is primarily due to over-clustering caused by CEM.

The CEM algorithms implemented in KlustaKwik assume a Gaussian distribution for the features; however, the LE features do not follow a Gaussian distribution. This could explain the ineffectiveness of LE/CEM combination.

The Amplitude-Only feature set yielded the poorest performance with large sorting error percentages as demonstrated in Table 2.1. This may be due to electrode drift or complex-spike cells whilst in other cases, the spikes of two neurons may have similar spike amplitude but different widths. The variation in single neuron amplitude can cause low spike sorting performance. In the case of *in-vivo* recordings results Table 2.3, individual channels yield high sorting error percentages or low sorting

accuracy. However, when the information from multichannel recordings is extracted, the performance of spike sorting using the simple amplitude features increases, thus illustrating the effect of multichannel recording in spike sorting.

The PCA feature set yields an excellent performance with data sets that are easy or contain low noise. However as data sets get nosier or difficult where spikes shapes are separated by small localized features, and in simulation of complex bursts and electrode drift the performance improvement of LE/*k*-means compared to methods based on PCA becomes more evident.

In some cases, (as shown in Figure 2.6b), over-clustering occurs. The performance of the spike sorting algorithms can be improved by an additional step that assess the similarity of the spikes in each cluster and merge the cluster of spikes that belong to a single neuron. A human operated method for merging spike clusters based on autocorrelograms and cross-correlograms is proposed in (Harris et al., 2000). Over-clustering was encountered in (Yang et al., 2009b) and clusters were merged based on boundary density estimation. Over-clustering is a challenge in spike sorting that has to be addressed. A possible solution to over-clustering is to consider the eigengap heuristic (von Luxburg, 2007), where the ratio between successive eigenvalues can indicate the number of clusters in a data set.

It has to be noted that in data sets where a high firing neurons and a sparse firing neurons are recorded the method proposed may not sort spikes of neurons with sparse firing due to its dependence on *k*-means clustering, since *k*-means is shown to produce clusters with approximately uniform sizes (Xiong et al., 2009). This issue can be addressed by using other nonparametric clustering methods such and mean shift

clustering (Comaniciu and Meer, 2002) to improve the sorting performance of the algorithm with sparse firing cells.

Overlapping spikes is one of the important challenges in automated spikes sorting algorithms, several methods have been proposed to address this problem explicitly (Atiya, 1992), this algorithm is criticized for being computationally expensive. Others have proposed solution to this problem which requires less computation power (Lewicki, 1994) however this algorithm is also criticized for underlying assumption of Gaussian noise (Segev et al., 2004). Recently more advancement in field is reported (Takahashi et al., 2003a, Segev et al., 2004, Hulata et al., 2002). The addition of algorithm that will resolve overlapping spikes to current method reported in this study can improve the performance of the proposed spike sorting algorithm.

It has to be noted that this algorithm is designed for offline spike sorting and one of the short-comings of this method is that this method does not allow online spike sorting. However the principles applied in this chapter can be employed, as an initial step of finding spike templates, and implementing template matching for online spike sorting.

2.9 Conclusion:

In this chapter, an automatic spike sorting method is proposed which is capable of spike detection, identifying the number of neurons recorded and assigning each spike to the neuron that produced it. This method yields significantly improved performance compared to previously reported methods based on PCA and Amplitude feature extraction. The method has the limitation of over-clustering in certain cases.

The proposed method is similar in principle to PCA based methods reported in the literature, hence this method can offer a better mechanism of extracting templates in spike sorting algorithms. This also allows for incorporation of algorithms that track non-stationary of spike waveform methods such as (Calabrese and Paninski, 2011).

Simulated data set and *in-vivo* recording were used to assess the performance of the proposed method. The simulated data set employed in this study was obtained from a publically available data, allowing objective comparison of spike sorting method across method compared in this study and others published in the literature.

Chapter 3. Spike waveform variability

3.1 Introduction:

Long-term recording of extracellular potentials, spikes, is an important experimental method in neural engineering and neuroscience research. Understanding the variability of spikes has important implications in many areas such as spike sorting (Fee et al., 1996b) and aiding the design of electrodes for chronic implantation (Linderman et al., 2006).

In the previous chapter a spike sorting method was introduced, the disadvantage of the method was that over clustering occurred. And that the method did not allow online spike sorting.

In this chapter the variability of spike recordings is examined, in terms focusing on noise characteristics and in successive recordings over several sessions. The findings of this chapter can aid future design of template matching and other spike sorting algorithms.

It has been established that the distance between the electrode and the neurons plays an important part in determining the amplitude recorded (Henze et al., 2000). It is also reported that spikes waveform vary (Fee et al., 1996b) within recording sessions. The changes in spike waveform can be attributed to two factors. The first factor is the background neural activity of other neighbouring cells, other neurons are capable of generating currents and this is a source of additive noise to the spike recordings. The

second factor is systematic change in the neuron's spike waveform. An example is seen in the case of spike burst where the spike amplitude decreases with successive spikes in the burst (Fee et al., 1996b).

Fee et al. (1996b) studied the variability of spikes recorded from layers 2/3 through layer 6 of primary somatosensory vibrissa cortex of the rat. They examined the variability within a session in terms of spike waveforms and spectral properties, and reported that spike variability does not follow a stationary Gaussian process. It was reported that half of the neurons recorded exhibited systematic changes as a function of inter-spike intervals.

Lin et al. (2003), studied the stability of neural recording of motor cortex neurons, recorded in the behaving monkey. The recording employed in the study included well isolated cells and spanned over 3 years. It was concluded that stability can last for long periods of time. However the challenge of identifying neurons across successive sessions using the spike waveform was noted.

Williams et al. (1999) implanted electrodes in the auditory cortex of guinea pigs. They examined the stability of one cell over a period of six weeks on a day to day basis. This cell was classified as a "stable unit", meaning that the waveform did not change from day to day, allowing then the cell to be identified across different sessions. Using Principal Component Stability Tube was used to track waveform changes.

Porada et al. (2000) examined the stability of neuron populations from the visual cortex of rabbits and monkeys. Stability was quantified by measuring the range of peak amplitudes, spike shape, spike frequency and the spike train autocorrelation histogram. The ability to record for periods up to 711 days was demonstrated.

However it was difficult to establish whether spikes recorded across different sessions originated from the same neuron.

Santhanam et al. (2007), recorded from motor cortex of a monkey for a period over two days. The stability of spike waveform during this period was examined. Neurons were identified across different 5 minute segment using the spike waveform, neurons with spike waveform that are distinct during the recordings were selected to ensure accurate tracking of waveform changes. Substantial variations up to 30% of the spike waveform were observed.

Suner et al. (2005), studied the variability of spike waveforms over a period of three months, to assess the viability of Bionic array electrode. No attempts were made to determine whether the same neuron was present across different session. Within short period no systematic change in spike amplitudes were observed.

In studying variability of spike waveforms it is difficult to determine if a single cell is recorded over long period of time, hence some studies consider the "stable cells" (Lin et al., 2003, Porada et al., 2000, Williams et al., 1999) where the waveform is distinct and does not fluctuate largely.

To overcome these challenges in this thesis we examined the variability of the spikes, using a novel method of identifying cells across session using the information rather than spike waveform to examine variability within and between recording sessions. Place cell recordings were only included in this study, in order to identify spikes of the neurons across consecutive sessions. The place field of these place cells provides a marker independent of the waveform, allowing objective tracking of waveforms across different sessions.

The main finding of this chapter was reported in:

Chah, E., Hok, V., O'Mara, S. M. & Reilly R. B., A Waveform Independent Cell Identification Method to Study Long-Term Variability of Spike Recordings. *Conference Proceedings of Annual International IEEE EMBS Conference*, Boston, USA. Aug 2011.

3.2 Methods:

3.2.1 Place cells:

Place cells have been first described in the rat hippocampus (O'Keefe and Dostrovsky, 1971). These pyramidal cells emit complex spikes when the animal is in a specific location within a particular environment, and are thought to provide the animal with an internal sense of it's location in space (Moser et al., 2008). Place cell activity can be visually ascertained by plotting the trajectory of the rodent in the environment, and superimposing the spike occurrences (Figure 3.1A). The place field (the location where the cell is active) can be examined in more detail using firing frequency plots (Figure 3.1B). Place cells generally have only one firing field in an environment of this size (Moser et al., 2008).

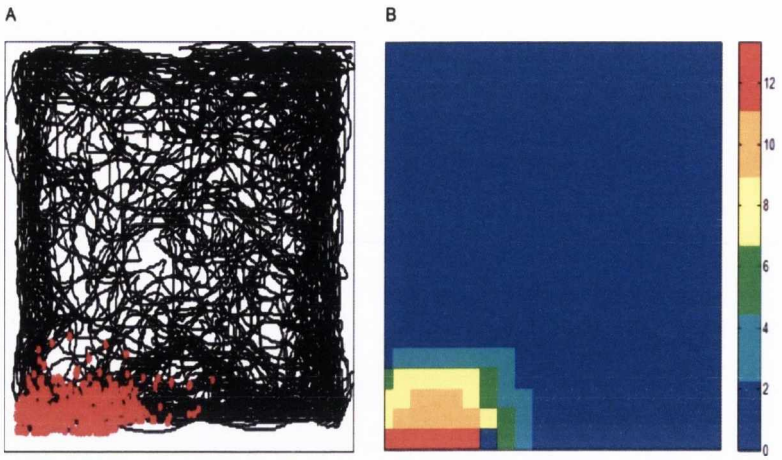

Figure 3.1. Example of a place cell recorded in the hippocampal CA1 subregion (A) black line indicates the trajectory of the animal in the environment (square box) red dots correspond to the location of the animal when the cell fired a spike (B) firing frequency plot of the same place cell; the environment is divided by a set of squares (bins) (3x3 cm) and the number of spikes in each bin is divided by the time spent by the rat in that bin. The firing rate in each bin was smoothed using a 5 X 5 kernel, meaning that the firing rate for each bin was calculated as the average of the 5 X 5 bin square centred on that bin. The six colours of firing-rate maps were autoscaled to represent 20% of the peak rate (red to dark blue).

Objective measures can be used to characterize and identify place cells activity such as the spatial information content (SIC) (Skaggs et al., 1993). This specificity index quantifies the amount of information (in bits) that a single spike conveys about the animal's location. (Markus et al., 1994). The SIC is calculated as follows:

$$SIC = \sum P_i \left(\frac{R_i}{R} \right) \log_2 \left(\frac{R_i}{R} \right) \tag{3.1}$$

Where i is the bin index, P_i is the probability of occupancy of the bin, R_i is the mean firing rate of the cell in bin i, and R is the overall firing rate of the cell during the session.

Spatial coherence is the z-transform of the correlation between the firing rate in each bin and the average firing rate of the eight surrounding bins (Muller and Kubie, 1989). It quantifies the extent to which firing rate in a particular bin is predicted by the average rate of the eight surrounding bins. Thus, high positive values result if the rate for each bin could be better predicted given the firing frequency in its neighbours.

Average firing rate is the total number of spikes emitted during the session divided by the recording duration. The measure insures that low firing cells are not misclassified as place cells due to low sampling.

3.2.2 Subjects:

Male Han Wistar rats (540–650 g) were housed individually in Perspex cages and maintained on a 12:12 h light:dark schedule with lights off at 8 p.m. All experimental procedures (behavioural, electrophysiological, and surgical) fulfilled the EU guidelines on protection of vertebrates used for experimentation (European Community Council Directive 86/609/EEC).

3.2.3 Surgery:

Prior to the beginning of the experiment the rats underwent surgical implantation of drivable microwires for collecting multiple single neurons activity. The recording electrodes consisted of eight bundles of four platinum-iridium wires (90% platinum, 10% iridium; HM-L insulated, 25μm bare wire diameter, California Fine Wire Ltd., California, USA) twisted together. Tetrodes were threaded through a 25 gauge guide cannula, and protected with 21 gauge cover. Tetrodes were then mounted on a lightweight microdrive (Axona Ltd.), cut flat and implanted in the dorsal hippocampus (-3.8 to -4.2 AP, ±3.0 to ±3.6 ML and 1.2 to 1.5 mm dorsoventral to dura). The microdrives used here are built around a precision screw, machined to a pitch of 200 μm, which advances the electrodes in 25 μm steps (1/8th turns). A spring tensions the screw and prevents it from moving spontaneously, therefore allowing recording of the same cell over several days.

3.2.4 Spike recording:

After a one week recovery, animals were connected, via a thirty-two channel headstage (Axona Ltd.) to a recording system which also allowed for animal position tracking. Signals were amplified between 3000 to 12000 and bandpass filtered between 380 Hz and 6 kHz for spike detection. In order to maximize spike separation, only waveforms of sufficient amplitude (at least three times noise threshold) were acquired. Spike waveforms were sampled at 48 kHz, with each spike represented by 50 samples corresponding to ~1ms. Candidate waveforms were then discriminated off-line using graphical cluster-cutting software (TINT, Axona Ltd.), which allows waveform separation based on multiple features. Such features include spike amplitude, spike duration, maximum and minimum spike voltage, and the time of occurrence of maximum and minimum spike voltages. It was also possible for the experimenter to discriminate the waveforms according to the voltage at a specified time. Autocorrelation histograms were built for each unit and the whole unit was removed from analysis if the histogram revealed the existence of correlations within the first 2ms (refractory period), inconsistent with good cell isolation. Similar to others (Fenton et al., 2010, Leutgeb et al., 2007), place cells were selected for study if their spatial firing patterns were location-specific (spatial coherence $\geq$ 0.25; spatial information content $\geq$ 0.5 bits/AP) and robust (average firing rate $\geq$ 0.25Hz).

The recordings took place in a square arena (64 x 64 x 25 cm high) located in the centre of a room with multiple cues available. Rats were food-deprived to 85% of their original weight. Rats were then placed in the open field and 20 mg food pellets were thrown in every 20 seconds to random locations within the open field; in this way, animals were in continuous locomotion, allowing for complete sampling of the environment. Each recording session lasted for 20 minutes.

3.2.5 Within session variation:

Similar to Fee et al. (Fee et al., 1996b), we defined the action potential residuals as the difference between a particular instance of a spike waveform and the average waveform. The distributions of these residues were then compared to normal and *t*-distributions.

Probability plots (Mullins, 2003) were used to determine if either normal or *t*-distributions would fit the residues distributions. This comparison was carried out on each cell recording. Only the channel with the largest amplitude recorded was considered in this analysis, as this electrode is the closest to the neuron and records the maximum voltage deflections.

Figure 3.2 shows an example of spike recording using a tetrode (four channels), one of the channels (largest amplitude) captures the largest voltage deflection.

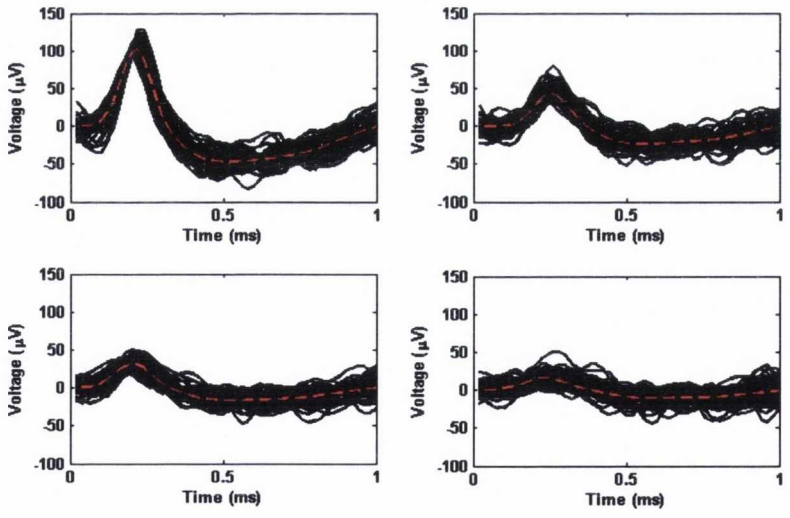

Figure 3.2. Example of spike waveform recorded using a tetrode (four channels), the black solid lines represent the spikes and red dashed line represents the average waveform.

3.2.5.1 Normal distribution:

The normal distribution or Gaussian distribution is a well-known distribution; one of its properties is that the mean and variance are independent of each other. The probability density function of a normal distribution is characterised by the following equation:

$$f(x) = \frac{1}{\sigma\sqrt{2\pi}} e^{\frac{-(x-\mu)^2}{2\sigma^2}} \tag{3.2}$$

Where μ is the mean and σ is the standard deviation. By calculating the two parameters mean and standard deviation the entire distribution can be modelled.

3.2.5.2 t-distribution:

A *t*-distribution has a bell curve similar to the normal distribution however in a *t*-distribution the tails fall with slower rate, in other words the areas under the tails are larger in a *t*-distribution than a normal distribution and its probability density function is represented by:

$$f(x) = \frac{\Gamma\left(\frac{\nu+1}{2}\right)}{\sqrt{\upsilon\pi\sigma^2}\,\Gamma\left(\frac{\nu}{2}\right)}\left(1+\frac{(x-\mu)^2}{\nu\sigma^2}\right)^{-(\nu+1)/2} \tag{3.3}$$

Where υ is the degrees of the freedom, Γ is the gamma function, μ is the mean and σ is the standard deviation. As the degrees of freedom increase the *t*-distribution curve can be approximated by a normal curve (Spiegel et al., 2009).

3.2.6 Between session variations:

Place cells were identified across different sessions using the Pearson correlation coefficient. The coefficient was calculated between the firing frequency plots (as described in Figure 3.1b) between all cells recorded from the same electrode across all

recording sessions. Cells that yielded an average correlation coefficient higher than 0.8, were added to the group and assumed to be the same cell (computed between the cell and the members of the group). Identifying the cells using their place field characteristics, which are independent of the spikes' waveform, this procedure allows for the comparison of spike waveforms across different sessions while guaranteeing the sameness of the neuron being studied. Figure 3.3 shows spatial firing frequency plots of a place cell tracked across several sessions where the average correlation coefficient between the sessions shown is 0.90.

The average amplitude was computed from each cell recording. The amplitude is defined as the peak-to-trough amplitude of the spike. Percentage change of the amplitude was computed and compared between successive sessions. The slope of these changes was also examined to test for systematic slow changes in the amplitude across the entire recording period of individual cells.

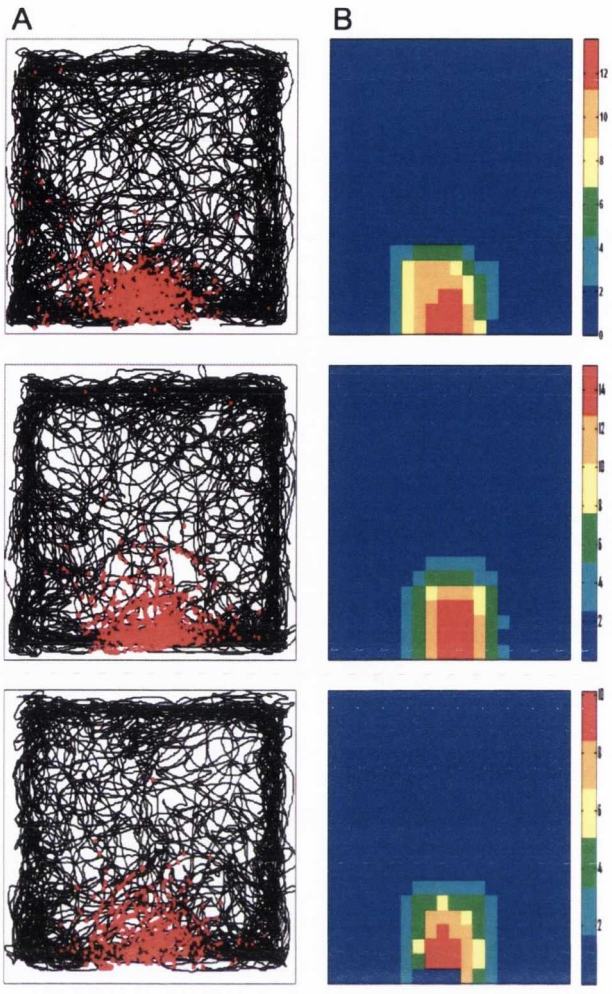

Figure 3.3. Comparing place field of a place cell across three successive sessions, the similarity between the place fields allows for objective and simple identification of the cell across these sessions. The average correlation between the sessions is 0.9.

3.2.7 Cell identification test:

Using the data set recorded in this study, the effectiveness of methods to identify whether two spike waveform recordings originated from a single cell is presented in this chapter. Two methods are proposed, the first is based on inverted wilks' lamda statistics which is has the advantage of being intuitive with normalized values between 0-1, and the second is based on Principal Component Analysis.

The methods were also tested on control conditions, where waveforms of two distinct cells were compared. The control condition was obtained by comparing cells recorded from different rats.

3.2.7.1 Wilks' lambda test:

Wilks' lambda (Johnson and Wichern, 2007) is used as a test to compare several multivariate population means. Consider a data collected at random from g populations.

Where $X_{11}, X_{12}, \ldots\ldots, X_{1n_1}$. are samples from population 1 and population g samples are $X_{g1}, X_{g2}, \ldots\ldots, X_{gn_g}$.

Any observation $\mathbf{x}_{\ell j}$ can be represented by Eq. (3.4).

$$\mathbf{x}_{\ell j} = \bar{\mathbf{x}} + (\bar{\mathbf{x}}_{\ell} - \bar{\mathbf{x}}) + (\mathbf{x}_{\ell j} - \bar{\mathbf{x}}_{\ell}) \tag{3.4}$$

Where $\bar{\mathbf{x}}$ is the overall mean, $\bar{\mathbf{x}}_{\ell}$ is the mean of the population ℓ. The term $(\bar{\mathbf{x}}_{\ell} - \bar{\mathbf{x}})$ represents the estimated method (or treatment) effect and the term $(\mathbf{x}_{\ell j} - \bar{\mathbf{x}}_{\ell})$ represents the error in the estimation.

Eq. (3.4) can be decomposed into a sum of squares Eq. (3.5).

$$\begin{aligned} \sum_{\ell=1}^{g} \sum_{j=1}^{n_\ell} (\mathbf{x}_{\ell j} - \bar{\mathbf{x}}_{\ell})(\mathbf{x}_{\ell j} - \bar{\mathbf{x}})' &= \sum_{\ell=1}^{g} n_\ell (\mathbf{x}_{\ell} - \bar{\mathbf{x}})(\mathbf{x}_{\ell j} - \bar{\mathbf{x}})' \\ + \sum_{\ell=1}^{g} \sum_{\ell=1}^{g} (\mathbf{x}_{\ell j} - \bar{\mathbf{x}}_{\ell})(\mathbf{x}_{\ell j} - \bar{\mathbf{x}}_{\ell})' & \end{aligned} \tag{3.5}$$

Where the first term is the total sum of squares and cross products, second term represents the between sum of squares and the final term is the within sum of squares and cross products.

The wilks' lambda (Λ) is the ratio between the within sum of squares and cross products and the total sum of squares and cross products.

$$\Lambda = \frac{\left| \sum_{\ell=1}^{g} \sum_{\ell=1}^{g} (\mathbf{x}_{\ell j} - \bar{\mathbf{x}}_{\ell})(\mathbf{x}_{\ell j} - \bar{\mathbf{x}}_{\ell})' \right|}{\left| \sum_{\ell=1}^{g} \sum_{j=1}^{n_{\ell}} (\mathbf{x}_{\ell j} - \bar{\mathbf{x}}_{\ell})(\mathbf{x}_{\ell j} - \bar{\mathbf{x}})' \right|} = \frac{|\mathbf{W}|}{|\mathbf{B} + \mathbf{W}|} \tag{3.6}$$

Higher values of wilks' lambda obtained when the between sum of squares and cross products (***B***) is small, hence indicating no difference between the populations. For simplicity in this study inverted wilks' lambda is referred to as $1-\Lambda$ i.e larger values correspond to larger separation and vice versa.

In this chapter wilks' lambda was calculated for spike recordings of two different sessions. The wilks' lambda results were used to assess the applicability of the method to identify if the recordings were from the same neuron.

3.2.7.2 Principal Component Analysis test:

Principal Component Analysis (PCA) is used in data reduction, i.e. the aim of PCA is to find *k* set of linear combinations that explains the maximum variability of the data. PCA is widely used in spike sorting algorithms (Abeles and Goldstein, 1977, Lewicki, 1998). The principal components are calculated by computing the eigenvalues and eigenvectors $\boldsymbol{\lambda}_i$ of the covariance matrix of data ***X***.

$$PC_i = \sum_t \boldsymbol{\lambda}_i(t).\mathbf{X}(t) \tag{3.7}$$

In this study the first three components were calculated, since these components are commonly used in spikes sorting algorithms, and they explain most of the variation within the spikes.

The Euclidian distance ratio of between and within cluster were calculated. This measure was used to assess the usefulness of PCA in identifying the cells across different sessions.

$$PCA\ dist = \frac{\|CC_1 - CC_2\|^2}{\frac{1}{N_t}\sum_{i=1}^{2}\sum_{A\in N_i}\|PC - CC_i\|^2} \tag{3.8}$$

Where CC_1 and CC_2 are the cluster centres, the term $\|CC_1 - CC_2\|^2$ corresponds to the between cluster distance. The denominator represents the average within cluster distance. Where N_t is the total number of spikes, PC is the principal components calculated and CC_i is the cluster centre.

Higher values indicate greater separation between the clusters hence indicating the spikes might originate to two different cells.

3.3 Data sets:

Data set recording were obtained from four rats. A total of 438 cell recordings were included in examining the within session variability in this study. From these recordings a total of 19 cells were identified across different sessions using their respective place fields. The cells were tracked up to a maximum of 46 days. Cells that were tracked for more than four sessions were only included in examination of the between sessions variability.

3.4 Results:

3.4.1 Within session variation:

We examined the distribution of the residues of the spikes recorded from the largest amplitude channel. We found that in 80% of these recording the residues followed a *t*-distribution. By contrast a low percentage (15%) of the cases the residues followed a normal distribution. Figure 3.4 shows two examples of the residues distribution, where

t-distribution can be used to approximate the residues distribution (Figure 3.4A), Figure 3.4C plot shows a rare case where normal distribution can be used to model the residues distribution.

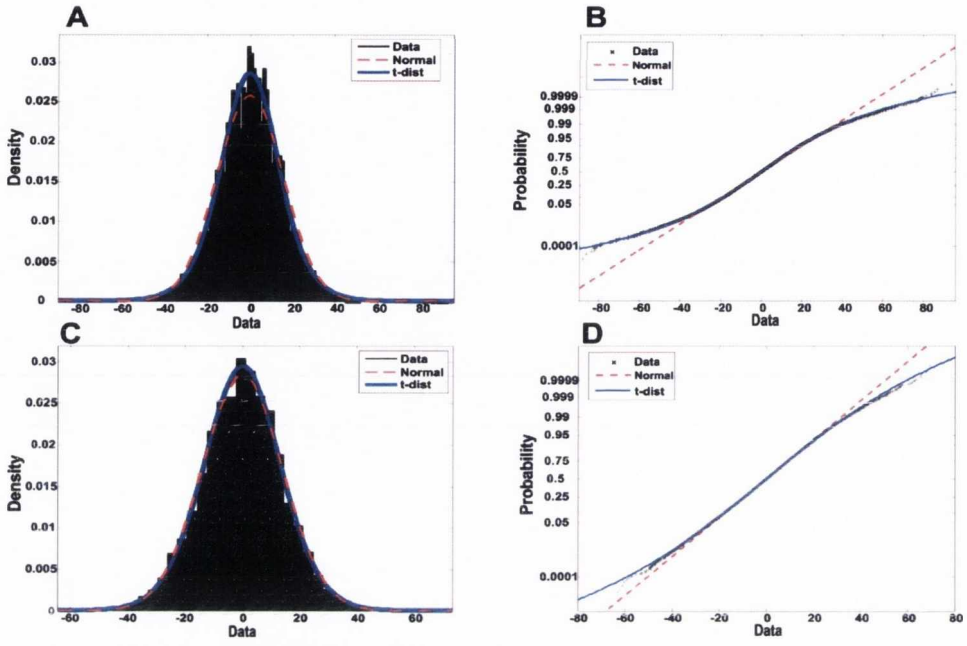

Figure 3.4. Residues distribution within a session. (A) distribution of residues where t-distribution fits the data better than normal distribution, (B) corresponding probability plot(C) rare case where both distribution are similar. (D) Corresponding probability plot for the data represented in C.

3.4.2 Between session variation:

An examination of the average amplitude percentage change, between successive sessions was carried out using the entire cell population in this study. It is evident that the change in amplitude is random varying around zero (Figure 3.5). A *t*-test showed that mean percentage change of the amplitude is not significantly different from zero.

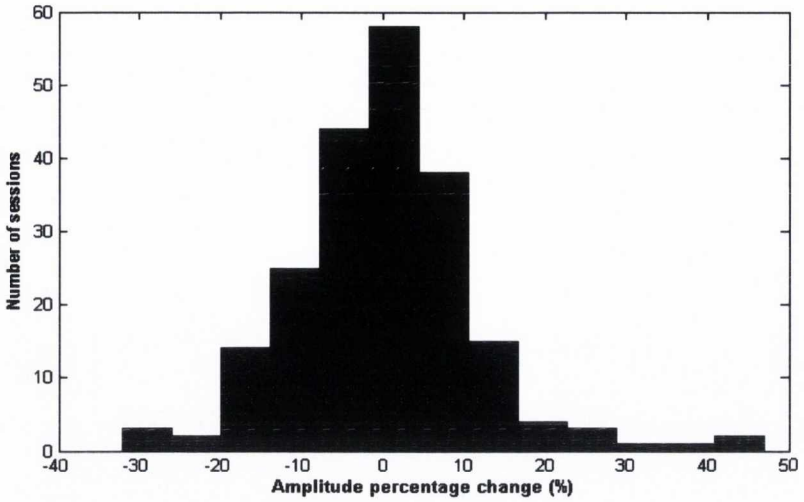

Figure 3.5. Histogram of the average amplitude percentage change between successive sessions for the entire cell population recorded in this study. The average is 0.02 (not significantly different from zero) standard deviation is 11.32. The range of the values is between (-32, 47).

A linear function was fitted to the percentage change of the cells' average amplitude, across all the sessions where the cell was recorded, 15 cells that were tracked for the largest number of session are displayed in Figure 3.6. A line was fitted to the data of each cell so that systematic changes across the entire recording period of the cell can be examined. The fitted line had the following equation:

$$Y = a*(x)+b \tag{3.9}$$

Where a is the slope of the line and b is the initial offset.

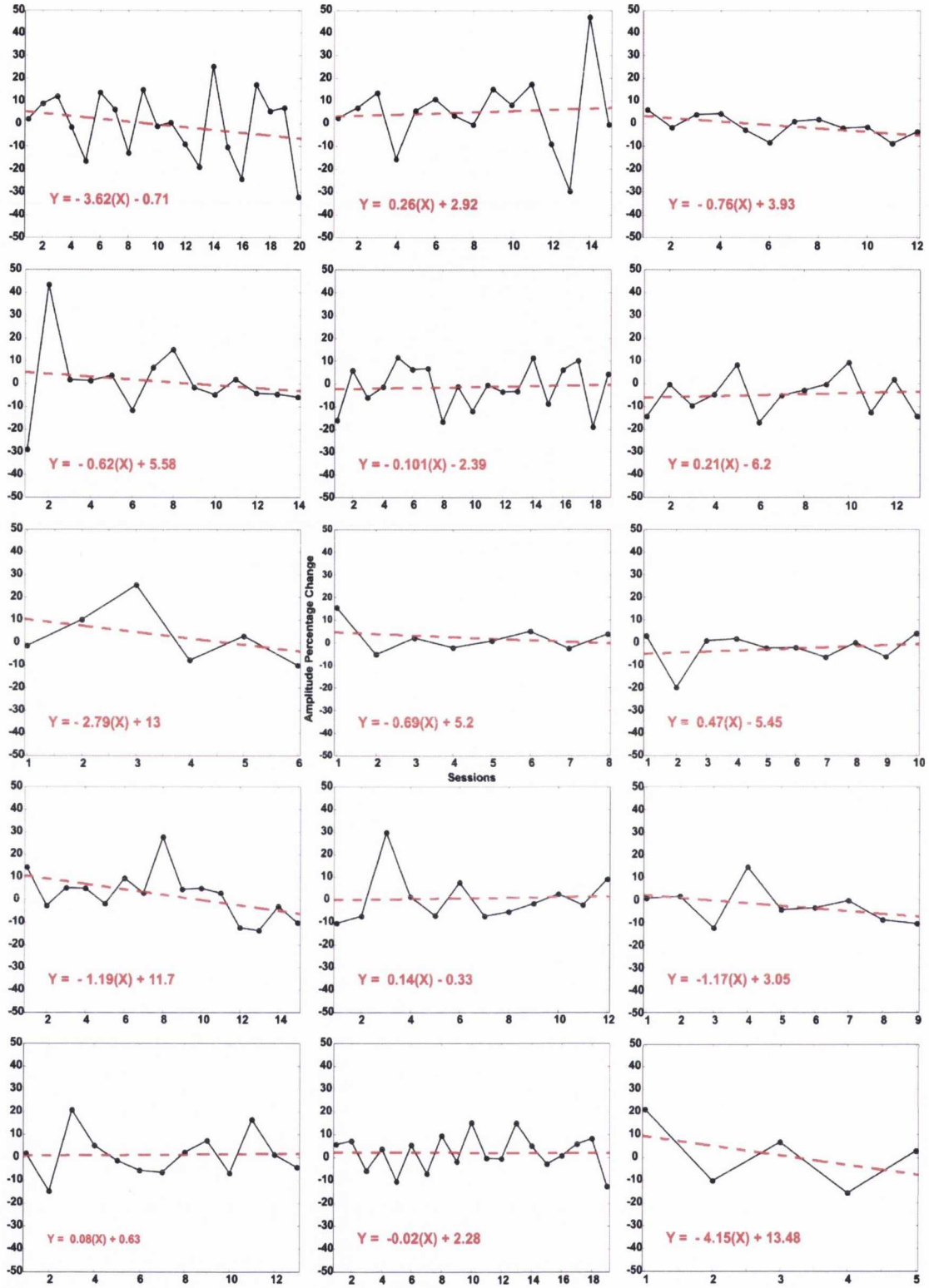

Figure 3.6. Selected cell examples illustrating the percentage change in amplitude. The x-axis represents the number of session where the cell was successfully sorted and identified. y-axis represents the percentage change in amplitude between successive sessions. The solid line represents with circular markers represent the amplitude percentage change between the successive sessions. The dashed line is a linear line fitted through the data, the equation of the lines is displayed within each plot.

By calculating the slope it is possible to quantify the slow changes in average amplitude. The average slope for all cells tracked is -0.98, most of the cells yielded a negative slope indicating that the amplitude change systematically decreased over the longer time periods. However as it can be seen in Figure 3.7 there are exceptions where the cells change in amplitude increased after longer periods or the slope was close to zero.

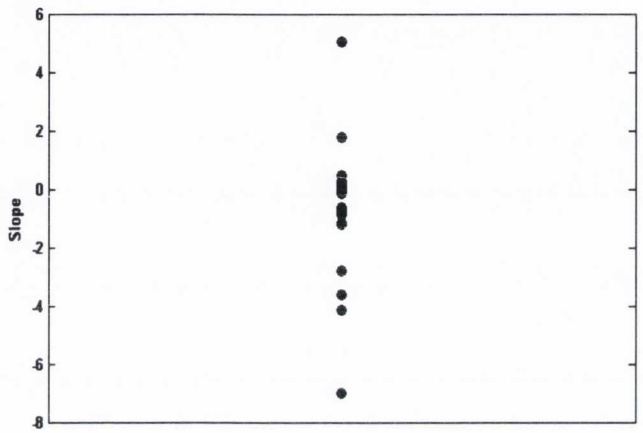

Figure 3.7. Dot plot of the slopes of the lines fitted to the average amplitude change for all the tracked cells across different sessions. Most of these values are close to zero.

3.4.3 Cell identification test:

As described in the methods Wilks' lambda and PCA distance was calculated between successive sessions, to design a test to assess the similarity of spike waveform.

3.4.3.1 Inverted Wilks' lambda:

For each tracked cell Wilks' lambda as described in Eq. (3.6) was calculated between successive recording sessions, and control comparisons. The result is shown in Figure 3.8 where the threshold was varied between 0 and 1. Accuracy indicates that the optimum threshold is 0.41 where sensitivity is 80% and specificity 100%.

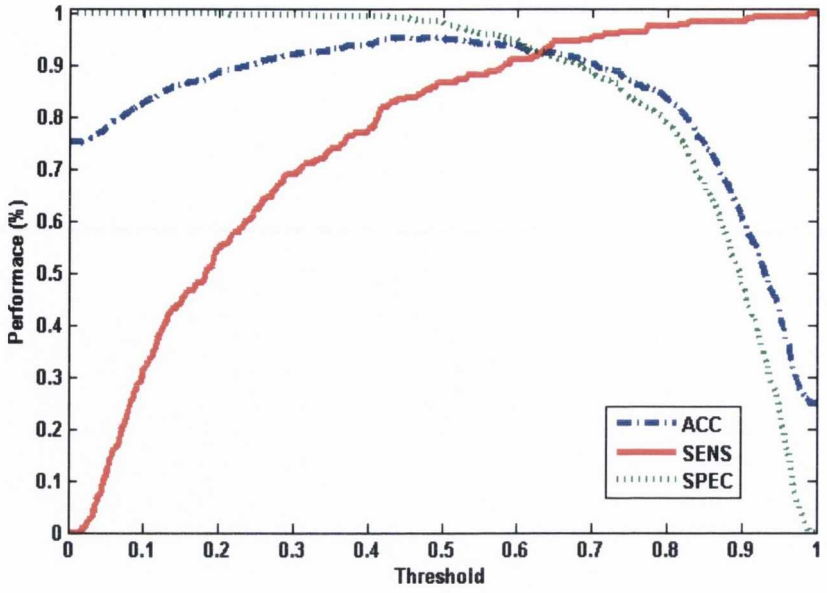

Figure 3.8. Wilks' lambda test performance, the threshold was varied from 0 up to 1.

3.4.3.2 PCA distance

Similarly PCA distance was computed between successive sessions of identical cells. The results are shown in Figure 3.9 where the threshold is varied between 0 and 10. The Accuracy indicates that the optimum threshold would be 0.93, with Sensitivity of 83% and specificity of 97%.

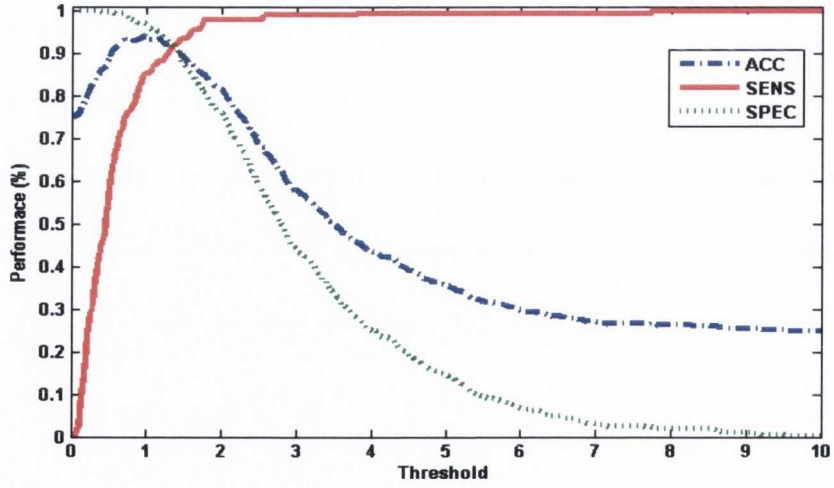

Figure 3.9. PCA performance test when the threshold is varied between 0-10

3.5 Discussion:

In this chapter the variability of spike waveforms between and within sessions were examined. The place field of the place cells was chosen as a marker to identify the cells across successive recording sessions. This criterion is independent of the spike waveform. Hence the results obtained are not affected by large variation in the spike waveform. The results show that the distribution of the residues do not follow a normal distribution in line with previous findings (Fee et al., 1996b).

A *t*-distribution fits the residues in the majority of cases. This could be attributed to the fact that place cells are complex spikes cells and the amplitude of the spikes can vary largely with short inter-spike intervals (Harris et al., 2001), hence the larger areas under the curves compared to what is expected from a normal distribution. The distribution of the residues has important implication for spike sorting analysis as many studies assume a Gaussian variability of spike waveforms.

The results show that amplitude average variation can be up to ~47%. This variation is large and it has important implications for long term neural recording systems. For example, in automatic spike sorting methods it cannot be assumed that spike waveforms are stationary for long periods of time. (Santhanam et al., 2007) recorded, using an accelerometer, rapid head movements along with neural recordings. It was shown that in some cases large amplitude variation of spikes was a result of vigorous head movement. Although in this study surgical procedures were followed to prevent the electrode from moving spontaneously, the possibility of electrode drifts causing large amplitude variations cannot be ruled out. In this study both decrease and increase in amplitude change were observed, indicating that the amplitude change is

not due to deterioration in the electrode. This is expected as the cells were recorded for a maximum of 46 days. It has been reported that "stable recordings" for periods longer than 6 months can be obtained (Lin et al., 2003, Porada et al., 2000), while the recording period in this study is relatively short. There are two possible mechanisms for the slow changes; the first is a slow drift of electrode through the tissue, which explains increase or decrease in average amplitude as the electrode moves closer or further away from the cell body. The second mechanism is the brain tissue response to the electrode where the gliosis pushes the cells away from the electrode (Polikov et al., 2005). The results demonstrate the need for improved electrode implantation procedures to reduce the effects of electrode movements after implantation, and also the need for flexible spike analysis to account for changes in spike waveform. Understanding the long term changes in spike waveform has particular importance in long term studies or in neural prosthesis where signals are acquired over long periods.

While in this chapter it was shown that variability of spike waveform follows a *t*-distribution, it has to be noted that the variability was studied on a small subset of cell types (namely pyramidal cells or place cells). However it cannot be assumed that all neurons have the same waveform variability. The method applied in this chapter can be extended to other types of cells to study if their variability is similar to place cells.

In this chapter variability of spike recordings with large amplitude are examined, since sorting spikes of a large amplitude recording are relatively easier than lower amplitude recordings. It can be expected that the variability to be larger in lower amplitude recordings although in those cases the reliability of spike sorting can suffer and bias the results.

Quian Quiroga (2009) demonstrate that the shape of the spikes can be distorted depending on the filtering procedure, however filtering procedures were not changed during the course of the study hence the effect of filtering should not influence the result reported in this chapter.

In this chapter two methods are proposed to test whether spike recording from two different sessions are generated by the same cell. Both methods yield similar results, this could be due to the fact that most of variation within spike clusters are represented by the first three principal component hence the two method become mathematically equivalent.

The optimum threshold for Wilks' lambda statistics is 0.41 while for the PCA method is 0.93. However these thresholds can be chosen differently depending on the experiment requirement. For example if it is important to exclude false positives then the threshold can be lowered to a value were Specificity is 100% rather than choosing the optimum trade-off between sensitivity and specificity.

While both tests yield similar performance, the Wilks' lambda statistics provides easier interpretation since the value of this statistics can range only from 0-1. This can be used as an objective measure to determine if the same cells are analysed across different sessions.

3.6 Conclusions:

In this chapter of the thesis, the variability of spike waveforms is studied. Understanding the variability is important in terms of spike sorting, and has important implications in studies recording spikes over long periods.

In line with other studies (Fee et al., 1996b) it is shown that the assumption of Gaussian waveform variability is not valid. The results also show that amplitude variability over long period recording can be large, violating the assumption of stationary. Hence spike sorting methods should consider these two factors in their design.

For example (Calabrese and Paninski, 2011), propose a method to account for non-stationary during spike recordings. This algorithm can be incorporated with the method proposed in the previous chapter, to enhance the performance of spike sorting methods during long recording sessions.

Chapter 4. Spike as information

4.1 Introduction:

In the previous chapters of this thesis, methods were proposed for the basic processing of spike information extraction, more attention was given to spike waveform to carry the task of spike sorting, and also the waveform variability of *in-vivo* spike recordings were reported. It has to be noted that the main purpose of spike waveform analysis is to extract the information carried by these spikes through the brain. In fact spike sorting is the first step in the extraction of information from spike recordings. The focus of this chapter is on the subsequent steps after spike sorting which is examining the information carried by these spikes. In chapter 1 a brief overview of information transmitted by these cells are presented namely, place cells, head-direction cells and grid cells which are thought to be important for spatial navigation. In this chapter the spiking properties of head-direction cells are examined in greater detail, specifically the relation between spikes in head-directional cells and theta rhythms are closely studied.

The first evidence that there is a population of cells that integrate head direction and theta oscillation in the thalamic anteroventral nucleus are presented.

Head-direction cells are neurons encoding the animal's directional heading in the horizontal plane, originally it was discovered in the postsubiculum by (Taube et al., 1990), head-directional cells subsequently were found in several other locations

within the brain (Taube, 1995, Mizumori and Williams, 1993, Sargolini et al., 2006) (Figure 4.1). Therefore that head-directional cells is accepted to act as an internal compass providing an innate sense of direction (Knierim et al., 1998).

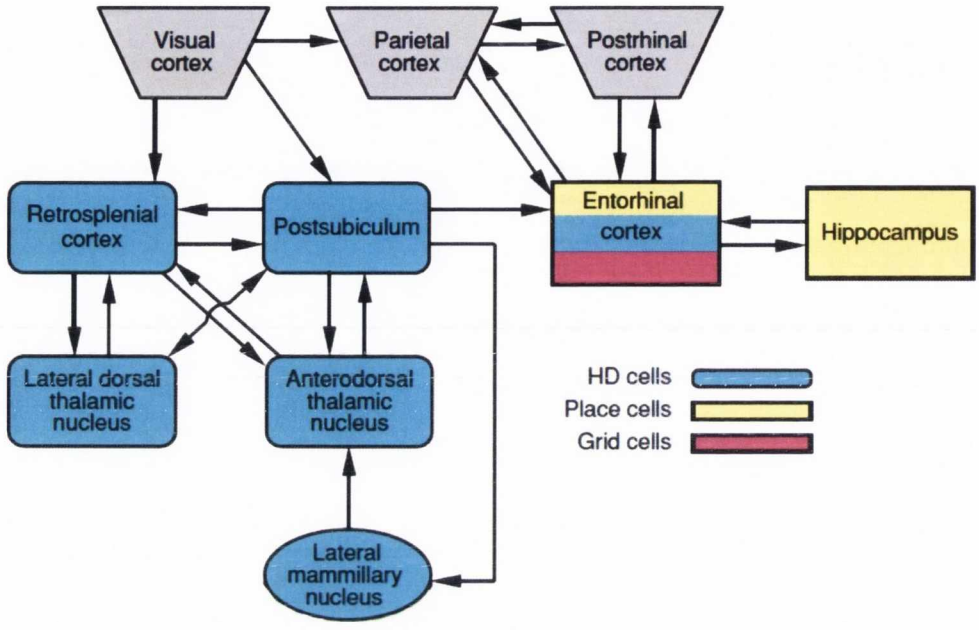

Figure 4.1: Major Regions in the rodent brain involved in the head-direction circuit blue areas indicate regions where head-directional cells have been identified (Taube, 2007).

The firing of these cells is determined by the animal's head direction, and is independent of other factors such as behaviour, location in the environment and trunk position (Taube, 1995). Figure 4.2 shows an example of head-directional cell. With the firing rate that is maximum in the preferred head direction, and as the animal head moves away from this direction the firing rate decreases.

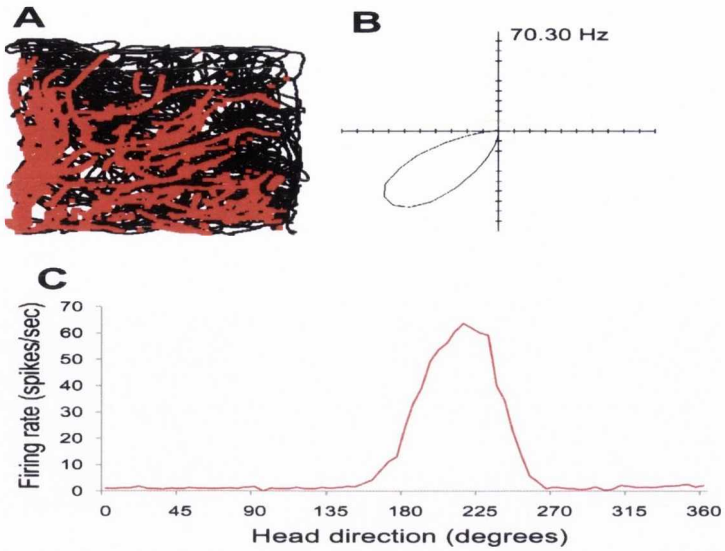

Figure 4.2: Example of head-directional cell. (A) Shows the trajectory of the animal (black line), coloured dots represent the location of the animal when a spike was emitted. (B-C) shows head directional preference of the cell.

Head-direction cells integrate external sensory inputs (visual, auditory and tactile) as well as internal idiothetic (self-motion) signals (Knierim et al., 1998, Goodridge et al., 1998, Zugaro et al., 2000, Kudrimoti et al., 1996). These idiothetic signals are driven by the combination of vestibular and proprioceptive inputs (Stackman and Taube, 1997, Stackman et al., 2003, van der Meer et al., 2007).

The anatomical pathways mediating head-direction signals share remarkably similar connectivity to those mediating theta rhythm (a sinusoidal oscillation of 6 to 12 Hz). Both pathways involve the tegmental nuclei → mammillary bodies → anterior thalamic nuclei → subicular/entorhinal cortices (Swanson and Cowan, 1977, Witter et al., 1990, Van Groen and Wyss, 1995, Gonzalo-Ruiz et al., 1997, Shibata, 1993b, van Groen et al., 1999). Previous studies suggest that the head-direction and theta systems involve parallel subcomponents of this circuitry (Vertes et al., 2004, Vann and Aggleton, 2004). Neurons possessing both theta and head-directional properties have been described at the highest level of this circuitry, namely the pre-/parasubicular

region, where a subset of cells encoding both direction and location with theta firing modulation is reported in those regions (Cacucci et al., 2004, Boccara et al., 2010). The proposal that theta and head-directional processing might converge at an earlier stage is supported by the findings that head-direction cells are present in anteroventral thalamic nucleus (Yoganarasimha et al., 2006), which is known to be the locus of theta oscillations (Vertes et al., 2001). The anterior thalamus has already been shown to integrate angular head velocity and head directionality, this was demonstrated by examining the spiking patterns of anterodorsal thalamic neurons (Blair and Sharp, 1995, Goodridge and Taube, 1997).

This chapter examines the integration of directional and theta-related information in thalamic anteroventral nucleus (AV). It has been reported that AV possess neurons that fire with theta-bursting and theta-modulated patterns (Vertes et al., 2001, Tsanov et al., 2011); suggesting the importance of theta oscillation in information encoding in AV.

Theta rhythm appears to serve a critical role for spatial and nonspatial mnemonic functions of the limbic system (Buzsáki, 2005). Consistent with this view, electrophysiological studies in rats have found that synaptic plasticity occurs between sequentially-activated hippocampal place cells during theta epochs (Mehta et al., 2000, Ekstrom et al., 2001). This line of research illustrates the importance of "limbic theta" cycle in the temporal coding and decoding of neuron populations (Buzsáki, 2002, Skaggs et al., 1996).

Firing pattern can also augment the thalamic responsiveness to sensory processing. Ventrobasal thalamic neurons show rhythmic burst firing to incoming somatosensory stimuli (Fanselow et al., 2001, Swadlow and Gusev, 2001).

This chapter examines the rhythmic modulation of the head-direction thalamic signal. The spiking properties of thalamic anteroventral head-direction cells are analysed and it is found that a population of neurons fire rhythmically at theta frequency. This chapter also shows that theta-bursting cells in AV that display directional modulation. These data further elaborate the interaction of theta and head directional processing within the structures of the hippocampo-diencephalic circuitry (Kocsis and Vertes, 1994, Vertes et al., 2001).

The main finding of this chapter was published:

Tsanov, M., **Chah, E.,** Vann, S. D., Reilly, R. B., Erichsen, J. T., Aggleton, J. P. & O'Mara, S. M. 2011. Theta-modulated head direction cells in the rat anterior thalamus. *J Neurosci,* 31**,** 9489-502.

4.2 Methods:

4.2.1 Surgical implantation of electrodes:

The recording electrodes consisted of eight bundles of four platinum-iridium wires (90% platinum, 10% iridium; HM-L insulated, 25μm bare wire diameter, California Fine Wire Ltd., California, USA) twisted together. Tetrodes were threaded through a 25 gauge guide cannula, and protected with a 21 gauge cover. Tetrodes were then mounted in a small microdrive (Axona Ltd., UK) and implanted in the anteroventral thalamus (-1.5 AP, -1.4 ML and 5.0 mm dorsoventral to dura).

For the cases with parallel hippocampal recordings, a recording electrode was implanted in CA3 subregion (-3.8 AP, -3.0 ML and 3.0 mm dorsoventral to dura). Experiments were conducted in accordance with European Community directive, 86⁄609⁄EC, and the Cruelty to Animals Act, 1876, and followed Bioresources Ethics

Committee, Trinity College, Dublin, Ireland, and international guidelines of good practice.

4.2.2 Neural recording:

After at least one week's recovery, rodents were connected, via a sixteen channel headstage (Axona Ltd.), to a recording system, which also allowed for animal position tracking. Signals were amplified (x 10000 to 30000) and band-pass filtered between 380 Hz and 7 kHz for single-unit detection. To maximize cell separation, only waveforms of sufficient amplitude (at least three times noise threshold) were acquired. Candidate waveforms were discriminated off-line using graphical cluster-cutting software (Axona Ltd.), which allows waveform separation based on multiple features including spike amplitude, spike duration, maximum and minimum spike voltage, and the time of occurrence of maximum and minimum spike voltages. Autocorrelation histograms were calculated for each unit, and the unit was removed from further analysis if the histogram revealed the existence of correlations within the first 2ms (refractory period), inconsistent with good unit isolation. Autocorrelograms were plotted between -1000, 1000 ms, with a bin width of 1 ms.

4.2.3 Recording sessions:

The recordings took place in a square arena (64 x 64 x 25 cm high) situated in the centre of a room with multiple background cues available (surrounding curtains were open). Rats were placed in the open field and 20mg food pellets (TestDiet, Formula 5TUL) were thrown in every 20 sec to random locations within the open field; in this way, animals locomoted continuously, allowing for complete sampling of the environment. The duration of each experimental session was 16 min, allowing the recording of the local field signal with predominant theta periods.

4.2.4 Criteria for data inclusion:

Cells were selected on the basis of their directional properties, rhythmicity of their firing, and spike isolation.

A total 226 well-isolated units were identified within the anterior thalamic nuclei from 12 male (250-350g) Lister-Hooded rats (Harlan, UK). Based on electrophysiological and post-mortem histological criteria, it was estimated that 135 of these units were from anteroventral nucleus (AV), while 91 were from anterodorsal nucleus (AD).

For a cell to be classified as head direction-by-theta (HD-by-theta), it had to meet the following criteria:

1. Peak rate in the directional field exceeding 1 Hz.
2. Peak firing rate (preferred direction) ≥30% higher than the non-preferred (background) firing rate.
3. The value of the autocorrelogram calculated theta index > 0.01.

Only units that fired a sufficient number of spikes for the duration of the 16 min recording sessions to allow the theta index analysis (see below) were included.

Besides the head-direction and HD-by-theta cells we also analysed a population of thalamic theta cells. Thalamic units were classified as theta cells based on their phase locking to local theta oscillations, their bursting firing properties and their spike shape (Christian and Deadwyler, 1986).

A theta unit was defined as a directional theta cell if the peak firing rate was ≥30% higher than the non-preferred firing rate. The non-preferred firing rate represents the unit's activity when the animal is facing the non-preferred heading direction of the unit.

Theta cells were defined as fast spiking for units with average firing rate >30Hz, while the slow spiking units' average firing rate was ≤30Hz.

4.2.5 Theta index calculations:

A sine wave with decaying amplitude was fitted to the autocorrelograms Eq. (4.1) (Royer et al., 2010):

$$[a(\sin(\frac{\pi}{2} - \omega t)) + b].e^{\frac{-|t|}{\tau_1}} + ce^{\frac{-t^2}{\tau_2}} \quad (4.1)$$

Where t refers to time and a, b, c, τ_1, τ_2 and ω are the fit parameters. Initially the parameters were estimated by smoothing the autocorrelgram and the peaks and troughs of the oscillation is estimated, these values are used to estimate a, b, τ_1, ω. Then the initial estimations are used as initial guess for the least squares fitting method and fit parameters are estimated more accurately.

The theta index is defined as the ratio of the fitted parameters, a/b, where a is amplitude of oscillation and b is the offset of the oscillation. Only autocorrelograms for all spikes with values of the theta index higher than zero were analysed, excluding the units with low firing rates.

4.2.6 Head-direction analysis:

Directional analyses were only performed for experiments with two LEDs (for all head-direction cells in anterodorsal and anteroventral thalamic nuclei, 101 units in total). The rat's head direction was calculated for each tracker sample from the projection of the relative position of the two LEDs onto the horizontal plane. The directional tuning function for each cell was obtained by plotting the firing rate as a function of the rat's directional heading, divided into bins of 5 degrees. Similar to others the firing rate was computed based on the total number of spikes divided by the

total time in that bin (Taube et al., 1990). To restrict the influence of inhomogeneous sampling on directional tuning, only recordings sampling all directional bins by the rat were included.

The directionality of the HD units in the horizontal plane (measured in degrees) was normalized for comparison of the HD firing rate properties. The peak firing rate of cells that respond to different direction of heading was aligned to a head-direction of 180° (Bassett et al., 2005). The firing rate was normalized (with values between 0 and 1) with respect to the peak firing rate for each unit (Bassett et al., 2005).

4.2.7 Gaussian function:

The Gaussian function or the Gaussian distribution is described mathematically by Eq. (4.2):

$$f(x) = \frac{G}{\sigma\sqrt{2\pi}} e^{\frac{-(x-\mu)^2}{2\sigma^2}} \tag{4.2}$$

Where G represents the peak of the curve, μ is the mean and σ is the standard deviation. The Gaussian distribution has the property that the majority of values 68% fall between ±σ (standard deviation) away from the mean.

4.2.8 Directional and locational information content:

The recording environment was divided into set boxes of (3cm x 3cm). Firing maps were calculated by dividing the number of spikes which occurred in each box by the total trial time the animal spent in that box (Cacucci et al., 2004). This produced maps showing the firing of cells (Hz) with respect to the location of the rodent.

To correct sampling bias and to quantify the influence of location on head-direction cells, the maximum likelihood model (MLM) analyses (Cacucci et al., 2004) were

employed. After the MLM correction, we calculated the locational and directional information (Skaggs et al., 1993):

$$I = \sum p_j \frac{\lambda_j}{\lambda} \log_2 \left(\frac{\lambda_j}{\lambda} \right) \tag{4.3}$$

Where I refers to Information content, p_j is the probability of the rat occupying bin j, λ_j is the average firing rate in bin j, and λ is the average firing rate of the cell.

4.2.9 Distributive ratio analyses:

To overcome the problems of sampling bias, The "distributive hypothesis" method was also included in the analysis (Muller et al., 1994, Cacucci et al., 2004). Similar to the MLM correction, the distributive hypothesis procedure was applied to quantify the influence of head direction on the spatial firing. The calculation of locational distributive ratio is based on the estimation of directional firing that one would predict under the null hypothesis that a cell's firing is only modulated by location and that the only influence of head direction arises from the sampling bias discussed above. The predicted rate as a function of direction is as follows:

$$R_{pred}(\theta) = \frac{\sum (R_p T_p(\theta))}{\sum T_p(\theta)} \tag{4.4}$$

Where R_P is the firing rate in one pixel and $T_P(\theta)$ is the time spent facing head-direction θ in that pixel. Then this tests whether the observed directional tuning for the cell, $R_{Obs}(\theta)$, differs from the one calculated under the assumption that the effect of direction is purely artificial, $R_{Pred}(\theta)$. This is achieved by computing a "distributive ratio" (DR) as follows:

$$DR = \sum \left| \frac{\ln((1 + R_{Obs}))}{((1 + R_{Pred}(\theta)} \right| \Big/ N \qquad (4.5)$$

Where N is the number of directional bins considered. For a perfect prediction, DR is zero. A perfect prediction indicates that the null hypothesis is true, namely place-cell firing is only modulated by location and the directional influence on place-cell firing is only attributable to the inhomogeneity of sampling referred to above, whereas high values of this ratio would indicate a poor prediction (indicating that head direction accounts for some of the variability in the firing rate of the cell).

4.2.10 Definition of compact spike trains:

For HD-by theta units, the trains included three or more spikes with inter-spike interval of 10 ms and 15-250 ms pause, preceding the first spike of the train.

The burst mode was defined with maximal ISI interval of 4 ms to the preceding spike (Ramcharan et al., 2005).

4.2.11 Inter-spike interval analysis:

The inter-spike (ISI) scatter plot, each dot on the scatter plots a spike where the time interval of the spike to the preceding one is on the (x-axis) and the time interval of the spike to the following one is on the (y-axis). The inter-spike (ISI) ratio represents the ratio between the number of spikes from the largest cluster marked with red on the ISI plots and the summation of spikes in the second and third largest clusters in the ISI scatter plot (marked in green/blue on the ISI plots) Figure 4.8.

Mean shift clustering was used to cluster the spikes in the ISI scatter plots. The principle of this clustering method is that assuming the feature space can be modelled by a probability density function then dense regions (local maxima) correspond to

cluster centres, using mean shift procedure points in the feature space that converge onto the same local maxima are assumed to belong to the same cluster. Mean shift clustering allows the locating of the maxima of a density function given, discrete data sampled from that function (Cheng, 1995). This function determines the weight of nearby points for re-estimation of the mean. Mean shift clustering is a non-parametric clustering method that does not require prior knowledge of the number of clusters and it will produce arbitrarily-shaped clusters that depend upon the topology of the data (Comaniciu and Meer, 2002). This clustering method was employed in this study since no prior assumptions are necessary for the clustering procedure.

The mean shift clustering procedure (Comaniciu and Meer, 2002) is as follows given n data points $\boldsymbol{x}_i$, for i values $(1,...n)$, in the d-dimensional space R^d (in this case $d = 2$), the multivariate kernel density estimate for the kernel $K(x)$ is then given by Eq. (4.6).

$$f(x) = \frac{1}{nh^d} \sum_{i=1}^{n} K\left(\frac{\mathbf{x} - \mathbf{x_i}}{h} \right) \tag{4.6}$$

h is the bandwidth ($h = 0.2$). Assuming that the kernel $K(x)$ (in this chapter a flat kernel was employed) is symmetric, it integrates to 1 and satisfies Eq. (4.7).

$$K(\mathbf{x}) = c_{k,d} k\left(\|\mathbf{x}\|^2 \right) \tag{4.7}$$

Where the $k(\boldsymbol{x})$ is the "profile kernel" and $c_{k,d}$ is the positive normalization constant which insures $K(\boldsymbol{x})$ integrate to one.

Using Eq. (4.7) to write Eq. (4.6) the following equation is obtained:

$$f(x) = \frac{c_{k,d}}{nh^d} \sum_{i=1}^{n} k\left(\left\| \frac{\mathbf{x} - \mathbf{x}_i}{h} \right\|^2 \right) \tag{4.8}$$

The first step is then to find modes of the density; these modes are located at the zeros of the gradient i.e. $\nabla f(x) = 0$.

Using the linearity of the previous equation the gradient can be written as:

$$\nabla f(x) = \frac{2c_{k,d}}{nh^{d+2}} \sum_{i=1}^{n} (\mathbf{x_i} - \mathbf{x}) g\left(\left\| \frac{\mathbf{x} - \mathbf{x_i}}{h} \right\|^2 \right) \tag{4.9}$$

$$\nabla f(x) = \frac{2c_{k,d}}{nh^{d+2}} \left[\sum_{i=1}^{n} g\left(\left\| \frac{\mathbf{x} - \mathbf{x_i}}{h} \right\|^2 \right) \right] \left[\frac{\sum_{i=1}^{n} \mathbf{x}_i g\left(\left\| \frac{\mathbf{x} - \mathbf{x_i}}{h} \right\|^2 \right)}{\sum_{i=1}^{n} g\left(\left\| \frac{\mathbf{x} - \mathbf{x_i}}{h} \right\|^2 \right)} - \mathbf{x} \right] \tag{4.10}$$

Where the $g(x) = -k`(x)$. Similar to $k(x)$ the $g(x)$ is the profile kernel of $G(x)$.

$$G(x) = c_{g,d} k\left(\|\mathbf{x}\|^2 \right) \tag{4.11}$$

The first term in Eq. (4.10) is proportional to the density estimate at $\boldsymbol{x}$, while the second term is the mean shift $\boldsymbol{m}$. in other terms it represents the difference between the weighted mean, using kernel G for weights, and $\boldsymbol{x}$ the centre of the kernel window. Hence it always moves towards the direction of maximum density.

$$\mathbf{m}(x) = \left[\frac{\sum_{i=1}^{n} \mathbf{x}_i g\left(\left\| \frac{\mathbf{x} - \mathbf{x_i}}{h} \right\|^2 \right)}{\sum_{i=1}^{n} g\left(\left\| \frac{\mathbf{x} - \mathbf{x_i}}{h} \right\|^2 \right)} - \mathbf{x} \right] \tag{4.12}$$

Finally the mean shift procedure is calculated by successive computation of shift vector $\boldsymbol{m(x)}$, and translation of the kernel window $G(\boldsymbol{x})$ by $\boldsymbol{m(x)}$ until a stationary point is reached.

4.2.12 Measurement of local field activity:

The local field potential (LFP) was sampled at 250 Hz and stored for further off-line analysis. LFP signal frequency analysis was carried, where the power was calculated using the short-time Fourier transform of the signal (hanning window of 2s, with overlap of 1 s) and interpolated into colour-coded power spectrograms. Information was displayed as the magnitude of the time-dependent Fourier transform versus time in a colour gradient graph with the maximum corresponding to 0 Db. The LFP from 32 channels (8 tetrodes), in AV was correlated to the LFP of two channels in CA3 of five rats. Three recording sessions with duration of 16 min each were conducted for five animals.

4.2.13 Cross-spectral analyses:

The coherence between sniff and hippocampal LFP was calculated using NeuroSpec (Halliday et al., 1995). The coherence uses a method of disjoint sections, where the recording (R) is divided in to L non-overlapping epochs each of time length T, where $R=LT$. For the segmented signal $\boldsymbol{x}$ Discrete Fourier Transforms is used to estimate the auto-spectrums of the signals $f_{xx}(\lambda)$, where λ is a particular frequency. The linear relations (coherence) between signals $\boldsymbol{x}$ and $\boldsymbol{y}$ is R_{xy} is then estimated using auto and cross spectra's.

$$\left|R_{xy}(\lambda)\right|^2 = \frac{\left|f_{xy}(\lambda)\right|^2}{f_{xx}(\lambda) f_{yy}(\lambda)} \tag{4.13}$$

The significance of the coherence was determined as in (Halliday et al., 1995):

$$1-(0.05)^{\frac{1}{L-1}} \tag{4.14}$$

4.2.14 Sniffing and theta cells:

It is reported that odour discrimination is depended on sniffing at frequencies of 6-9 Hz, anticipation of reward was associated with sniffing at frequency of 9-12Hz (Kepecs et al., 2007). Similar to frequency band of theta oscillations. Hence in this chapter the potential relation between theta cells and sniffing was investigated.

4.2.14.1 Measuring the sniffing activity:

Similar to (Kepecs et al., 2007) a thermocouple was implanted in the nasal passage through the nasal bone (Figure 4.3) of the rodents to measure the sniffing activity during the recording sessions.

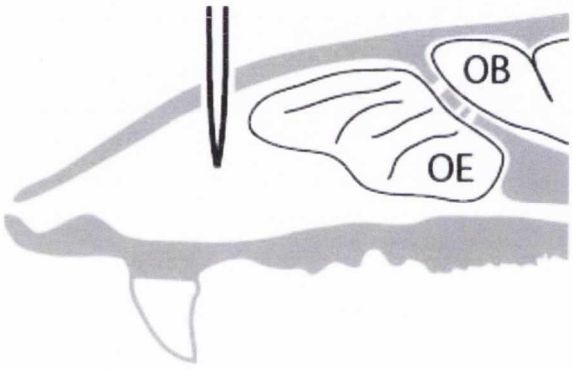

Figure 4.3: schematic of thermocouple placement in the nasal passage (Kepecs et al., 2007)

The electrical noise was large hence a second method of measuring sniffing was adopted (Verhagen et al., 2007), where a hollow metal cylinder was implanted in the nasal passage to allow passage of air through the cylinder. A plastic tube was attached to metal cylinder and connected to a pressure sensor (24PCAFA6G, Honeywell, Morristown, NJ). The output of the pressure sensor was connected to a differential amplifier with a gain of 10 and the sniffing signal was sampled at 250Hz.

4.2.14.2 Sniffing phase and theta firing cells:

To measure if the firing of the cells occurs at specific period of sniffing cycle, each sniffing cycle was modelled as a sinusoidal wave; first the sniffing signal was up sampled to 1 kHz in order to achieve better phase resolution. The peaks were then detected by estimating the gradient, the peaks then correspond to locations where the gradient switches from positive to negative. Each sniffing cycle was considered as the period between two successive peaks, where the phase of the peak was considered as zero. The best fit cosine was then found for each cycle using least square fit (an example is shown Figure 4.4A).

For each spike of the theta cell, the phase of the sniffing cycling corresponding to the time of the spike was obtained. Polar plots displaying the frequency of the spikes versus phase of the sniffing cycle were used to determine, if the firing of these cells occur at specific phase.

4.2.14.3 Similarity measure between Silent periods and sniffing cycle:

The spike similarity measure proposed by (Lyttle and Fellous, 2011) was modified to suit analysing continuous and a point processes.

First the sniffing signal was transformed as described in the previous in series of cosine waves, and the entire signal was presented by their phase. This transforms the signal from a cosine waveform to series of "triangular waves" (Figure 4.4A (bottom)). Similarly the spikes timing can be transformed in a series of triangular waves (Figure 4.4B (bottom)). Assuming a spike train with timings $\boldsymbol{d} = d_1, d_2, \ldots\ldots d_n$ Where n is the number of spikes detected for the cell during the recording.

The transformation *f(t)* is then:

$$f(t) = \begin{cases} 0 & for \quad t \in [d_i, d_i + \tau) \\ t - (d_i + \tau) & for \quad t \in [x_i + \tau, x_{i+1}) \end{cases} \tag{4.15}$$

Where τ was selected to 10 ms, this insures spike trains are considered as one event. Finally the Pearson correlation can be calculated between both signals at time lags to determine the silence and sniffing cycle relationship. Where a value of one indicated perfect relationship between the two signals, as the time lag between signals increase, it is expected that a true correlation would decease, since the signals are not synchronised at longer time delays.

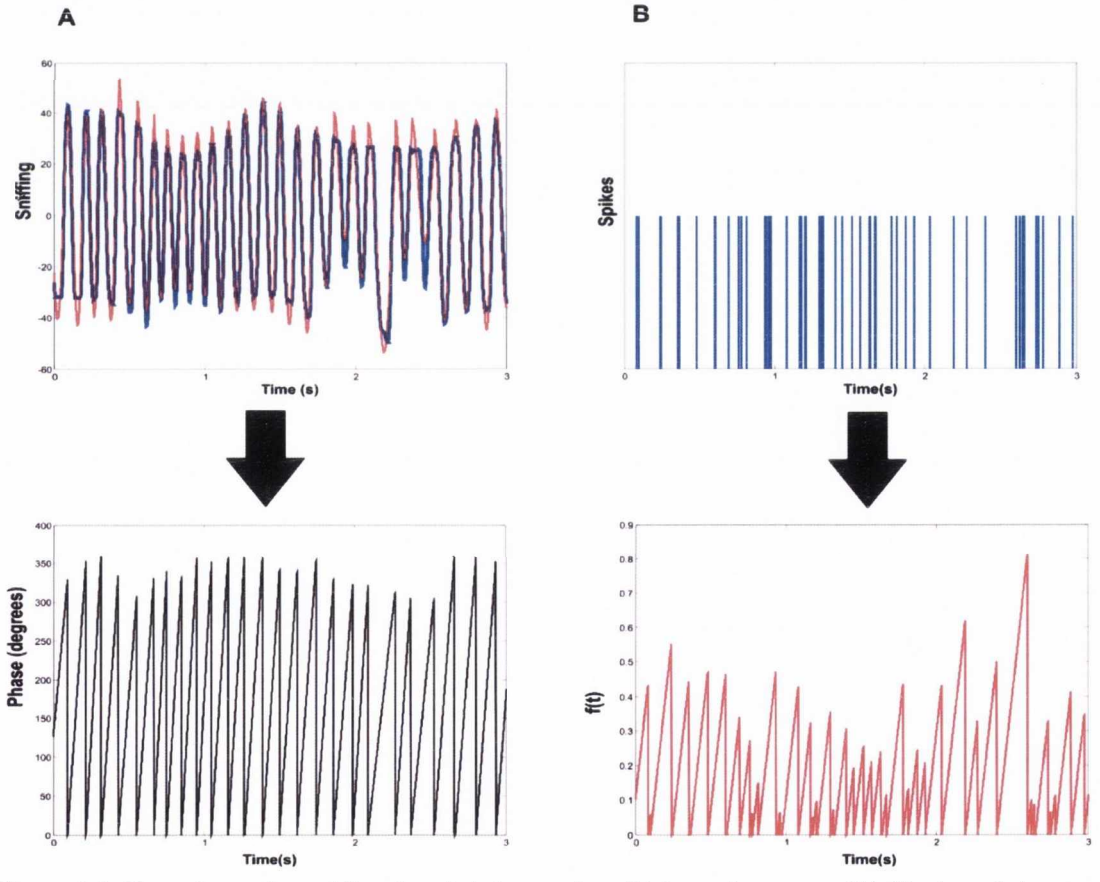

Figure 4.4: Transformation of the signals into a series of triangular waves (A) (first row) An snap shot of sniffing activity (blue) and the fitted cosine waves (red) (second row) transformed signal . (B) Spiking activity of theta cells (up), and the transformation in continuous signal (bottom).

4.2.15 Post-mortem verification of electrode site:

Rat brains were removed for histological verification of electrode localization, at the end of recordings session. The animals underwent transcardial perfusion with 0.1 M PBS followed by 10% formol-saline. The brains were postfixed in 10% formol-saline and then transferred to 25% sucrose overnight. Brain sections (16 μm) were Nissl-stained, using 1% toluidine blue, and examined using brightfield microscopy.

4.2.16 Statistical Analysis:

All data were analysed using Prism software (GraphPad Software, Inc, La Jolla, CA). Statistical significance was estimated by using two-tailed *t*-test and two-way analysis of variance (ANOVA) paired with *post hoc* Newman–Keuls test. The probability level interpreted as statistically significant was $p < 0.05$. All data points are plotted ± sem.

4.3 Results:

4.3.1 Histological and electrophysiological identification of thalamic units:

High-frequency current lesions were induced through the electrodes that recorded theta-modulated head-direction cells, to determine the exact location of our electrode tips among the nuclei of the anterior thalamus (Figure 4.5A). A total of 226 well-isolated units were recorded from anteroventral (AV) and anterodorsal (AD) nuclei in 12 rats. All recordings were made during pellet-chasing in a square arena. On the basis of the histological verification, 135 cells from nine rats were assigned to AV (Figure 4.5B) and 91 cells from eight rats to AD (Figure 4.5C). The recording positions in anteroventral nucleus were distributed predominantly in its medial compartment (Figure 4.5).

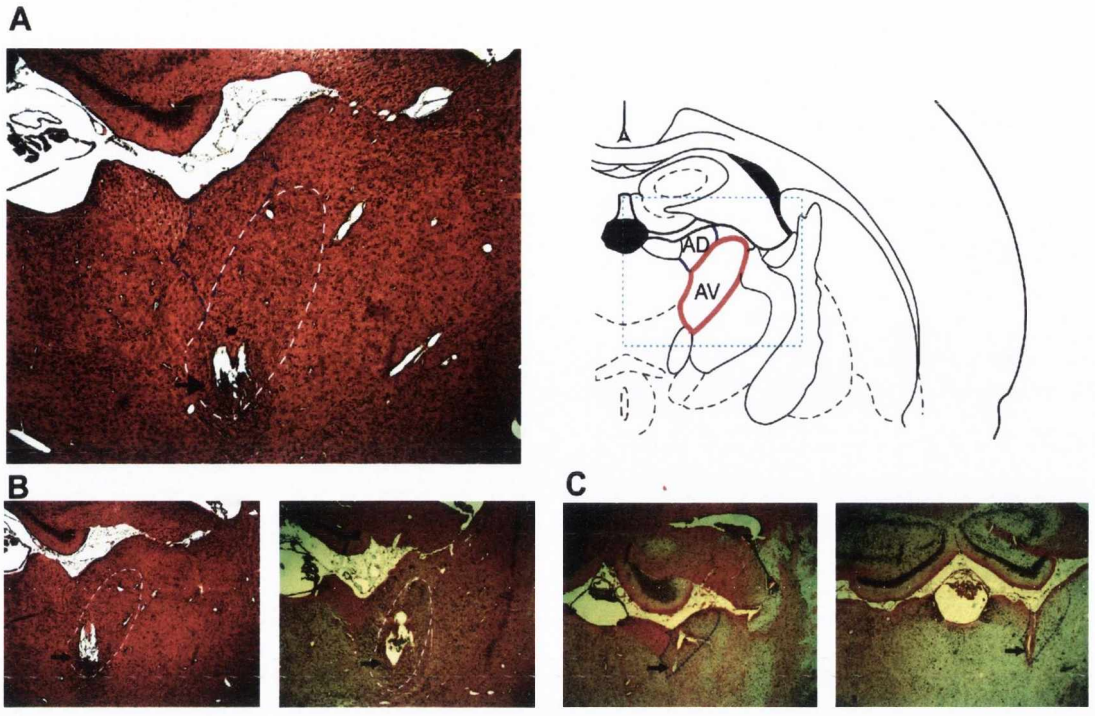

Figure 4.5: Anatomical location and electrophysiological detection of anteroventral units. (A) Coronal brain section from a rat where eight chronically-implanted tetrodes targeted the anteroventral nucleus (AV, indicated with dashed white line). The black arrow indicates the tip of the tetrodes. The dashed blue line indicates the adjacent anterodorsal nucleus (AD). Atlas schematic (right) shows rat anteroventral nucleus location (highlighted with red line). The dashed blue rectangle denotes the extent of the histological section on left. (B) coronal brain sections from two rats with chronically implanted tetrodes in AV (white line). High-frequency current was applied at the level of HD-by-theta units' identification. (C) coronal brain sections from two rats with chronically implanted tetrodes in AD (blue line).

To achieve maximum isolation of the extracellular signal, tetrode electrodes were used, which allowed clear identification of thalamic units (McNaughton et al., 1983, Gray et al., 1995). Head-direction (HD) cells are characterized by a tuning curve (Taube et al., 1990), where the firing rate is represented on the y-axis and the animal's head direction represented on the x-axis. Head directionality can be depicted using polar plots (Knierim et al., 1995), where HD-by-theta cells (Figure 4.6A) reveal similar to the putative HD cells directionality (Figure 4.6B). The average firing rate (33.5 ± 1.66 Hz) and maximal firing rate (109.3 ± 7.43 Hz) of HD-by-theta units (n = 36) were comparable to the average (31.5 ± 1.55 Hz) and maximal (98.7 ± 5.9 Hz) firing rates of the HD units (n = 101), respectively (Table 4.1). The mean spike

amplitude (261.9 ± 22.6 μV) and spike width (189.5 ± 22.6 μs) of the HD-by-theta spikes (Figure 4.6C) showed similar values to the mean spike amplitude (251.1 ± 12.1 μV) and spike width (174.2 ± 6.5 μs) of the HD spikes, respectively (Figure 4.6D).

Table 4.1: Electrophysiological classification of thalamic units with head directional properties.

Cell types	Head-direction	Head-direction-by-theta	Directional theta
n	101	36	10
Mean spike width (μs)	174.2 ± 6.5	189.5 ± 22.6	186.1 ± 16.0
Average frequency (Hz)	31.5 ± 1.5	33.5 ± 1.6	26.8 ± 1.7
Maximal frequency (Hz)	98.7 ± 5.9	109.3 ± 7.4	133.7 ± 13.1
Theta index all spikes	0.0017 ± 0.0002	0.0217 ± 0.0004	0. 274 ± 0.0551

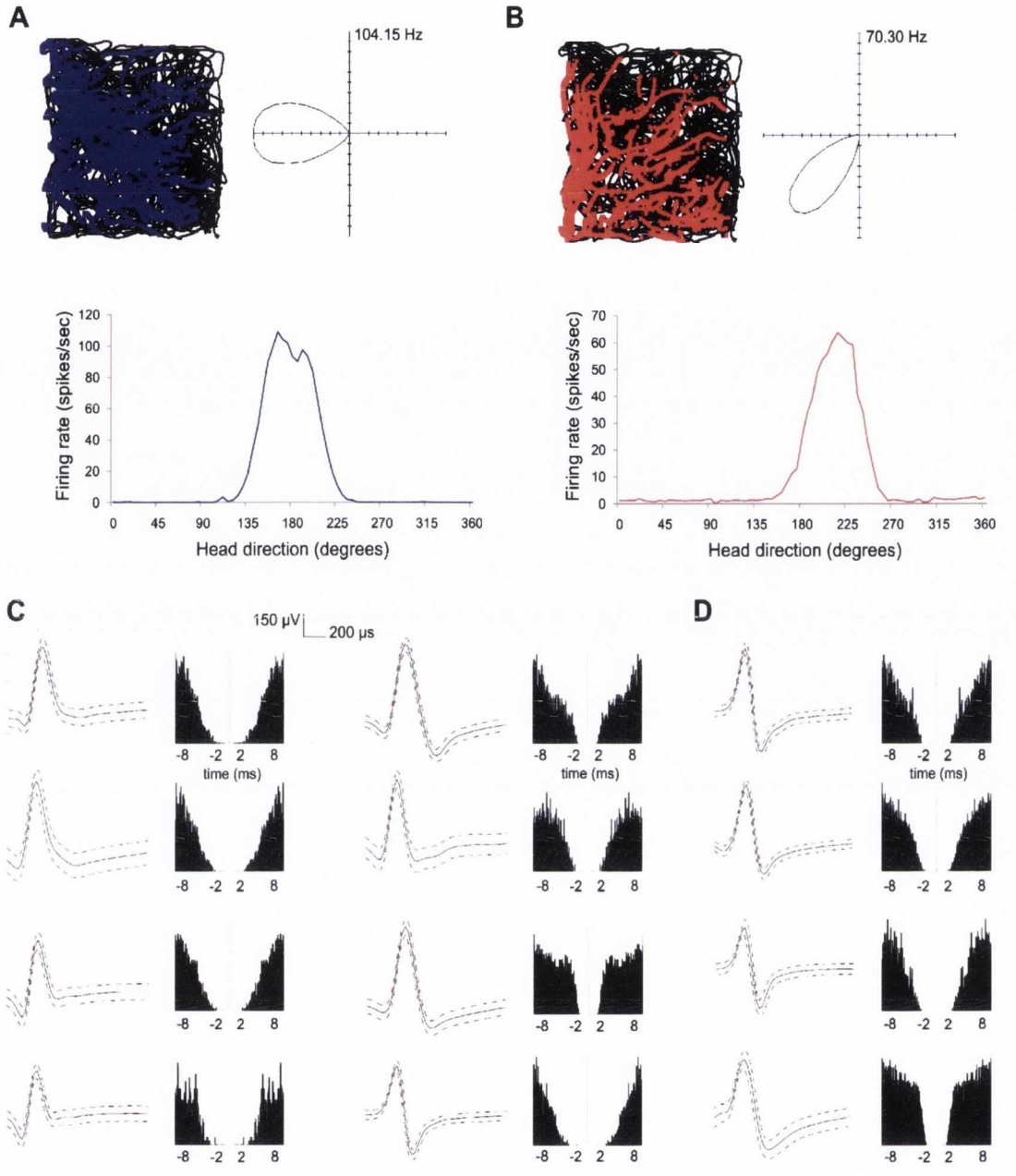

Figure 4.6: Spiking properties of anteroventral units. (A) Head-directional properties of HD-by-theta units. (B) and HD units. The spiking of HD-by-theta (A up, left, marked with purple symbols) and HD (*B* up, left, marked with red symbols) follows equivalent directional pattern. The experiments are conducted in rectangular recording arena and animal's path is marked with black line. Polar plot examples reveal the head directionality of HD-by-theta (A up, right) and HD (B up, right) units. The polar plots coordinate system denotes maximal firing frequency of the recorded unit with 0Hz in the centre and 104.15/70.30Hz on the edges for A and B respectively. The same signal can be plotted as firing rate versus head direction tuning plot for HD-by-theta (*A* bottom) and HD (*B* bottom) units. The spike waveform (left) and the autocorrelogram of spiking waveform (right) for eight anteroventral HD-by-theta units (*C*) and four HD units (*D*). For the spike waveform, the solid curve represents the mean and the dashed curve represents the standard deviation. Autocorrelation histograms were calculated for -10/10 ms. The clear isolation of the neuronal extracellular response was identified by the absence of correlations within the first 2 ms of the refractory period.

4.3.2 Tonic and rhythmic profiles of head-directional cells:

The occurrence of rhythmic patterns in neuronal spiking was estimated from the inter-spike intervals scatter plots of all AV neurons with head directional tuning. The two-dimensional inter-spike interval (ISI) scatter plot represents the action potentials as points, for which the x-axis indicates the time interval before and the y-axis indicates the time interval after the action potential. The ISI scatter plots of 101 head-direction units (44 from AD and 57 from AV) with predominantly tonic spiking were characterized with one major ISI cluster and defined as putative HD cells (Figure 4.7A). The tonic ISI profile of HD cells can also be visualized by sample spike traces (Figure 4.7B).

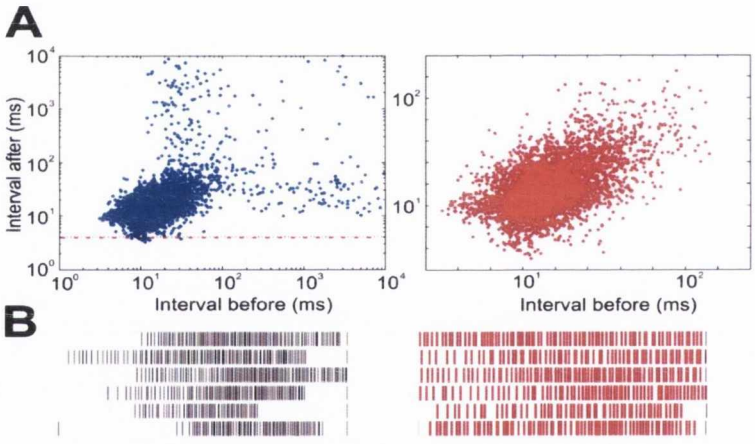

Figure 4.7: (A) Inter-spike interval scatter plot for head-direction unit, where the clustering procedure finds one large cluster, indicating tonic firing of the cells. The points below the dashed horizontal red line represent the action potentials within the 4ms range that defines bursting mode. The ISI scatter plot on the right presents the action potentials from the central cluster (marked with red). (B) Sample recordings of the same head-direction unit for 1 sec duration (left) and 500 msec duration (right, marked with red).

36 head-directional units (HD-by-theta group, all of them from AV) showed an additional two ISI clusters, located in the 100 ms pre- and post-inter-spike intervals range (Figure 4.8A,B). As expected that the additional ISI clusters represent the first (Figure 4.8A bottom; marked with green) and the last spike (Figure 4.8A bottom,

marked with Blue) of rhythmically-grouped spike trains. These compact spike trains occur at a frequency of 6-9 Hz (Figure 4.8A,B bottom).

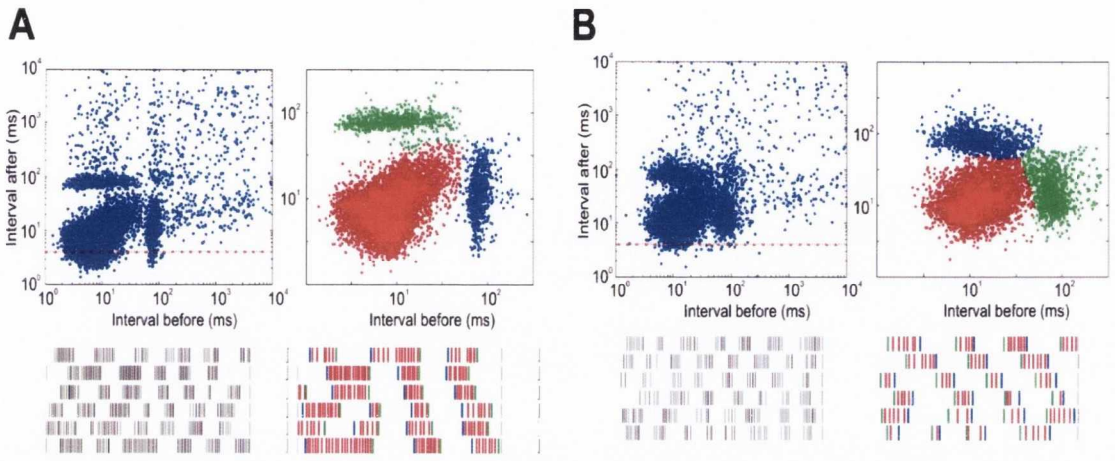

Figure 4.8: (A) ISI scatter plots for all spikes (left) and for the main clusters (right) of two HD-by-theta units. The central cluster is marked in red, with two further clusters (blue and green). Sample recordings of the same cell with 1 sec duration (below, left) and 500 ms duration (below, right). Note that the spikes from the green ISI cluster in *B* take first position in the spike trains, while the spikes from the blue ISI cluster are positioned last. The intermediate spikes correspond to the points from the central red ISI cluster.

The most frequent spike train parameters for the HD-by-theta cells included three or more spikes with an inter-spike interval of 10 ms and a 25-250 ms pause preceding the first spike of the train. The number of compact spike trains per total spikes from HD cells is much less compared to HD-by-theta cells ($P < 0.01$) (Figure 4.9A). This finding reflects the difference between the ISI profiles of these groups, represented by the ISI ratio (the ratio between the total number of spikes from additional ISI clusters, marked in green/blue and the number of spikes from the largest cluster, marked in red on the ISI scatter plots multiplied by 100). The ISI ratio for HD-by-theta cells is several-fold higher than the ISI ratio of HD cells ($P < 0.001$) (Figure 4.9B).

Figure 4.9: (A) Comparison between the relative number of spike trains between HD-by-theta and HD cell groups (left, $P<0.01$). (B) The ratio between additional green/purple clusters and central red cluster multiplied by 100 (ISI ratio) for the anteroventral HD-by-theta and HD cell groups (right, $P<0.001$).

The major ISI cluster and the additional two ISI clusters contain the spikes forming the compact spike trains Figure 4.10. ISI analyses therefore suggests the two main types of head-directional cells in AV: tonic and rhythmic units.

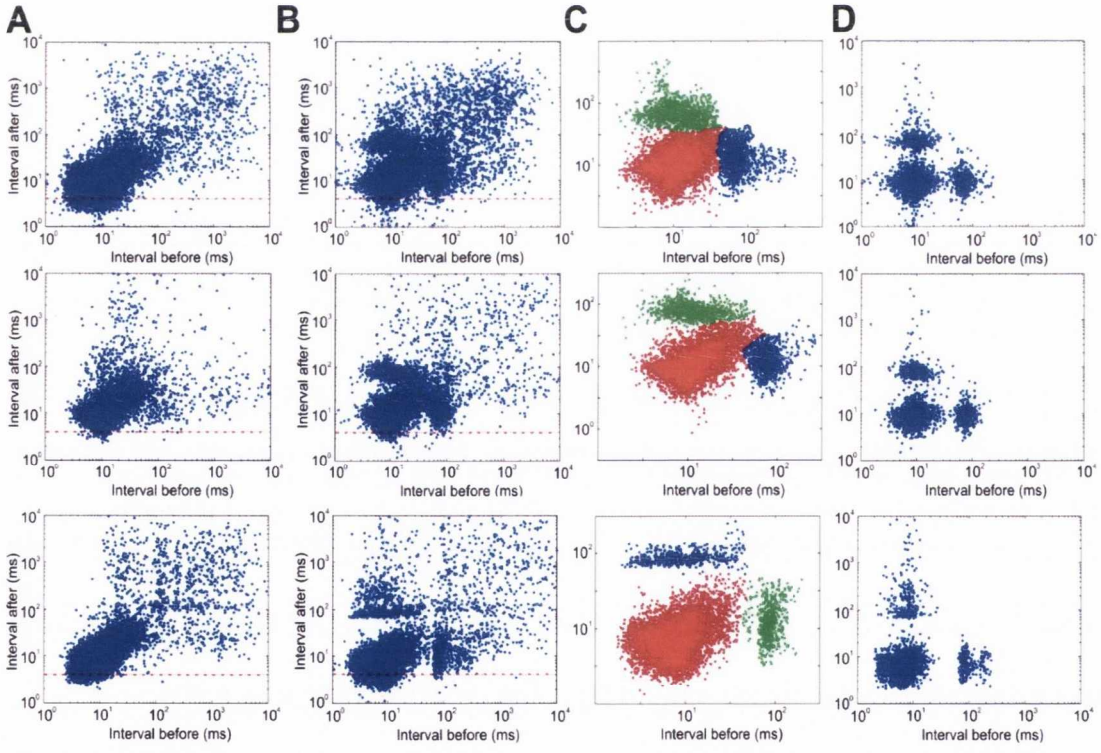

Figure 4.10: (A) Three examples of ISI scatter plot of HD cells. (B) ISI histograms of HD-by-theta units for all spikes (*C*) The main ISI clusters of plots in B. (D) ISI scatter plots when filtered for compact spike trains only.

The irregularity of the ISI can be also quantified using coefficient of variation, which is the ratio between the standard deviation to the mean of ISI's. The coefficient of variation is significantly different between the two groups ($P < 0.001$) where this coefficient was calculated for ISIs less than 200ms to exclude period's transition between preferred and non-preferred head direction. The HD-by-theta group yield a higher coefficient of variation (1.189 ± 0.03), and for HD group (0.995± 0.022). The ISIs of head-direction cells are highly irregular (Taube, 2010), hence the high values of coefficient of variation. While the coefficient of variation indicates the higher irregularity of ISIs between the two groups, the ISI scatter plots gives finer details where this irregularity originates from.

4.3.3 Theta rhythmicity of anteroventral neurons:

To quantify the rhythmicity of HD-by-theta cells, a sinusoidal function with decaying amplitude was fitted to the spike autocorrelogram of each neuron (the fitted curve is represented by the red line in Figure 4.11) and the relative amplitude of the fitting parameter were used to calculate the theta index (Royer et al., 2010). As described in the method section the theta index is the maximal amplitude of the sinusoidal fitted curve relative to the maximal value of the non-sinusoidal fitted curve of the autocorrelograms. The predominant tonic spiking of HD cells was non-rhythmic autocorrelograms (Figure 4.11A) with theta index values close to zero (0.0017 ± 0.0002). Rhythmic spiking resulted in theta-modulated autocorrelograms for HD-by-theta units (Figure 4.11B), with theta index values of 0.0217 ± 0.0004.

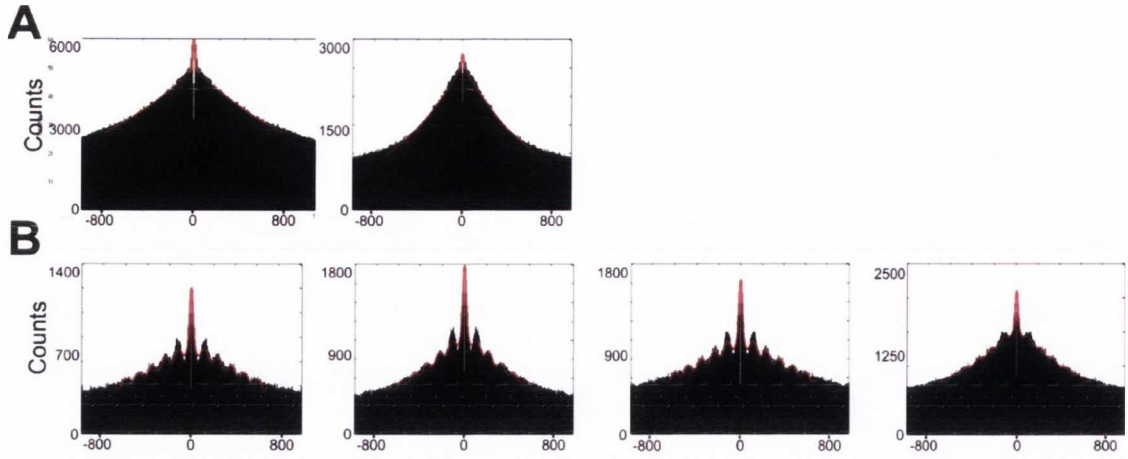

Figure 4.11: Evaluation of theta rhythmicity. (A) 1 s autocorrelograms of two HD units. (B) and four HD-by-theta units. The fitted vertical red line indicates the relative amplitude of the sinusoid component of the autocorrelogram, visualizing the degree of autocorrelogram rhythmicity (Royer et al., 2010).

To examine the head directional firing characteristics within periods of maximal firing it was assumed that head-directional tuning curves obey a Gaussian distribution. The rhythmicity of the spikes within the $\pm\sigma$ of the peak was examined to investigate how head-directional firing is modulated when the animal is facing the preferred direction for the recorded unit (Taube, 2010). This includes spikes from the central part of the head-directional tuning curve. By examining this central part of tuning curves It was found that the HD autocorrelogram (Figure 4.12A) yielded the HD theta index (0.0018 ± 0.0002) approximately the same value as the entire tuning curve, however HD-by-theta autocorrelograms (Figure 4.12B) showed higher rhythmicity, with values of 0.0484 ± 0.0064 double the previous value (0.0217 ± 0.0004).

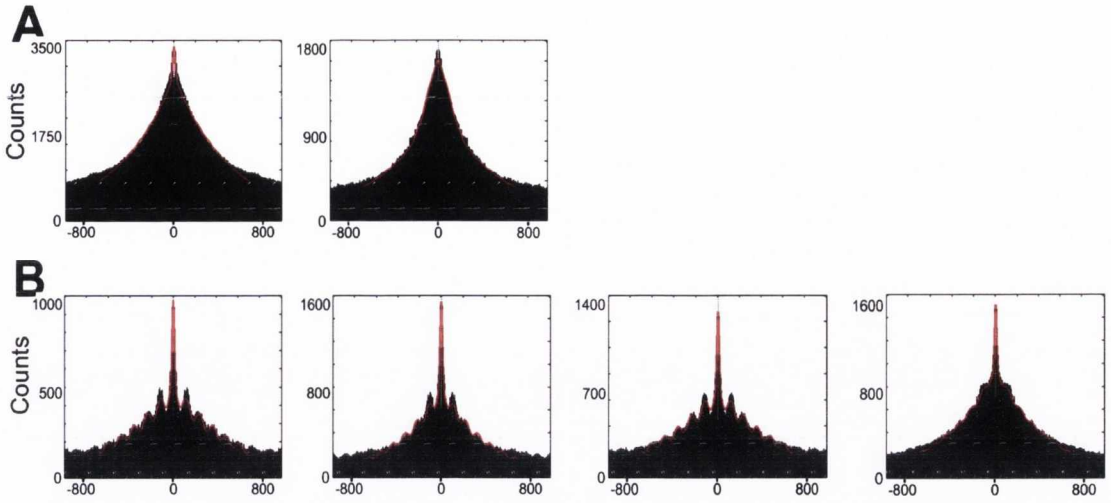

Figure 4.12: Evaluation of theta rhythmicity for HD preferred direction of firing which include all spikes from the central region ±σ peak and the lower panels include only the spike trains from the ±σ peak.. (A) 1s autocorrelograms of two HD units (B) and four HD-by-theta units.

To examine the rhythmic properties of the spike trains, the theta index only for the action potentials composing the spike trains were analysed (Figure 4.13). The theta index of HD-by-theta group reached values of 0.06255 ± 0.0086.

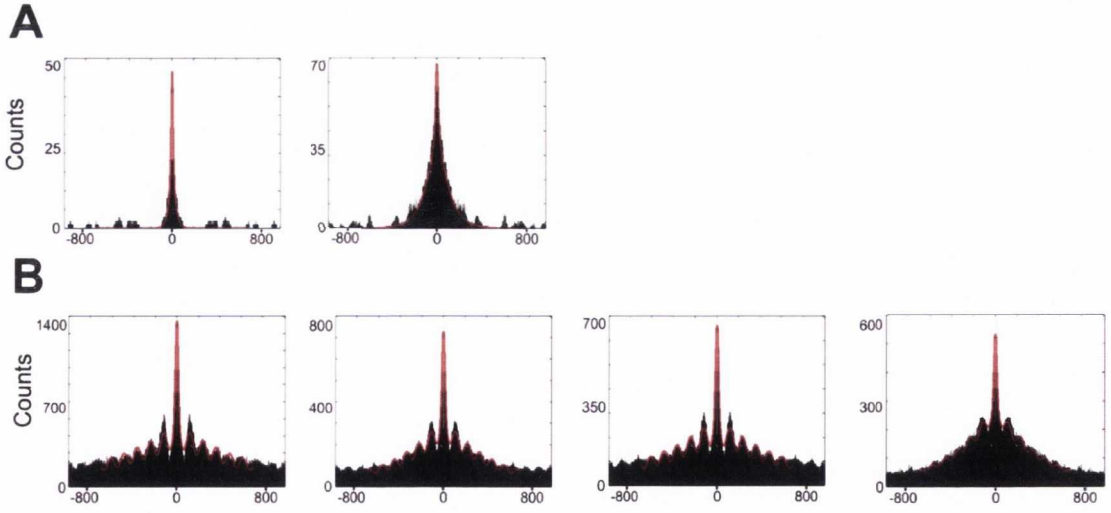

Figure 4.13: : Evaluation of theta rhythmicity for HD preferred direction which include all spike trains from the central region ±σ peak and the lower panels include only the spike trains from the ±σ peak.. (A) 1 s autocorrelograms of two HD units (B) and four HD-by-theta units.

Examining the peak firing regions of the spike trains showed that the theta index increased significantly, compared to all spikes of HD-by-theta units ($P < 0.01$,

Figure 4.14 C). In this case, the rhythmicity of the HD-by-theta autocorrelograms reached their maximal value (0.1870 ± 0.0265), while the HD autocorrelogram revealed zero values when filtered for spike trains.

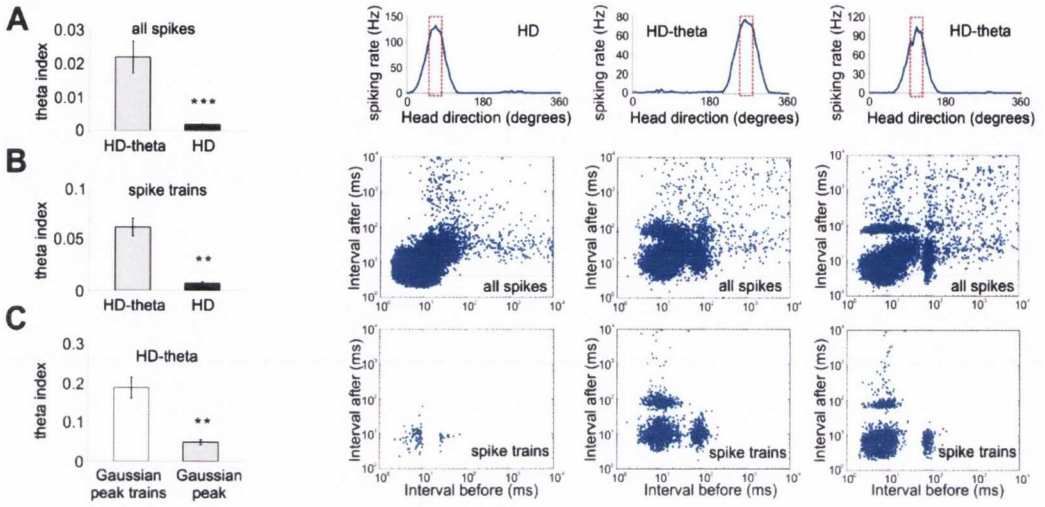

Figure 4.14: (A) Theta index of all spikes for HD-by-theta (n = 36) and HD (n = 101) cell groups. (B) Theta index of spike trains for HD-by-theta and HD cell groups (P<0.01). (C) Comparison between theta index values of all spikes within preferred direction of firing (grey bar) and spike trains Gaussian peak (white bar) for HD-by-theta units (P<0.01).

To determine the frequency with which the compact spike trains of thalamic head-directional units occur. Figure 4.15A shows a plot of inter-train interval. The sequence of HD-by-theta spike trains predominated in the range of 80 and 170 ms, corresponding to the frequency range of 6-12 Hz (Figure 4.15A, black). In comparison, the HD spike trains did not show a preferred frequency range (Figure 4.15A, grey). To determine the spike train frequency, the mean spike train frequency for each HD-by-theta unit across all recording sessions was analysed (Figure 4.15B). We found a distribution of the spike train frequency in the range of 7.89 ± 0.15Hz. These data show that HD-by-theta units exhibit a constant preference for their spiking frequency (which is around 8Hz).

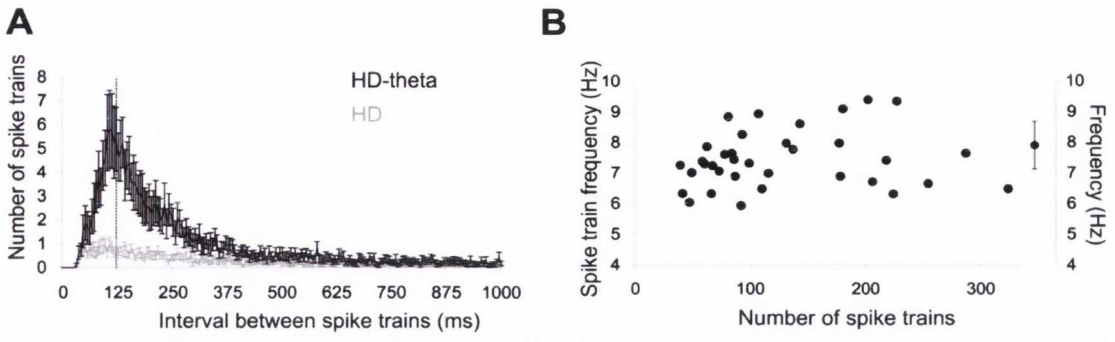

Figure 4.15: Theta rhythmicity of anteroventral spike clusters. (A) Distribution of spike train intervals (mean ± sem) for HD-by-theta units. Dashed vertical line denotes interval of 125 ms (8Hz). The values of HD cells are indicated with grey. (B) Mean values of the spike train frequency (Hz) for all HD-by-theta cells. The inset on the right represents the averaged frequency for all HD-by-theta cells (along with their standard deviation).

4.3.4 Theta cells correspond to HD rhythmicity:

The AV is also a location of theta cells (Tsanov et al., 2011). Next the aim was to determine if the firing pattern of HD-by-theta units is related to thalamic theta cells. To achieve this, recordings were analysed where both theta- and HD-by-theta units were detected on the same channel of the same tetrode. This proximity suggests with a high probability that both cells are close enough to be innervated with the axonal branches of the same presynaptic afferent. The crosscorrelograms between these cell pairs demonstrated the synchronous rhythmicity for both units (Figure 4.16A). Furthermore, the crosscorrelation was negative at time lag 0 between theta and HD-by-theta spikes for all pairs (marked with a vertical white line). When compared to a crosscorrelograms between theta and putative HD cells recorded from the same channel, we found no evidence of synchronization (Figure 4.16B). The negative crosscorelation between theta and HD-by-theta spikes can be seen in sample traces of these cell pairs (Figure 4.16*C*). The rhythmic bursts of theta cells (red traces) were paralleled occasionally by pauses of HD-by-theta spiking activity (purple traces). The subsequent pauses formed compact spike trains, which were evident during the firing

of HD-by-theta cell in the preferred head direction (Figure 4.16*C* black trace, bottom). These parallel events occurred at the troughs (marked with dotted rectangles) of the simultaneously-recorded local field potential (green trace). Thus, the intervals between the spike trains of HD-by-theta cells corresponded to the local field troughs, which in turn are phase-locked to theta cell bursts.

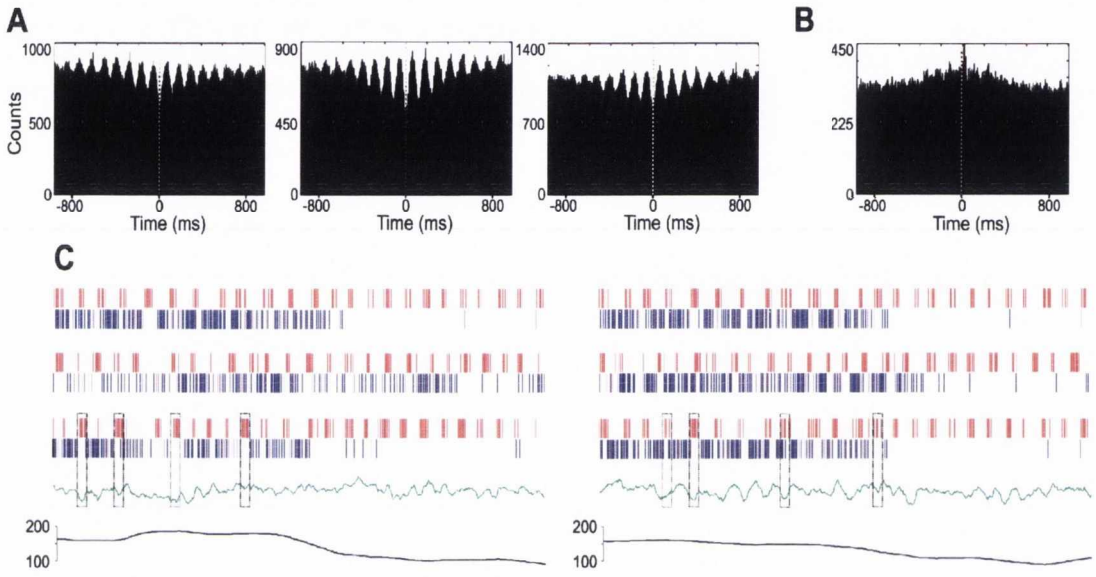

Figure 4.16: Rhythmic modulation of anteroventral units corresponds to the activity of theta cells. (A) Three examples of crosscorrelograms between theta and HD-by-theta units recorded from the same tetrode channel. Time 0 is denoted by dashed white line. (B) Crosscorrelogram between theta and HD units recorded from the same tetrode channel. (C) Sample recordings, representing the parallel activity of theta (red) and HD-by-theta (purple) units. The left panels represent the recorded activity [from three different cells] in one animal, while the right panels show similar episodes [from three different cells] in a second animal. Simultaneously recorded LFP (green trace) is below. The rectangular box denotes parallel theta cell activity, HD-by-theta pause and LFP oscillation trough. Bottom: concurrent head direction (black trace) measured in degrees (y-axis).

4.3.5 Directionally-modulated theta cells in anteroventral nucleus:

In the previous sections theta modulation of the head-directional signal in AV was reported. Next the goal was to examine if there was a reciprocal influence of the head-directional system on the theta signal. For this purpose the directional characteristics of all theta-bursting cells recorded within the population of head-direction cells was analysed, located in the medial part of AV. The small sample size of all theta cells

recorded in this region (31/23%) is comparable to the low density of theta cells in the hippocampal formation (Jung et al., 1994). A small group of theta-bursting cells was identified (10/7%), for which the difference between maximal and average firing frequency for preferred head direction reached 40%, and this population of cells is defined as directional theta cells.

Directional theta units possessed an intermediate firing frequency with an average rate of 26.8 ± 1.7 Hz and a maximal rate of 133.7 ± 13.1 Hz (Figure 4.17A, first row). The remaining theta units were grouped as slow- (Figure 4.17A, second row) and fast-spiking (Figure 4.17A, last row) theta cells, depending on their absolute frequency. For slow-spiking units, the average firing rate was 18.5 ± 1.7 Hz and the maximal firing rate was 76.1 ± 10.5 Hz. For the fast-spiking units, the average firing rate was 63.6 ± 6.4 Hz and the maximal firing rate was 208.8 ± 24.1 Hz. The theta-spiking profile of thalamic theta units is evident when expressed through an autocorrelogram (Figure 4.17B) and ISI plots (Figure 4.17C).

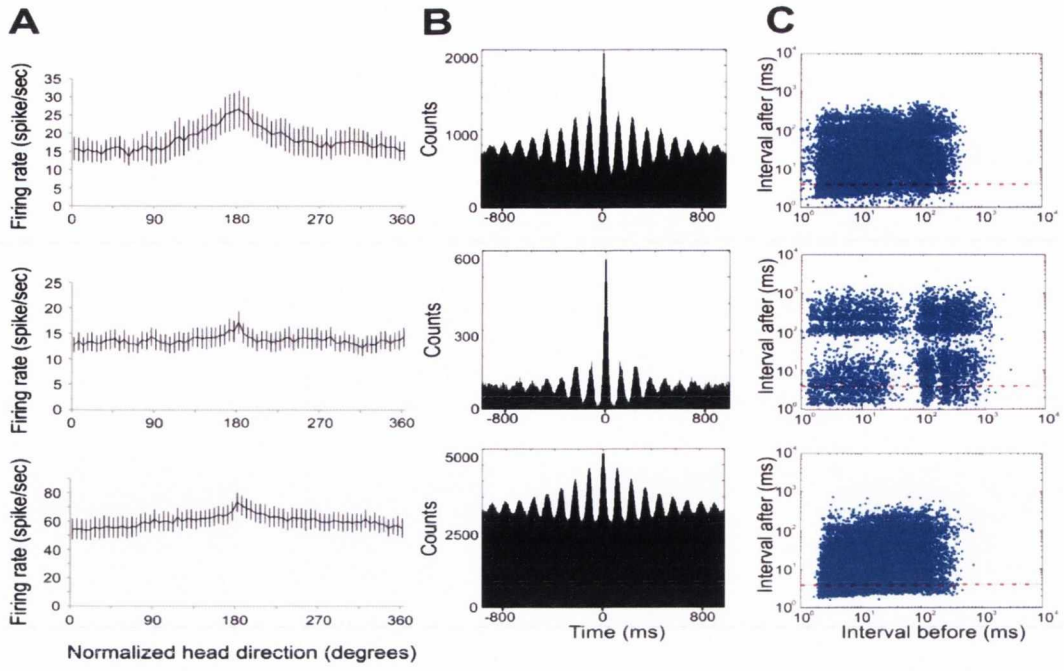

Figure 4.17: (A) Firing rate versus head-direction tuning plot for directional theta (first row), slow-spiking theta (second row) and fast-spiking theta (last row) cells. The x-axis presents normalized head direction degrees that set the peak of tuning curve for all units to 180^0. The y-axis represents absolute firing frequency in spikes per sec (mean ± sem). (B) Sample 1 s autocorrelograms for directional theta (first row), slow-spiking theta (second row) and fast-spiking theta (last row) cells. (C) Sample ISI scatter plots for directional theta (up), slow-spiking theta (middle) and fast-spiking theta (bottom) cells.

The place and directional information content of all thalamic theta cells was computed and the values of these parameters for the directional theta group, the fast-spiking and slow-spiking theta groups. The information content quantifies the amount of spatial information (locational or directional) carried by each spike, expressed in bits per spike (Skaggs et al., 1993). The directional information of directional theta spikes was significantly higher than the directional information of fast-spiking ($P < 0.01$) and slow-spiking ($P < 0.01$) theta units (Figure 4.18A). In comparison, the locational information of directional theta spikes did not show significantly different values (Figure 4.18B).

Distributive ratios for both the directional and locational component of the units' firing between directional theta cells and fast-/slow-spiking theta cells was also

compared. Distributive ratios measure the goodness-of-fit between a predicted and an observed firing distribution (Muller et al., 1994). Similarly, the directional (Figure 4.18C), but not locational (Figure 4.18D), distributive ratio was significantly higher for directional theta cells, compared to fast-spiking ($P < 0.01$) and slow-spiking ($P < 0.01$) theta cells. These data demonstrate that the firing of directional theta cells is modulated by the animal's head direction. It has to be noted that the directional information content for these cells is low, and as locational distributive ratio indicates, the firing of the cell is not entirely explained by head direction.

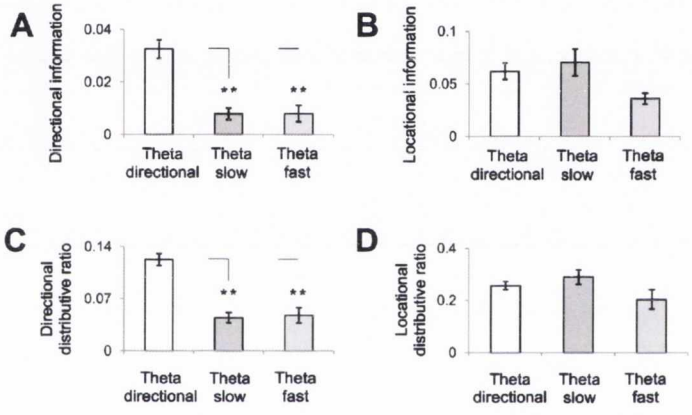

Figure 4.18: Comparison of the directional (left) and locational (right) information for the directional theta (n = 10), slow-spiking theta (n = 12) and fast-spiking theta (n = 10) cells ($P < 0.01$). *G*, Comparison of the directional (C) and locational (D) distributive ratio for the same cells.

4.3.6 HD cells correspond to theta units' directionality:

Although the rhythmic properties of directional theta units are similar to the other theta-bursting cells with a comparable spike train frequency (Figure 4.19A), spike distribution (Figure 4.19D) and theta index (Figure 4.19E), the preferred direction of spiking suggests that these cells receive a distinct afferent signal.

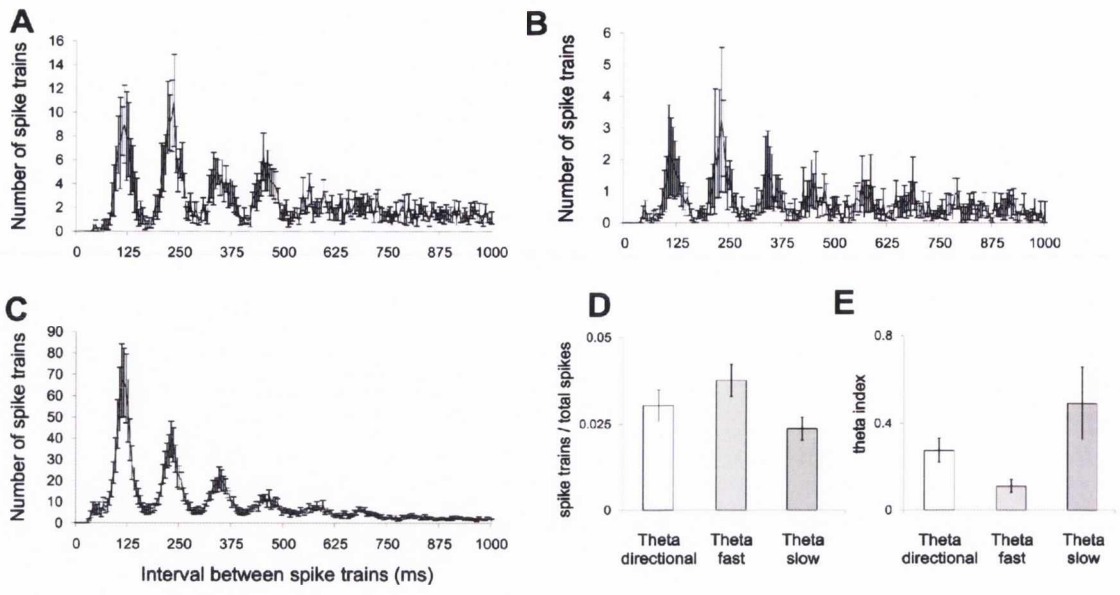

Figure 4.19: Comparison of the rhythmic properties between anteroventral theta cells classes. (A) Inter-train intervals distribution (mean ± sem) for directional theta, (B) slow-spiking theta (C) fast-spiking theta cells. Note that the peaks and troughs for all cell classes share the same rhythmic pattern, with the highest peak located at 125 ms (8Hz). (D) Relative number of spike trains (E) and theta index values for directional theta unit, fast-spiking theta and slow-spiking theta cells.

Directional theta and HD units, recorded on the same tetrode channel showed similar directionality (Figure 4.20A). The crosscorrelograms between these cell pairs revealed synchronous activity with a positive correlation at time lag 0 (Figure 4.20B, marked with a vertical dashed white line). This suggests that the common head directional input induces increased spiking of directional theta units during the preferred head direction of the HD cell (Figure 4.20*C*), compared to the inactive period of a HD unit (Figure 4.20D) when the animal was heading in a non-preferred head-direction (Figure 4.20D bottom, HD degrees are indicated with black trace).

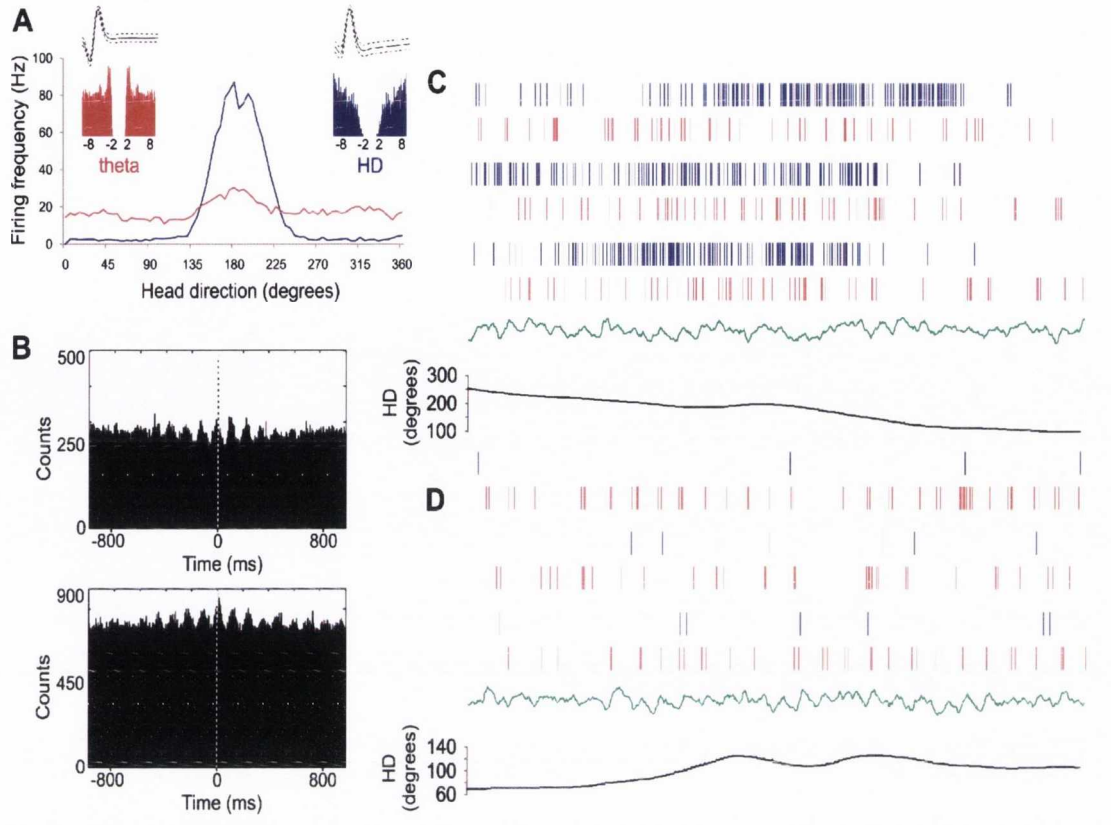

Figure 4.20: Directional modulation of anteroventral theta cells corresponds to HD activity. (A) Firing rate versus head-direction tuning plot for a directional theta (red) and a HD cell (purple) recorded from the same tetrode channel. The inset on the left represents the spike waveform (above) and -10/10ms autocorrelogram (below) for the theta-bursting unit, while the inset on the right represents the same parameters for the HD unit. (B) Two examples of crosscorrelograms between proximally located directional theta and HD cells. Time 0 is denoted by dashed white line. (C) Sample recordings, representing the parallel activity of directional theta (red) and HD (purple) units and recorded during the preferred direction for the HD unit. Simultaneously-recorded LFP (green trace) and the concurrent heading direction, measured in degrees (black trace) are plotted below. (D) Sample recordings of the same pair during non-preferred for the HD unit direction. Simultaneously-recorded LFP (green trace) and the concurrent heading direction, measured in degrees (black trace) are plotted below. Note the decreased number of directional theta spikes, compared to *C*.

4.3.7 Thalamic and hippocampal theta are functionally related:

In this section the aim was to determine if the rhythmic activity observed in the anteroventral thalamic nucleus expresses the same frequency and temporal resolution as hippocampal theta rhythm. This would address the question of whether theta rhythm in anterior thalamus is a functional part of the limbic theta oscillation. For this, simultaneous recordings of local field potentials (LFP) from hippocampal area CA3 (Figure 4.21A) and AV (Figure 4.21B) in five rats were carried out.

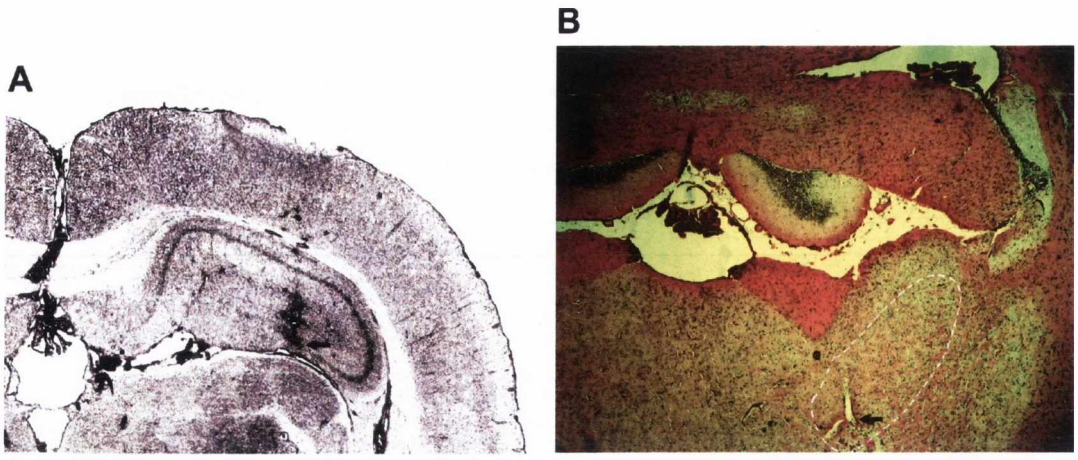

Figure 4.21: Parallel recordings from hippocampus and anterior thalamus. Coronal section shows the trace of recording electrode in hippocampal CA3 region (*A*) and anteroventaral thalamic nucleus (*B*, marked with white). The black arrows indicate the tip of the recording electrodes.

Thalamic LFP theta power is dependent on the proximity of theta cells to the recording tetrodes (Tsanov et al., 2011), and as a result, the LFPs recorded by different tetrodes in anterior thalamus (in total 32 channels per rat) can be divided into theta and non-theta groups. During the pellet-chasing task, the LFP power reached its peak in the range of 7-10 Hz for hippocampal and thalamic theta recordings (Figure 4.22A). Coherence analysis showed that the highest degree of coherence between hippocampal and thalamic theta signal is in the range of 7-10 Hz (Figure 4.22B). The synchronization of concurrent hippocampal and thalamic theta oscillations (Figure 4.22*C*) is apparent. In comparison, hippocampal and thalamic non-theta signals are less correlated (Newman–Keuls, $P<0.001$, Figure 4.22*B*, below, grey line).

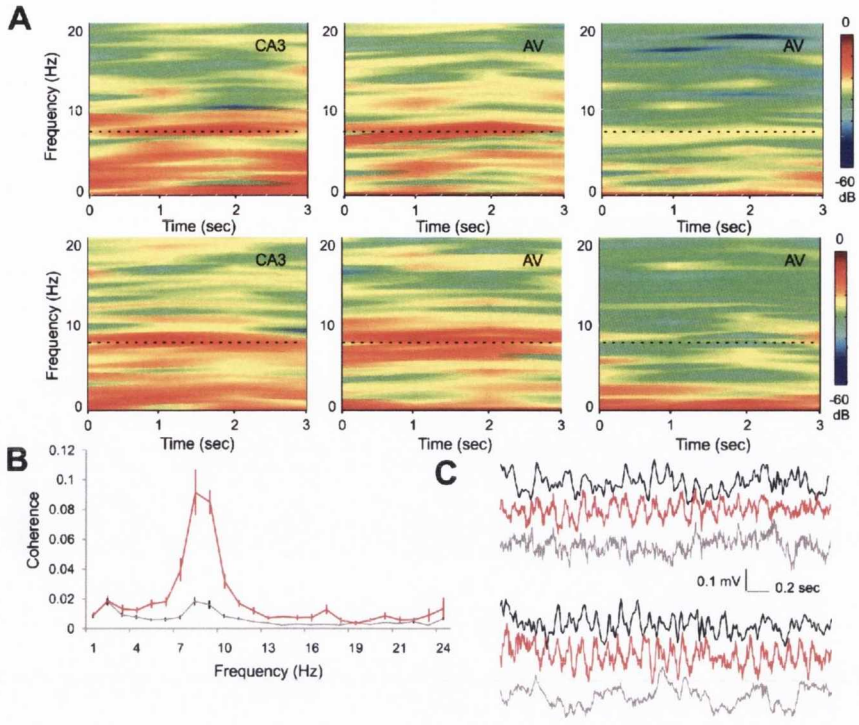

Figure 4.22: Synchronous hippocampal and thalamic theta oscillations. (*A*) Colour-coded 3 sec power spectrograms, representing simultaneous recording of local field potential (LFP) from hippocampal area CA3 (left panels), anteroventral theta (middle panels) and anteroventral non-theta (right panels) signal. The black dashed line indicates the frequency level of 8 Hz. (*B*) Coherence plot between hippocampal LFP and anteroventral theta (red trace) and non-theta (grey trace) LFP (mean ± sem). (*C*) Sample LFP traces for the simultaneously recorded hippocampal (black), anteroventral theta (red) and anteroventral non-theta (grey) LFPs.

4.3.8 Sniffing and theta cells:

Three rats were implanted with tetrodes and pressure sensor was used to monitor the sniffing activity during free exploration of the environment. 17 theta cells were analysed, polar plots depicting the sniffing phase at which theta cells fired an action potentials were used to determine if these cells had a preferred sniffing phase of firing (Figure 4.23). None of these cells in the AV showed preference of firing rate at a specific sniffing.

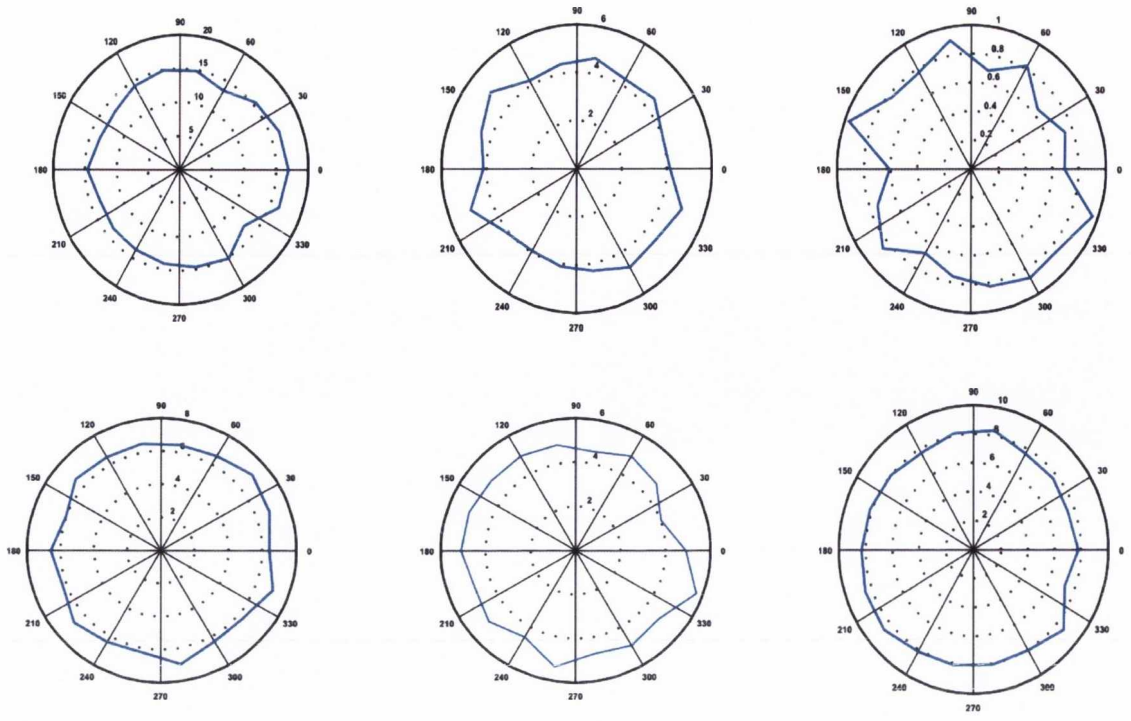

Figure 4.23: polar plots depicting the theta cells and sniffing phase relationship. Six examples are shown where none of these cells showed a preferred sniffing phase.

To investigate the relation between the silence period between theta cells spikes and sniffing, both signals were transformed and correlation at different time lags (-1,1) sec was computed between the transformed signals. In all cases the correlations were lower than 0.05 and the correlation coefficient at short time lags were not different from longer time lags which indicated the low correlation is random chance (Figure 4.24).

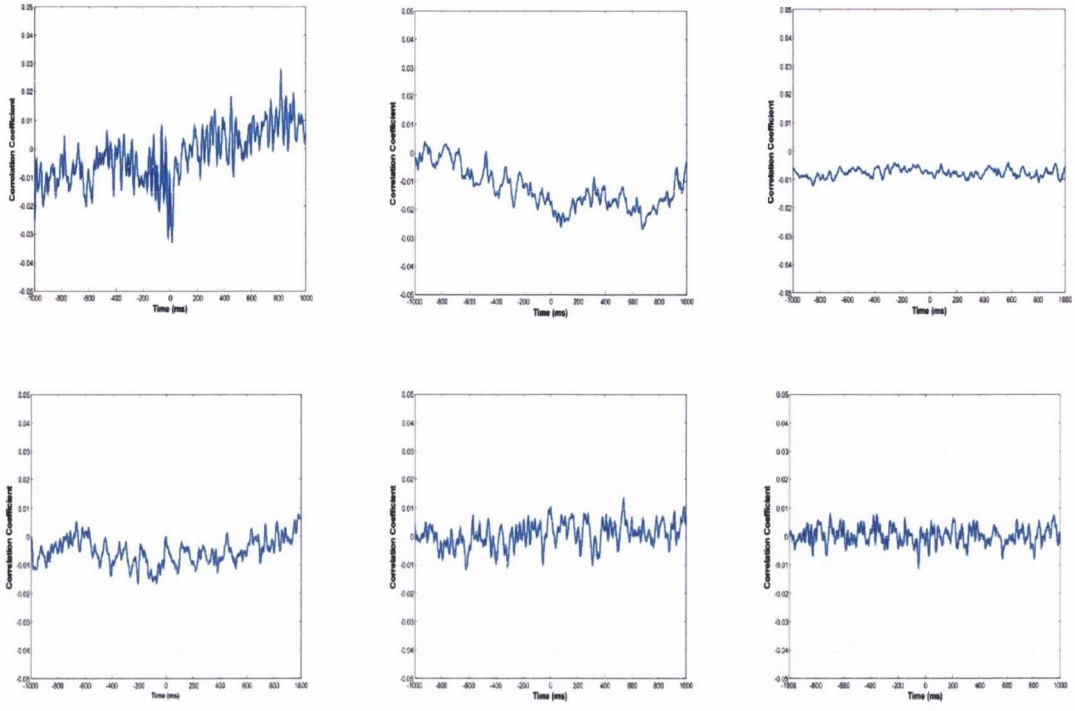

Figure 4.24: theta cells silence period and sniffing cycle correlation. Six examples are shown, y-axis indicates correlation coefficient and x-axis is time (-1,1) sec. all correlation were lower than 0.05 and correlation at short time lags is similar to those at longer time lags indicating these low correlation are random chance.

Results examining at the relationship between sniffing cycle and theta cells in AV, does not indicate a relation between the two processes. Hence further experimentation was not carried out.

4.4 Discussion:

In this chapter it is shown that a substantial population of head-direction cells in the thalamic anteroventral nucleus is able to spike rhythmically in the theta frequency range. The single-unit recordings from anteroventral thalamic nucleus revealed that the spiking activity of local theta cells can undergo head directional modulation. The spectral power from this region shows coherence with hippocampal theta rhythm, suggesting that the anterior thalamus is a functional component of limbic theta

processing. Together, these results demonstrate integration of directional and theta processing at the level of the anterior thalamus. The result supports the importance of theta within the limbic system and demonstrates the significance of cell firing patterns in decoding activity of neurons.

4.4.1 Cell types in anterior thalamus:

Based on its anatomical and cytoarchitectonic properties, the anterior thalamus is subdivided into anterodorsal (AD), anteroventral (AV) and anteromedial nuclei (Kruger et al., 1995). Electrophysiologically, anterodorsal neurons exhibit head-direction properties (Taube, 1995), whereas anteroventral and anteromedial nuclei are linked to theta rhythm (Albo et al., 2003). Numerous electrophysiological investigations have targeted AD in freely-behaving rats, revealing that anterodorsal neurons function as head-direction (HD) cells (Goodridge and Taube, 1997, Zugaro et al., 2001, Zugaro et al., 2002, Taube, 1995, Yoganarasimha et al., 2006). By comparison, most data reported from the adjacent anteroventral nucleus have been conducted without concurrent measures of head-directionality (Vertes et al., 2001, Albo et al., 2003, Talk et al., 2004). HD cells in AV have previously been described (Taube, 1995, Yoganarasimha et al., 2006), but have not been quantified. In this chapter it is shown that the medial part of anteroventral nucleus is a locus of HD cells, where 69% of recorded units expressed a clear head-directional tuning curve. A population of anteroventral cells fires rhythmically at theta frequency (5-12Hz) (Vertes et al., 2001), and these neurons are defined as theta cells (Tsanov et al., 2011).

An interesting question was whether thalamic neurons can integrate head direction and theta rhythm. The possibility that head-directional and theta signals might merge in anterior thalamus was suggested by observations that anterodorsal HD cells

gradually developed rhythmic firing in the slow theta frequency range (6 Hz) after bilateral destruction of the lateral mammillary bodies (Blair et al., 1999).

In this chapter three independent criteria were used to estimate theta modulation of anteroventral head-direction neurons:

1) Inter-spike interval ratio.
2) Theta index.
3) Spike train frequency.

Inter-spike interval histograms reveal the temporal relationship between HD spikes and ISI is important part of cells coding process (Taube, 2010). Inter-spike interval ratio shows the number of spikes clustered around the 100ms inter-spike interval. These ISI clusters are formed from the first and the last spike of the spike groups, occurring at frequency of 6-12 Hz. These rhythmic groups of spikes are referred to in this chapter as compact spike trains, but not as bursts because of their long inter-spike interval (> 10ms) that reached values of 10ms. The definition of burst mode in thalamus varies from 4ms (Ramcharan et al., 2005) up to 10ms (Fanselow et al., 2001) inter-spike interval. To avoid misinterpretation of the observed spike pattern, in here the bursting in the recordings was defined with a maximum of 4 ms inter-spike interval.

Measurement of autocorrelogram parameters is the most conventional method to identify rhythmic pattern in neuronal spiking (Steriade et al., 1991, O'Keefe and Recce, 1993), and on that basis, theta rhythmicity was evaluated using the theta index (Royer et al., 2010). It was found that the value of the theta index for the preferred direction of the spiking trains reaches values of 0.18 for HD-by-theta units. Importantly, these values are comparable to the theta index of anteroventral theta

cells, which are 0.11 and 0.49 for the fast- and slow-spiking theta cells (Tsanov et al., 2011). For comparison, the theta index of putative HD cells was close to zero (0.0018).

The third measurement with which spiking rhythmicity was evaluated is the spiking train frequency. This parameter demonstrates the predominant frequency with which rhythmic spike groups are distributed. It was estimated that the frequency of the spike train distribution to be 6-12 Hz, which represents theta frequency modulation. Based on the abovementioned analyses, these cells were defined as head direction-by-theta (HD-by-theta) units, and this cell type comprised 26% of all recorded units in medial AV or 39% of the head-directional units in AV.

4.4.2 Theta processing in hippocampo-diencephalic system:

One of the major inputs to AV arises from the medial mammillary bodies (Seki and Zyo, 1984), which in turn receive projections from the ventral tegmental nucleus (Cruce, 1977, Hayakawa and Zyo, 1984), hippocampal formation (Ishizuka, 2001, Swanson and Cowan, 1977), medial septum and supramammillary nucleus (Gonzalo-Ruiz et al., 1992). Thus, the mammillary bodies project to AV a theta signal that integrates tegmental, septal and reciprocal hippocampal theta activity (Pan and McNaughton, 1997, Pan and McNaughton, 2002, Bassant and Poindessous-Jazat, 2001, Kocsis et al., 2001). The generation of theta rhythm *per se* is proposed to be in medial septum and the propagation of theta signal to the hippocampus and the diencephalon (thalamus and hypothalamus) is mediated via mammillary and supramamillary nuclei.

Studies have found that theta rhythm in the mammillary bodies and hippocampus is abolished after procaine injections in the medial septum (Kirk et al., 1996, Kirk and

McNaughton, 1991). The supramammillary nucleus is a part of an ascending system involving the medial septum (Borhegyi et al., 1998, Vertes, 1992) and this system is proposed as the cholinergic pacemaker of theta in the hippocampo-diencephalic circuit (Brazhnik and Vinogradova, 1986).

The theta oscillations has been shown to be important in spatial learning (Pan and McNaughton, 1997, O'Keefe and Recce, 1993) and plasticity (Mehta et al., 2000, Ekstrom et al., 2001). Studies have shown a strong link between navigation and theta rhythms (Buzsáki, 2005, Cacucci et al., 2004), in place cells it is reported that the firing of these cells and their relation to theta rhymes can improve the accuracy of locational coding (O'Keefe and Recce, 1993). Since head-directional cells have a large firing range (~90 degrees) (Taube et al., 1990), it can be hypothesised theta modulation of head-direction cells can improve the accuracy of directional coding.

The major finding described in this chapter is that AV contains HD-by-theta cells suggesting a convergence of the highly-processed theta signal and the head-direction signal. This convergence suggests another level of integration additional to visual and idiothetic information reported in HD cells (Hargreaves et al., 2007, Yoganarasimha and Knierim, 2005, Knierim et al., 1998).

The existence of similar information integration is demonstrated by postsubicular units that integrate place and direction (Taube et al., 1990, Sharp, 1996). Neurons that express spatial, head-directional and theta properties are found in presubicular and parasubicular cortices and are named theta-modulated place-by-direction (TPD) units (Cacucci et al., 2004). Recent findings have also shown concurrent directional- and theta-modulation of grid cells in the same region (Boccara et al., 2010). This line of research supports current oscillatory interference models which suggest that grid cell

firing in entorhinal/parasubicular cortices is highly dependent on a combination of theta and grid cell activity (Hasselmo and Brandon, 2008, Burgess, 2008a, Burgess et al., 2007). Thalamic signals from anterodorsal and anteroventral nuclei may update grid cell firing via the pre- and parasubicular cortices (Shibata, 1993a, Van Groen and Wyss, 1995, van Groen and Wyss, 1990). These afferents define the thalamo-cortical connection of the extended hippocampal system (Vann and Aggleton, 2004). Functionally, this system is involved in episodic memory formation (Burgess et al., 2002, Buzsáki, 2005), and the anterior thalamic nuclei are a vital component of this system (Aggleton and Sahgal, 1993, Harding et al., 2000). Studies have shown that the patterns of episodic memory loss seen in patients with anterior thalamic pathology are similar to those seen in patients with lesions in the medial temporal lobe (Harding et al., 2000, Van der Werf et al., 2000).

The information flow within the hippocampo-diencephalic circuitry has been studied through lesion studies of the head-direction system. Lesions of the dorsal presubiculum (postubiculum) (Goodridge and Taube, 1997) and hippocampus (Golob and Taube, 1997) did not disrupt the HD signal in anterodorsal thalamic nucleus. In contrast, lesions of the anterodorsal nucleus disrupted the HD signal in the postsubiculum (Goodridge and Taube, 1997), suggesting that the propagation of HD signal is ascending (i.e. in a bottom-up direction). Coherence analyses of simultaneously recorded local field potentials from hippocampus and anterior thalamus showed larger coherence between these structures in the theta range. The HD system complements anatomically the theta system in hippocampo-diencephalic circuitry (Vann and Aggleton, 2004).

In this chapter it is shown that these two systems are functionally integrated and actively interacting during the signal propagation. The results show that

approximately one-third (32%) of theta-bursting cells, which generate thalamic theta local field potential (Tsanov et al., 2011), display head-directional modulation in the medial part of anteroventral nucleus. The observed crossover between head-direction and theta processing may functionally implicate an oscillatory enhancement of the HD signal. This hypothesis is suggested by the finding that rhythmic oscillations generate a period during which thalamic neurons are highly sensitive to incoming sensory stimuli (Nicolelis et al., 1995) and that the rhythmic mode can enhance the detection of incoming stimuli (Guido and Weyand, 1995, Sherman and Guillery, 1996, Sherman, 2001).

4.5 Conclusion:

The data demonstrate that AV neurons integrate head-directional and theta information. This data shows the importance of oscillation and the rhythmic firing patterns in extracting information from spikes. It further supports the theory that spikes encode timing as well firing rates (Buzsáki, 2002).

Chapter 5. Summary and future work

The aims of this thesis were to research methods of extracting information from implanted recording technology and to contribute towards understanding of the brain function using *in-vivo* recordings.

The second chapter of this thesis presents a method of automated spike sorting which is the first step in extracting information from spike recordings. As mentioned in the introduction chapter and frequently stated in the literature (Buzsaki, 2004, Brown et al., 2004) this is an important part of neural *in-vivo* recording analysis. As the trend of neuron recording technology is progressing towards multiple simultaneous recording of neurons (Stevenson and Kording, 2011), automated accurate spike sorting becomes a vital step making manual sorting too time consuming.

The second chapter outlined the spike sorting algorithm and the results demonstrated that improved performances can be obtained using the proposed method of spike sorting when compared to other methods reported previously in the literature. Since there are many algorithms proposed in the literature the comparison between these can provide insights on which method would be more suitable for different experiment requirements. It is important to compare spike sorting algorithms with both standard data sets and standard tests to provide objective and fair comparison across all methods reported in the literature. Quiroga et al. (2004) provide standard data sets for testing the performance of these methods and as a result have been used in this study. Data sets should simulate real feature of extracellular recordings (Martinez et al.,

2009). Data set for example can exclude overlapping spikes which may bias test result. Therefore it is important any future progress of research in this area to set international standard tests to provide an objective comparison of spike sorting methods, across several factors:

1. Isolating the spikes of all neurons close to the recording electrode
2. Minimal human intervention
3. Resolving overlapping spikes
4. Taking into account non-stationary recordings
5. Ability to carry spike sorting online i.e. during the recording session
6. Computational complexity

In chapter 3 the variability of spike waveforms associated with place cells are reported. The results demonstrated that place cell waveform residues follow a *t*-distribution. This has important implications in the assumption of spike sorting methods. Similar analysis can be applied to other type of cells, for example grid cells and head-directional cells. Confirming the validity of this assumption would be important topic for *in-vivo* electrophysiology.

The result reported in the third chapter also demonstrates large amplitude fluctuations between sessions. Certainly such a large amplitude change can affect spike sorting algorithms. This indicates the need for improvement in electrode and headset designs to minimise electrode movements. It can be concluded that in long term recordings of spikes algorithms must take into account the non-stationary nature of data.

Following the findings of chapters 2 and 3, the spike sorting proposed in this thesis can be developed further, to provide online sorting. Where initially the spikes were sorted using the method proposed in chapter 2, and those initial sorting results may

then be employed to construct templates following expected *t*-distribution waveform variability. Template matching then can be carried for online sorting and clustering can be continued in the background to verify any new spike clusters or any drift in the cluster centres. In online sorting other factors such as computational complexity should also be considered.

An emerging need in spike sorting is to generate confidence levels of the sorting reliability (Einevoll et al., (in press)). An intriguing question to consider in future is whether the information relating to the distribution, variation of the spike waveform and the similarity measures introduced in chapter 3 can aid in providing a measure of sorting reliability.

As the neural electrode technologies advance towards simultaneous recordings from hundreds of electrodes, an important challenge to consider in the future of spike sorting is how to efficiently incorporate multichannel incoming information in order to improve the sorting algorithm and also possibility to detect electrode drifts. Tetrodes have been reported to provide better spike isolation (Gray et al., 1995). Recent advancement of electrode technology also allow greater control distances between of the recording sites, in order to achieve better spike sorting performances using information from multi-channel electrodes rather than single channel electrodes.

In the fourth chapter of the thesis the process following spike sorting in neural recordings is examined in detail. The focus here is on the information carried by the spikes in the thalamic anteroventral nucleus (AV), where a population of cells were reported that integrates theta oscillation and head-direction. In the chapter the conclusion drawn is that there is coherence between theta oscillations of hippocampus

CA3 and AV, demonstrating the importance of this oscillation in conveying information within the limbic system.

In this thesis it was possible to study the interaction between a few cell types. It has been established that the head-direction system involves several brain structures and similarly several brain nuclei are involved in the generation of theta rhythm. Figure 5.1A shows a schematic of the brain nuclei involved in head-direction network and their respective connections, similarly Figure 5.1B is a schematic of the brain nuclei where theta responsive cells are reported.

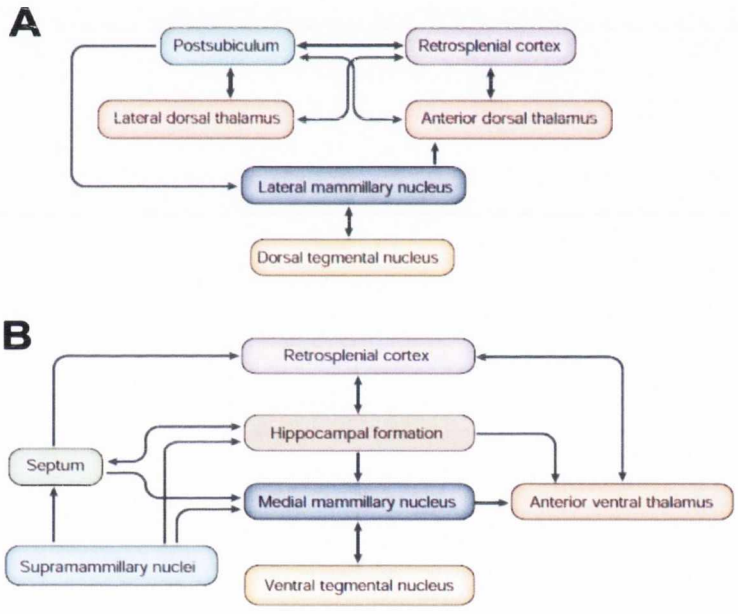

Figure 5.1: (A) Regions of the rodent brain involved with head-direction system (B) Regions of the brain where theta-responsive cells are reported (Vann and Aggleton, 2004).

Examining the interaction between population of theta cells and head-direction using parallel simulations recording of hundreds neurons would provide an improved basis for interpretation of the importance of these cells, and also the influence of these cells reported in this thesis on the head-direction network.

Grid cells and theta modulated grid cells recorded from medial entorhinal cortex were reported to degrade their spatial periodicity, while head-directional cells retained their firing properties after reduction of theta rhythm. The reduction in theta rhythm was achieved by inactivation of medial septum (Brandon et al., 2011). Arising from this is an interesting question to consider for future research whether reducing theta rhythm can change the firing properties of head-directional cells recorded from anteroventral (AV) and anterodorsal (AD) nuclei. This may provide further insight into the role of theta oscillations in the head direction network. It can also elaborate the role of theta modulated HD cells in the head direction network.

In summary the first challenge in extracting information from neural *in-vivo* recording has been addressed in this thesis. The method of spike sorting is introduced to provide automated and improved spike isolation.

The method proposed does not address all the challenges of spike sorting however the subsequent studies reported on variability of spike waveforms of place cells, within short periods and longer time frames. The aim of the study was to provide insights into observed variations of *in-vivo* spike recordings, therefore aiding the design of future spike sorting methods and providing a basis where the spike sorting method proposed may be extended to address further challenges of spike recordings.

In the study reported in the fourth chapter of the thesis, subsequent challenges of spike recording were investigated. The study examined the information carried by these neurons and provides insights into the brain function. More specifically the information carried by so called head-direction cells is extensively examined. The chapter reports on subset of head-direction cells that are modulated by theta oscillation. The theta oscillations has been shown to be important in spatial learning

(Pan and McNaughton, 1997, O'Keefe and Recce, 1993) and plasticity (Mehta et al., 2000, Ekstrom et al., 2001). The findings of this chapter further support the importance of theta oscillation in hippocampo-diencephalic circuitry. This raises questions about the significance of theta modulation in head direction network and how this modulation encodes information.

This thesis contributes towards the research of methods of extracting information from the neuron code and understanding the function of the brain using recordings obtained from implanted microelectrodes.

Bibliography

Abeles, M. & Goldstein, M. H., Jr. 1977. Multispike train analysis. *Proceedings of the IEEE,* 65, 762-773.

Adamos, D. A., Laskaris, N. A., Kosmidis, E. K. & Theophilidis, G. 2010. NASS: an empirical approach to spike sorting with overlap resolution based on a hybrid noise-assisted methodology. *J Neurosci Methods,* 190, 129-42.

Aggleton, J. P. & Sahgal, A. 1993. The contribution of the anterior thalamic nuclei to anterograde amnesia. *Neuropsychologia,* 31, 1001-19.

Aghagolzadeh, M., Zhang, F. & Oweiss, K. 2010. An implantable VLSI architecture for real time spike sorting in cortically controlled Brain Machine Interfaces. *Conf Proc IEEE Eng Med Biol Soc,* 2010, 1569-72.

Akay, M. (ed.) 2007. *Handbook of Neural Engineering*: John Wiley & Sons.

Aksenova, T. I., Chibirova, O. K., Dryga, O. A., Tetko, I. V., Benabid, A. L. & Villa, A. E. 2003. An unsupervised automatic method for sorting neuronal spike waveforms in awake and freely moving animals. *Methods,* 30, 178-87.

Albo, Z., Viana Di Prisco, G. & Vertes, R. P. 2003. Anterior thalamic unit discharge profiles and coherence with hippocampal theta rhythm *Thalamus and Related Systems,* 2, 133-144.

Albright, T. D., Jessell, T. M., Kandel, E. R. & Posner, M. I. 2000. Neural science: a century of progress and the mysteries that remain. *Cell,* 100 Suppl, S1-55.

Andreassen, S., Stein, R. B. & Oguztoreli, M. N. 1979. Application of optimal multichannel filtering to simulated nerve signals. *Biol Cybern,* 32, 25-33.

Atiya, A. F. 1992. Recognition of multiunit neural signals. *IEEE Trans Biomed Eng,* 39, 723-9.

Balasubramanian, K. & Obeid, I. 2011. Fuzzy logic-based spike sorting system. *J Neurosci Methods,* 198, 125-34.

Bar-Hillel, A., Spiro, A. & Stark, E. 2006. Spike sorting: Bayesian clustering of non-stationary data. *J Neurosci Methods,* 157, 303-16.

Bassant, M. H. & Poindessous-Jazat, F. 2001. Ventral tegmental nucleus of Gudden: a pontine hippocampal theta generator? *Hippocampus,* 11, 809-13.

Bassett, J. P., Zugaro, M. B., Muir, G. M., Golob, E. J., Muller, R. U. & Taube, J. S. 2005. Passive movements of the head do not abolish anticipatory firing properties of head direction cells. *J Neurophysiol,* 93, 1304-16.

Belkin, M. & Niyogi, P. 2003. Laplacian Eigenmaps for Dimensionality Reduction and Data Representation. *Neural Computation,* 15, 1373-1396.

Blair, H. T., Cho, J. & Sharp, P. E. 1999. The anterior thalamic head-direction signal is abolished by bilateral but not unilateral lesions of the lateral mammillary nucleus. *J Neurosci,* 19, 6673-83.

Blair, H. T. & Sharp, P. E. 1995. Anticipatory head direction signals in anterior thalamus: evidence for a thalamocortical circuit that integrates angular head motion to compute head direction. *J Neurosci,* 15, 6260-70.

Boccara, C. N., Sargolini, F., Thoresen, V. H., Solstad, T., Witter, M. P., Moser, E. I. & Moser, M. B. 2010. Grid cells in pre- and parasubiculum. *Nat Neurosci,* 13, 987-94.

Borhegyi, Z., Magloczky, Z., Acsady, L. & Freund, T. F. 1998. The supramammillary nucleus innervates cholinergic and GABAergic neurons in the medial septum-diagonal band of Broca complex. *Neuroscience,* 82, 1053-65.

Brandon, M. P., Bogaard, A. R., Libby, C. P., Connerney, M. A., Gupta, K. & Hasselmo, M. E. 2011. Reduction of theta rhythm dissociates grid cell spatial periodicity from directional tuning. *Science,* 332, 595-9.

Brazhnik, E. S. & Vinogradova, O. S. 1986. Control of the neuronal rhythmic bursts in the septal pacemaker of theta-rhythm: effects of anaesthetic and anticholinergic drugs. *Brain Res,* 380, 94-106.

Brown, E. N., Kass, R. E. & Mitra, P. P. 2004. Multiple neural spike train data analysis: state-of-the-art and future challenges. *Nat Neurosci,* 7, 456-61.

Burgess, N. 2008a. Grid cells and theta as oscillatory interference: theory and predictions. *Hippocampus,* 18, 1157-74.

Burgess, N. 2008b. Spatial cognition and the brain. *Ann N Y Acad Sci,* 1124, 77-97.

Burgess, N., Barry, C. & O'keefe, J. 2007. An oscillatory interference model of grid cell firing. *Hippocampus,* 17, 801-12.

Burgess, N., Maguire, E. A. & O'keefe, J. 2002. The human hippocampus and spatial and episodic memory. *Neuron,* 35, 625-41.

Buzsaki, G. 2004. Large-scale recording of neuronal ensembles. *Nat Neurosci,* 7, 446-51.

Buzsáki, G. 2002. Theta oscillations in the hippocampus. *Neuron,* 33, 325-340.

Buzsáki, G. 2005. Theta rhythm of navigation: link between path integration and landmark navigation, episodic and semantic memory. *Hippocampus,* 15, 827-40.

Cacucci, F., Lever, C., Wills, T. J., Burgess, N. & O'keefe, J. 2004. Theta-modulated place-by-direction cells in the hippocampal formation in the rat. *J Neurosci,* 24, 8265-77.

Calabrese, A. & Paninski, L. 2011. Kalman filter mixture model for spike sorting of non-stationary data. *J Neurosci Methods,* 196, 159-69.

Celeux, G. & Govaert, G. 1992. A classification EM algorithm for clustering and two stochastic versions. *Computational Statistics & Data Analysis,* 14, 315-332.

Chandra, R. & Optican, L. M. 1997. Detection, classification, and superposition resolution of action potentials in multiunit single-channel recordings by an on-line real-time neural network. *IEEE Trans Biomed Eng,* 44, 403-12.

Cheeseman, P. & Stutz, J. 1996. Bayesian classification (AutoClass): theory and results. *Advances in knowledge discovery and data mining.* American Association for Artificial Intelligence.

Chelaru, M. I. & Jog, M. S. 2005. Spike source localization with tetrodes. *J Neurosci Methods,* 142, 305-15.

Chen, C., Zhang, L., Bu, J., Wang, C. & Chen, W. 2010. Constrained Laplacian Eigenmap for dimensionality reduction. *Neurocomputing,* 73, 951-958.

Cheng, Y. 1995. Mean Shift, Mode Seeking, and Clustering. *IEEE Transactions on Pattern Analysis and Machine Intelligence,* 17, 790 - 799.

Christian, E. P. & Deadwyler, S. A. 1986. Behavioral functions and hippocampal cell types: evidence for two nonoverlapping populations in the rat. *J Neurophysiol,* 55, 331-48.

Comaniciu, D. & Meer, P. 2002. Mean shift: a robust approach toward feature space analysis. *Pattern Analysis and Machine Intelligence, IEEE Transactions on,* 24, 603-619.

Cruce, J. A. 1977. An autoradiographic study of the descending connections of the mammillary nuclei of the rat. *J Comp Neurol,* 176, 631-44.

Csicsvari, J., Henze, D. A., Jamieson, B., Harris, K. D., Sirota, A., Bartho, P., Wise, K. D. & Buzsaki, G. 2003. Massively parallel recording of unit and local field potentials with silicon-based electrodes. *J Neurophysiol,* 90**,** 1314-23.

D'hollander, E. H. & Orban, G. A. 1979. Spike recognition and on-line classification by unsupervised learning system. *IEEE Trans Biomed Eng,* 26**,** 279-84.

Delescluse, M. & Pouzat, C. 2006. Efficient spike-sorting of multi-state neurons using inter-spike intervals information. *J Neurosci Methods,* 150**,** 16-29.

Dilorenzo, D. J. & Dronzino, J. D. (eds.) 2008. *neuroengineering*: CRC Press.

Ding, W. & Yuan, J. 2008. Spike sorting based on multi-class support vector machine with superposition resolution. *Med Biol Eng Comput,* 46**,** 139-45.

Dinning, G. J. & Sanderson, A. C. 1981. Real-time classification of multiunit neural signals using reduced feature sets. *IEEE Trans Biomed Eng,* 28**,** 804-12.

Einevoll, G. T., Franke, F., Hagen, E., Pouzat, C. & Harris, K. D. (in press). Towards reliable spike-train recordings from thousands of neurons with multielectrodes. *Current Opinion in Neurobiology.*

Ekstrom, A. D., Meltzer, J., Mcnaughton, B. L. & Barnes, C. A. 2001. NMDA receptor antagonism blocks experience-dependent expansion of hippocampal ''place fields''. *Neuron,* 31**,** 631–638.

Fanselow, E. E., Sameshima, K., Baccala, L. A. & Nicolelis, M. A. 2001. Thalamic bursting in rats during different awake behavioral states. *Proc Natl Acad Sci U S A,* 98**,** 15330-5.

Farashi, S., Abolhassani, M. D., Salimpour, Y. & Alirezaie, J. 2010. Combination of PCA and undecimated wavelet transform for neural data processing. *Conf Proc IEEE Eng Med Biol Soc,* 2010**,** 6666-9.

Fee, M. S., Mitra, P. P. & Kleinfeld, D. 1996a. Automatic sorting of multiple unit neuronal signals in the presence of anisotropic and non-Gaussian variability. *J Neurosci Methods,* 69, 175-88.

Fee, M. S., Mitra, P. P. & Kleinfeld, D. 1996b. Variability of extracellular spike waveforms of cortical neurons. *J Neurophysiol,* 76, 3823-33.

Fenton, A. A., Lytton, W. W., Barry, J. M., Lenck-Santini, P.-P., Zinyuk, L. E., Kubík, S., Bures, J., Poucet, B., Muller, R. U. & Olypher, A. V. 2010. Attention-like modulation of hippocampus place cell discharge. *J Neurosci,* 30, 4613-4625.

Franke, F., Natora, M., Boucsein, C., Munk, M. H. & Obermayer, K. 2010. An online spike detection and spike classification algorithm capable of instantaneous resolution of overlapping spikes. *J Comput Neurosci,* 29, 127-48.

Friedman, M. 1937. The Use of Ranks to Avoid the Assumption of Normality Implicit in the Analysis of Variance. *Journal of the American Statistical Association,* 32, 675-701.

Fyhn, M., Molden, S., Witter, M. P., Moser, E. I. & Moser, M. B. 2004. Spatial representation in the entorhinal cortex. *Science,* 305, 1258-64.

Gerstein, G. L. & Clark, W. A. 1964. Simultaneous Studies of Firing Patterns in Several Neurons. *Science,* 143, 1325-7.

Ghanbari, Y., Papamichalis, P. & Spence, L. 2010. Graph-Spectrum-Based Neural Spike Features for Stereotrodes and Tetrodes. *IEEE International Conference on Acoustics, Speech, and Signal Processing* 598-601.

Ghanbari, Y., Papamichalis, P. E. & Spence, L. 2011. Graph-Laplacian features for neural waveform classification. *IEEE Trans Biomed Eng,* 58, 1365-72.

Ghanbari, Y., Spence, L. & Papamichalis, P. 2009. A graph-Laplacian-based feature extraction algorithm for neural spike sorting. *Conf Proc IEEE Eng Med Biol Soc,* 2009**,** 3142-5.

Gibson, S., Judy, J. W. & Markovic, D. 2008. Comparison of spike-sorting algorithms for future hardware implementation. *Conf Proc IEEE Eng Med Biol Soc,* 2008**,** 5015-20.

Gibson, S., Judy, J. W. & Markovic, D. 2010. Technology-aware algorithm design for neural spike detection, feature extraction, and dimensionality reduction. *IEEE Trans Neural Syst Rehabil Eng,* 18**,** 469-78.

Glaser, E. M. & Marks, W. B. 1968. On-line separation of interleaved neuronal pulse sequences. *Data Acquisition Process Biol Med,* 5.

Golob, E. J. & Taube, J. S. 1997. Head direction cells and episodic spatial information in rats without a hippocampus. *Proc Natl Acad Sci U S A,* 94**,** 7645-50.

Gonzalo-Ruiz, A., Alonso, A., Sanz, J. M. & Llinas, R. R. 1992. Afferent projections to the mammillary complex of the rat, with special reference to those from surrounding hypothalamic regions. *J Comp Neurol,* 321**,** 277-99.

Gonzalo-Ruiz, A., Morte, L. & Lieberman, A. R. 1997. Evidence for collateral projections to the retrosplenial granular cortex and thalamic reticular nucleus from glutamate and/or aspartate-containing neurons of the anterior thalamic nuclei in the rat. *Exp Brain Res,* 116**,** 63-72.

Goodridge, J. P., Dudchenko, P. A., Worboys, K. A., Golob, E. J. & Taube, J. S. 1998. Cue control and head direction cells. *Behav Neurosci,* 112**,** 749-61.

Goodridge, J. P. & Taube, J. S. 1997. Interaction between the postsubiculum and anterior thalamus in the generation of head direction cell activity. *J Neurosci,* 17**,** 9315-30.

Gozani, S. N. & Miller, J. P. 1994. Optimal discrimination and classification of neuronal action potential waveforms from multiunit, multichannel recordings using software-based linear filters. *IEEE Trans Biomed Eng,* 41, 358-72.

Gray, C. M., Maldonado, P. E., Wilson, M. & Mcnaughton, B. 1995. Tetrodes markedly improve the reliability and yield of multiple single-unit isolation from multi-unit recordings in cat striate cortex. *J Neurosci Methods,* 63, 43-54.

Guido, W. & Weyand, T. 1995. Burst responses in thalamic relay cells of the awake behaving cat. *J Neurophysiol,* 74, 1782-6.

Gustavsson, A., Svensson, M., Jacobi, F., Allgulander, C., Alonso, J., Beghi, E., Dodel, R., Ekman, M., Faravelli, C., Fratiglioni, L., Gannon, B., Jones, D. H., Jennum, P., Jordanova, A., Jönsson, L., Karampampa, K., Knapp, M., Kobelt, G., Kurth, T., Lieb, R., Linde, M., Ljungcrantz, C., Maercker, A., Melin, B., Moscarelli, M., Musayev, A., Norwood, F., Preisig, M., Pugliatti, M., Rehm, J., Salvador-Carulla, L., Schlehofer, B., Simon, R., Steinhausen, H.-C., Stovner, L. J., Vallat, J.-M., Den Bergh, P. V., Van Os, J., Vos, P., Xu, W., Wittchen, H.-U., Jönsson, B. & Olesen, J. 2011. Cost of disorders of the brain in Europe 2010. *European Neuropsychopharmacology,* 21, 718-779.

Hafting, T., Fyhn, M., Molden, S., Moser, M. B. & Moser, E. I. 2005. Microstructure of a spatial map in the entorhinal cortex. *Nature,* 436, 801-6.

Halliday, D. M., Rosenberg, J. R., Amjad, A. M., Breeze, P., Conway, B. A. & Farmer, S. F. 1995. A framework for the analysis of mixed time series/point process data--theory and application to the study of physiological tremor, single motor unit discharges and electromyograms. *Prog Biophys Mol Biol,* 64, 237-78.

Harding, A., Halliday, G., Caine, D. & Kril, J. 2000. Degeneration of anterior thalamic nuclei differentiates alcoholics with amnesia. *Brain,* 123 (Pt 1), 141-54.

Hargreaves, E. L., Yoganarasimha, D. & Knierim, J. J. 2007. Cohesiveness of spatial and directional representations recorded from neural ensembles in the anterior thalamus, parasubiculum, medial entorhinal cortex, and hippocampus. *Hippocampus,* 17, 826-41.

Harris, K. D. Available: http://klustakwik.sourceforge.net/ [Accessed].

Harris, K. D., Henze, D. A., Csicsvari, J., Hirase, H. & Buzsaki, G. 2000. Accuracy of tetrode spike separation as determined by simultaneous intracellular and extracellular measurements. *J Neurophysiol,* 84, 401-14.

Harris, K. D., Hirase, H., Leinekugel, X., Henze, D. A. & Buzsáki, G. 2001. Temporal Interaction between Single Spikes and Complex Spike Bursts in Hippocampal Pyramidal Cells. *Neuron,* 32, 141-149.

Hasselmo, M. E. & Brandon, M. P. 2008. Linking cellular mechanisms to behavior: entorhinal persistent spiking and membrane potential oscillations may underlie path integration, grid cell firing, and episodic memory. *Neural Plast,* 2008, 658323.

Hayakawa, T. & Zyo, K. 1984. Comparative anatomical study of the tegmentomammillary projections in some mammals: a horseradish peroxidase study. *Brain Res,* 300, 335-49.

Henze, D. A., Borhegyi, Z., Csicsvari, J., Mamiya, A., Harris, K. D. & Buzsaki, G. 2000. Intracellular features predicted by extracellular recordings in the hippocampus in vivo. *J Neurophysiol,* 84, 390-400.

Herbst, J. A., Gammeter, S., Ferrero, D. & Hahnloser, R. H. 2008. Spike sorting with hidden Markov models. *J Neurosci Methods,* 174**,** 126-34.

Hodgkin, A. L. & Huxley, A. F. 1952. A quantitative description of membrane current and its application to conduction and excitation in nerve. *The Journal of physiology,* 117**,** 500-544.

Holtzheimer, P. E. & Mayberg, H. S. 2011. Deep brain stimulation for psychiatric disorders. *Annu Rev Neurosci,* 34**,** 289-307.

Horton, P. M., Nicol, A. U., Kendrick, K. M. & Feng, J. F. 2007. Spike sorting based upon machine learning algorithms (SOMA). *J Neurosci Methods,* 160**,** 52-68.

Hulata, E., Segev, R. & Ben-Jacob, E. 2002. A method for spike sorting and detection based on wavelet packets and Shannon's mutual information. *J Neurosci Methods,* 117**,** 1-12.

Hulata, E., Segev, R., Shapira, Y., Benveniste, M. & Ben-Jacob, E. 2000. Detection and sorting of neural spikes using wavelet packets. *Phys Rev Lett,* 85**,** 4637-40.

Ishizuka, N. 2001. Laminar organization of the pyramidal cell layer of the subiculum in the rat. *J Comp Neurol,* 435**,** 89-110.

Johnson, R. A. & Wichern, D. W. 2007. Applied Multivariate Statistical Analysis. New Jersey: Prentice Hall.

Jung, M. W., Wiener, S. I. & Mcnaughton, B. L. 1994. Comparison of spatial firing characteristics of units in dorsal and ventral hippocampus of the rat. *J Neurosci,* 14**,** 7347-56.

Kandel, E., Schwartz, J. H. & Jessell, T. 2000. *Principles of Neural Science*, McGraw-Hill Medical.

Kepecs, A., Uchida, N. & Mainen, Z. F. 2007. Rapid and precise control of sniffing during olfactory discrimination in rats. *J Neurophysiol,* 98**,** 205-13.

Kim, K. H. 2006. Improved Algorithm for Fully-automated Neural Spike Sorting based on Projection Pursuit and Gaussian Mixture Model. *Int. J. Control Autom. Syst.* , 4 705-13.

Kim, K. H. & Kim, S. J. 2003. Method for unsupervised classification of multiunit neural signal recording under low signal-to-noise ratio. *IEEE Trans Biomed Eng,* 50, 421-31.

Kirk, I. J. & Mcnaughton, N. 1991. Supramammillary cell firing and hippocampal rhythmical slow activity. *Neuroreport,* 2, 723-5.

Kirk, I. J., Oddie, S. D., Konopacki, J. & Bland, B. H. 1996. Evidence for differential control of posterior hypothalamic, supramammillary, and medial mammillary theta-related cellular discharge by ascending and descending pathways. *J Neurosci,* 16, 5547-54.

Knierim, J. J., Kudrimoti, H. S. & Mcnaughton, B. L. 1995. Place cells, head direction cells, and the learning of landmark stability. *J Neurosci,* 15, 1648-59.

Knierim, J. J., Kudrimoti, H. S. & Mcnaughton, B. L. 1998. Interactions between idiothetic cues and external landmarks in the control of place cells and head direction cells. *J Neurophysiol,* 80, 425-46.

Kocsis, B., Di Prisco, G. V. & Vertes, R. P. 2001. Theta synchronization in the limbic system: the role of Gudden's tegmental nuclei. *Eur J Neurosci,* 13, 381-8.

Kocsis, B. & Vertes, R. P. 1994. Characterization of neurons of the supramammillary nucleus and mammillary body that discharge rhythmically with the hippocampal theta rhythm in the rat. *J Neurosci,* 14, 7040-52.

Kruger, L., Saporta, S. & Swanson, L. W. 1995. Photographic Atlas of the Rat Brain: The Cell and Fiber Architecture Illustrated in Three Planes with Stereotaxic Coordinates, 299 pp. *Cambridge University Press, New York.*

Kudrimoti, H. S., Knierim, J. J. & Mcnaughton, B. L. 1996. Dynamics of visual cue control over head direction cells. *Ann N Y Acad Sci,* 781, 642-4.

Lai, H. Y., Chen, Y. Y., Lin, S. H., Lo, Y. C., Tsang, S., Chen, S. Y., Zhao, W. T., Chao, W. H., Chang, Y. C., Wu, R., Shih, Y. Y., Tsai, S. T. & Jaw, F. S. 2011. Automatic spike sorting for extracellular electrophysiological recording using unsupervised single linkage clustering based on grey relational analysis. *J Neural Eng,* 8, 036003.

Letelier, J. C. & Weber, P. P. 2000. Spike sorting based on discrete wavelet transform coefficients. *J Neurosci Methods,* 101, 93-106.

Leutgeb, J. K., Leutgeb, S., Moser, M.-B. & Moser, E. I. 2007. Pattern separation in the dentate gyrus and CA3 of the hippocampus. *Science,* 315, 961-966.

Lewicki, M. S. 1994. Bayesian Modeling and Classification of Neural Signals. *Neural Computation,* 6, 1005-1030.

Lewicki, M. S. 1998. A review of methods for spike sorting: the detection and classification of neural action potentials. *Network,* 9, R53-78.

Lin, W. S., Tillery, S. H. & Jiping, H. Year. Stability of the chronic multichannel recording neuron signals. *In:* Engineering in Medicine and Biology Society, 2003. Proceedings of the 25th Annual International Conference of the IEEE, 17-21 Sept. 2003 2003. 2193-2196 Vol.3.

Linderman, M. D., Gilja, V., Santhanam, G., Afshar, A., Ryu, S., Meng, T. H. & Shenoy, K. V. Year. Neural Recording Stability of Chronic Electrode Arrays in Freely Behaving Primates. *In:* Engineering in Medicine and Biology Society, 2006. EMBS '06. 28th Annual International Conference of the IEEE, Aug. 30 2006-Sept. 3 2006 2006. 4387-4391.

Lyttle, D. & Fellous, J. M. 2011. A new similarity measure for spike trains: sensitivity to bursts and periods of inhibition. *J Neurosci Methods,* 199, 296-309.

Markus, E. J., Barnes, C. A., Mcnaughton, B. L., Gladden, V. L. & Skaggs, W. E. 1994. Spatial information content and reliability of hippocampal CA1 neurons: effects of visual input. *Hippocampus,* 4, 410-21.

Martinez, J., Pedreira, C., Ison, M. J. & Quian Quiroga, R. 2009. Realistic simulation of extracellular recordings. *J Neurosci Methods,* 184, 285-93.

Mcnaughton, B. L., O'keefe, J. & Barnes, C. A. 1983. The stereotrode: a new technique for simultaneous isolation of several single units in the central nervous system from multiple unit records. *J Neurosci Methods,* 8, 391-7.

Mehta, M. R., Quirk, M. C. & Wilson, M. A. 2000. Experience-dependent asymmetric shape of hippocampal receptive fields. *Neuron,* 25, 707–715.

Mitra, P. P. & Bokil, H. 2009. *Observed brain dynamics,* New York, Oxford University Press.

Mizumori, S. J. & Williams, J. D. 1993. Directionally selective mnemonic properties of neurons in the lateral dorsal nucleus of the thalamus of rats. *J Neurosci,* 13, 4015-28.

Moffitt, M. A. & Mcintyre, C. C. 2005. Model-based analysis of cortical recording with silicon microelectrodes. *Clin Neurophysiol,* 116, 2240-50.

Moser, E. 2007. Grid cells. *Scholarpedia,* 2, 3394.

Moser, E. I., Kropff, E. & Moser, M. B. 2008. Place cells, grid cells, and the brain's spatial representation system. *Annu Rev Neurosci,* 31, 69-89.

Muller, R. U., Bostock, E., Taube, J. S. & Kubie, J. L. 1994. On the directional firing properties of hippocampal place cells. *J Neurosci,* 14, 7235-51.

Muller, R. U. & Kubie, J. L. 1989. The firing of hippocampal place cells predicts the future position of freely moving rats. *J Neurosci,* 9**,** 4101-10.

Mullins, E. 2003. *Statistics for the Quality Control Chemistry Laboratory*, The Royal Society of Chemistry.

Nguyen, D. P., Frank, L. M. & Brown, E. N. 2003. An application of reversible-jump Markov chain Monte Carlo to spike classification of multi-unit extracellular recordings. *Network,* 14**,** 61-82.

Nicolelis, M. A., Baccala, L. A., Lin, R. C. & Chapin, J. K. 1995. Sensorimotor encoding by synchronous neural ensemble activity at multiple levels of the somatosensory system. *Science,* 268**,** 1353-8.

Nicolelis, M. A., Dimitrov, D., Carmena, J. M., Crist, R., Lehew, G., Kralik, J. D. & Wise, S. P. 2003. Chronic, multisite, multielectrode recordings in macaque monkeys. *Proc Natl Acad Sci U S A,* 100**,** 11041-6.

O'keefe, J. & Dostrovsky, J. 1971. The hippocampus as a spatial map. Preliminary evidence from unit activity in the freely-moving rat. *Brain Research,* 34**,** 171-175.

O'keefe, J. & Recce, M. L. 1993. Phase relationship between hippocampal place units and the EEG theta rhythm. *Hippocampus,* 3**,** 317-30.

Pakhira, M. K., Bandyopadhyay, S. & Maulik, U. 2004. Validity index for crisp and fuzzy clusters. *Pattern Recognition,* 37**,** 487-501.

Pan, W. X. & Mcnaughton, N. 1997. The medial supramammillary nucleus, spatial learning and the frequency of hippocampal theta activity. *Brain Res,* 764**,** 101-8.

Pan, W. X. & Mcnaughton, N. 2002. The role of the medial supramammillary nucleus in the control of hippocampal theta activity and behaviour in rats. *Eur J Neurosci,* 16, 1797-809.

Pavlov, A., Makarov, V., Makarova, I. & Panetsos, F. 2007. Sorting of neural spikes: When wavelet based methods outperform principal component analysis. *Natural Computing,* 6, 269-281.

Peng, C. C., Sabharwal, P. & Bashirullah, R. 2008. Neural cache: a low-power online digital spike-sorting architecture. *Conf Proc IEEE Eng Med Biol Soc,* 2008, 2004-7.

Polikov, V. S., Tresco, P. A. & Reichert, W. M. 2005. Response of brain tissue to chronically implanted neural electrodes. *J Neurosci Methods,* 148, 1-18.

Porada, I., Bondar, I., Spatz, W. B. & Kruger, J. 2000. Rabbit and monkey visual cortex: more than a year of recording with up to 64 microelectrodes. *J Neurosci Methods,* 95, 13-28.

Pouzat, C., Delescluse, M., Viot, P. & Diebolt, J. 2004. Improved spike-sorting by modeling firing statistics and burst-dependent spike amplitude attenuation: a Markov chain Monte Carlo approach. *J Neurophysiol,* 91, 2910-28.

Pouzat, C., Mazor, O. & Laurent, G. 2002. Using noise signature to optimize spike-sorting and to assess neuronal classification quality. *J Neurosci Methods,* 122, 43-57.

Quian Quiroga, R. 2009. What is the real shape of extracellular spikes? *J Neurosci Methods,* 177, 194-8.

Quian Quiroga, R. & Panzeri, S. 2009. Extracting information from neuronal populations: information theory and decoding approaches. *Nat Rev Neurosci,* 10, 173-85.

Quiroga, R. Q., Nadasdy, Z. & Ben-Shaul, Y. 2004. Unsupervised spike detection and sorting with wavelets and superparamagnetic clustering. *Neural Comput,* 16, 1661-87.

Ramcharan, E. J., Gnadt, J. W. & Sherman, S. M. 2005. Higher-order thalamic relays burst more than first-order relays. *Proc Natl Acad Sci U S A,* 102, 12236-41.

Rizk, M., Bossetti, C. A., Jochum, T. A., Callender, S. H., Nicolelis, M. A., Turner, D. A. & Wolf, P. D. 2009. A fully implantable 96-channel neural data acquisition system. *J Neural Eng,* 6, 026002.

Roberts, W. M. & Hartline, D. K. 1975. Separation of multi-unit nerve impulse trains by a multi-channel linear filter algorithm. *Brain Res,* 94, 141-9.

Royer, S., Sirota, A., Patel, J. & Buzsaki, G. 2010. Distinct representations and theta dynamics in dorsal and ventral hippocampus. *J Neurosci,* 30, 1777-87.

Rutishauser, U., Schuman, E. M. & Mamelak, A. N. 2006. Online detection and sorting of extracellularly recorded action potentials in human medial temporal lobe recordings, in vivo. *J Neurosci Methods,* 154, 204-24.

Santhanam, G., Linderman, M. D., Gilja, V., Afshar, A., Ryu, S. I., Meng, T. H. & Shenoy, K. V. 2007. HermesB: a continuous neural recording system for freely behaving primates. *IEEE Trans Biomed Eng,* 54, 2037-50.

Sargolini, F., Fyhn, M., Hafting, T., Mcnaughton, B. L., Witter, M. P., Moser, M. B. & Moser, E. I. 2006. Conjunctive representation of position, direction, and velocity in entorhinal cortex. *Science,* 312, 758-62.

Sato, T., Suzuki, T. & Mabuchi, K. 2007. Fast automatic template matching for spike sorting based on Davies-Bouldin validation indices. *Conf Proc IEEE Eng Med Biol Soc,* 2007, 3200-3.

Schwartz, A. B., Cui, X. T., Weber, D. J. & Moran, D. W. 2006. Brain-controlled interfaces: movement restoration with neural prosthetics. *Neuron,* 52, 205-20.

Segev, R., Goodhouse, J., Puchalla, J. & Berry, M. J., 2nd 2004. Recording spikes from a large fraction of the ganglion cells in a retinal patch. *Nat Neurosci,* 7, 1154-61.

Seki, M. & Zyo, K. 1984. Anterior thalamic afferents from the mamillary body and the limbic cortex in the rat. *J Comp Neurol,* 229, 242-56.

Sharp, P. E. 1996. Multiple spatial/behavioral correlates for cells in the rat postsubiculum: multiple regression analysis and comparison to other hippocampal areas. *Cereb Cortex,* 6, 238-59.

Sheldon, M. R., Fillyaw, M. J. & Thompson, W. D. 1996. The use and interpretation of the Friedman test in the analysis of ordinal-scale data in repeated measures designs. *Physiother Res Int,* 1, 221-8.

Sherman, S. M. 2001. Tonic and burst firing: dual modes of thalamocortical relay. *Trends Neurosci,* 24, 122-6.

Sherman, S. M. & Guillery, R. W. 1996. Functional organization of thalamocortical relays. *J Neurophysiol,* 76, 1367-95.

Shibata, H. 1993a. Direct projections from the anterior thalamic nuclei to the retrohippocampal region in the rat. *J Comp Neurol,* 337, 431-45.

Shibata, H. 1993b. Efferent projections from the anterior thalamic nuclei to the cingulate cortex in the rat. *J Comp Neurol,* 330, 533-42.

Shoham, S., Fellows, M. R. & Normann, R. A. 2003. Robust, automatic spike sorting using mixtures of multivariate t-distributions. *J Neurosci Methods,* 127, 111-22.

Skaggs, W. E., Mcnaughton, B. L. & Gothard, K. M. 1993. An Information-Theoretic Approach to Deciphering the Hippocampal Code. *Advances in Neural Information Processing Systems 5, [NIPS Conference].* Morgan Kaufmann Publishers Inc.

Skaggs, W. E., Mcnaughton, B. L., Wilson, M. A. & Barnes, C. A. 1996. Theta phase precession in hippocampal neuronal populations and the compression of temporal sequences. *Hippocampus,* 6, 149–172.

Spiegel, M. R., Schiller, J. J. & Srinivasan, R. A. 2009. Schaum's Outlines - Probability and Statistics (3rd Edition). McGraw-Hill.

Stackman, R. W., Golob, E. J., Bassett, J. P. & Taube, J. S. 2003. Passive transport disrupts directional path integration by rat head direction cells. *J Neurophysiol,* 90, 2862-74.

Stackman, R. W. & Taube, J. S. 1997. Firing properties of head direction cells in the rat anterior thalamic nucleus: dependence on vestibular input. *J Neurosci,* 17, 4349-58.

Stein, R. B., Andreassen, S. & Oguztoreli, M. N. 1979. Mathematical analysis of optimal multichannel filtering for nerve signals. *Biol Cybern,* 32, 19-24.

Steriade, M., Dossi, R. C. & Nunez, A. 1991. Network modulation of a slow intrinsic oscillation of cat thalamocortical neurons implicated in sleep delta waves: cortically induced synchronization and brainstem cholinergic suppression. *J Neurosci,* 11, 3200-17.

Stevenson, I. H. & Kording, K. P. 2011. How advances in neural recording affect data analysis. *Nat Neurosci,* 14, 139-142.

Suner, S., Fellows, M. R., Vargas-Irwin, C., Nakata, G. K. & Donoghue, J. P. 2005. Reliability of signals from a chronically implanted, silicon-based electrode

array in non-human primate primary motor cortex. *IEEE Trans Neural Syst Rehabil Eng,* 13, 524-41.

Swadlow, H. A. & Gusev, A. G. 2001. The impact of 'bursting' thalamic impulses at a neocortical synapse. *Nat Neurosci,* 4, 402-8.

Swanson, L. W. & Cowan, W. M. 1977. An autoradiographic study of the organization of the efferent connections of the hippocampal formation in the rat. *J Comp Neurol,* 172, 49-84.

Takahashi, S., Anzai, Y. & Sakurai, Y. 2003a. Automatic sorting for multi-neuronal activity recorded with tetrodes in the presence of overlapping spikes. *J Neurophysiol,* 89, 2245-58.

Takahashi, S., Anzai, Y. & Sakurai, Y. 2003b. A new approach to spike sorting for multi-neuronal activities recorded with a tetrode--how ICA can be practical. *Neurosci Res,* 46, 265-72.

Takahashi, S. & Sakurai, Y. 2005. Real-time and automatic sorting of multi-neuronal activity for sub-millisecond interactions in vivo. *Neuroscience,* 134, 301-15.

Takekawa, T., Isomura, Y. & Fukai, T. 2010. Accurate spike sorting for multi-unit recordings. *Eur J Neurosci,* 31, 263-72.

Talk, A., Kang, E. & Gabriel, M. 2004. Independent generation of theta rhythm in the hippocampus and posterior cingulate cortex. *Brain Res,* 1015, 15-24.

Taube, J. S. 1995. Head direction cells recorded in the anterior thalamic nuclei of freely moving rats. *J Neurosci,* 15, 70-86.

Taube, J. S. 2007. The head direction signal: origins and sensory-motor integration. *Annu Rev Neurosci,* 30, 181-207.

Taube, J. S. 2010. Interspike interval analyses reveal irregular firing patterns at short, but not long, intervals in rat head direction cells. *J Neurophysiol,* 104, 1635-48.

Taube, J. S., Muller, R. U. & Ranck, J. B., Jr. 1990. Head-direction cells recorded from the postsubiculum in freely moving rats. I. Description and quantitative analysis. *J Neurosci,* 10, 420-35.

Thakur, P. H., Lu, H., Hsiao, S. S. & Johnson, K. O. 2007. Automated optimal detection and classification of neural action potentials in extra-cellular recordings. *J Neurosci Methods,* 162, 364-76.

Theodoridis, S. & Koutroumbas, K. 1998. *Pattern recognition,* San Diego,, Academic Press.

Tsanov, M., Chah, E., Wright, N., Vann, S. D., Reilly, R., Erichsen, J. T., Aggleton, J. P. & O'mara, S. M. 2011. Oscillatory entrainment of thalamic neurons by theta rhythm in freely moving rats. *J Neurophysiol,* 105, 4-17.

Van Der Meer, M. A., Knierim, J. J., Yoganarasimha, D., Wood, E. R. & Van Rossum, M. C. 2007. Anticipation in the rodent head direction system can be explained by an interaction of head movements and vestibular firing properties. *J Neurophysiol,* 98, 1883-97.

Van Der Werf, Y. D., Witter, M. P., Uylings, H. B. & Jolles, J. 2000. Neuropsychology of infarctions in the thalamus: a review. *Neuropsychologia,* 38, 613-27.

Van Groen, T., Kadish, I. & Wyss, J. M. 1999. Efferent connections of the anteromedial nucleus of the thalamus of the rat. *Brain Res Brain Res Rev,* 30, 1-26.

Van Groen, T. & Wyss, J. M. 1990. The connections of presubiculum and parasubiculum in the rat. *Brain Res,* 518, 227-43.

Van Groen, T. & Wyss, J. M. 1995. Projections from the anterodorsal and anteroventral nucleus of the thalamus to the limbic cortex in the rat. *J Comp Neurol,* 358, 584-604.

Vann, S. D. & Aggleton, J. P. 2004. The mammillary bodies: two memory systems in one? *Nat Rev Neurosci,* 5, 35-44.

Vargas-Irwin, C. & Donoghue, J. P. 2007. Automated spike sorting using density grid contour clustering and subtractive waveform decomposition. *J Neurosci Methods,* 164, 1-18.

Ventura, V. 2009. Automatic spike sorting using tuning information. *Neural Comput,* 21, 2466-501.

Verhagen, J. V., Wesson, D. W., Netoff, T. I., White, J. A. & Wachowiak, M. 2007. Sniffing controls an adaptive filter of sensory input to the olfactory bulb. *Nat Neurosci,* 10, 631-9.

Vertes, R. P. 1992. PHA-L analysis of projections from the supramammillary nucleus in the rat. *J Comp Neurol,* 326, 595-622.

Vertes, R. P., Albo, Z. & Viana Di Prisco, G. 2001. Theta-rhythmically firing neurons in the anterior thalamus: implications for mnemonic functions of Papez's circuit. *Neuroscience,* 104, 619-25.

Vertes, R. P., Hoover, W. B. & Viana Di Prisco, G. 2004. Theta rhythm of the hippocampus: subcortical control and functional significance. *Behav Cogn Neurosci Rev,* 3, 173-200.

Von Luxburg, U. 2007. A tutorial on spectral clustering. *Statistics and Computing,* 17, 395-416.

Waldert, S., Pistohl, T., Braun, C., Ball, T., Aertsen, A. & Mehring, C. 2009. A review on directional information in neural signals for brain-machine interfaces. *J Physiol Paris,* 103, 244-54.

Wang, G. L. & Liang, P. J. 2005. Method for robust spike sorting with overlap decomposition. *Conf Proc IEEE Eng Med Biol Soc,* 2, 2013-6.

Wang, G. L., Zhou, Y., Chen, A. H., Zhang, P. M. & Liang, P. J. 2006. A robust method for spike sorting with automatic overlap decomposition. *IEEE Trans Biomed Eng,* 53, 1195-8.

Weiland, J. D. & Humayun, M. S. 2008. Visual Prosthesis. *Proceedings of the IEEE,* 96, 1076-1084.

Wheeler, B. C. & Heetderks, W. J. 1982. A comparison of techniques for classification of multiple neural signals. *IEEE Trans Biomed Eng,* 29, 752-9.

Williams, J. C., Rennaker, R. L. & Kipke, D. R. 1999. Stability of chronic multichannel neural recordings: Implications for a long-term neural interface. *Neurocomputing,* 26-27, 1069-1076.

Wittchen, H. U., Jacobi, F., Rehm, J., Gustavsson, A., Svensson, M., Jonsson, B., Olesen, J., Allgulander, C., Alonso, J., Faravelli, C., Fratiglioni, L., Jennum, P., Lieb, R., Maercker, A., Van Os, J., Preisig, M., Salvador-Carulla, L., Simon, R. & Steinhausen, H. C. 2011. The size and burden of mental disorders and other disorders of the brain in Europe 2010. *Eur Neuropsychopharmacol,* 21, 655-79.

Witter, M. P., Ostendorf, R. H. & Groenewegen, H. J. 1990. Heterogeneity in the Dorsal Subiculum of the Rat. Distinct Neuronal Zones Project to Different Cortical and Subcortical Targets. *Eur J Neurosci,* 2, 718-725.

Wood, F. & Black, M. J. 2008. A nonparametric Bayesian alternative to spike sorting. *J Neurosci Methods,* 173**,** 1-12.

Wood, F., Black, M. J., Vargas-Irwin, C., Fellows, M. & Donoghue, J. P. 2004. On the variability of manual spike sorting. *IEEE Trans Biomed Eng,* 51**,** 912-8.

Wood, F., Goldwater, S. & Black, M. J. 2006. A non-parametric Bayesian approach to spike sorting. *Conf Proc IEEE Eng Med Biol Soc,* 1**,** 1165-8.

Xiaofei, H. & Partha, N. Year. Locality Preserving Projections. *In:* Proc. Conf. Advances in Neural Information Processing Systems, 2003.

Xiong, H., Wu, J. & Chen, J. 2009. K-means clustering versus validation measures: a data-distribution perspective. *IEEE Trans Syst Man Cybern B Cybern,* 39**,** 318-31.

Yang, X. W. & Shamma, S. A. 1988. A totally automated system for the detection and classification of neural spikes. *IEEE Trans Biomed Eng,* 35**,** 806-16.

Yang, Z., Hoang, L., Zhao, Q., Keefer, E. & Liu, W. 2011. 1/f neural noise reduction and spike feature extraction using a subset of informative samples. *Ann Biomed Eng,* 39**,** 1264-77.

Yang, Z., Zhao, Q. & Liu, W. 2009a. Energy based evolving mean shift algorithm for neural spike classification. *Conf Proc IEEE Eng Med Biol Soc,* 2009**,** 966-9.

Yang, Z., Zhao, Q. & Liu, W. 2009b. Improving spike separation using waveform derivatives. *J Neural Eng,* 6**,** 046006.

Yen, C. C., Shann, W. C., Yen, C. T. & Tsai, M. L. 2009. Spike sorting by a minimax reduced feature set based on finite differences. *J Physiol Sci,* 59**,** 143-7.

Yoganarasimha, D. & Knierim, J. J. 2005. Coupling between place cells and head direction cells during relative translations and rotations of distal landmarks. *Exp Brain Res,* 160**,** 344-59.

Yoganarasimha, D., Yu, X. & Knierim, J. J. 2006. Head direction cell representations maintain internal coherence during conflicting proximal and distal cue rotations: comparison with hippocampal place cells. *J Neurosci,* 26, 622-31.

Zhang, P. M., Wu, J. Y., Zhou, Y., Liang, P. J. & Yuan, J. Q. 2004. Spike sorting based on automatic template reconstruction with a partial solution to the overlapping problem. *J Neurosci Methods,* 135, 55-65.

Zhou, D. D. & Greenbaum, E. (eds.) 2009. *Implantable Neural Prostheses 1,* New York: Springer.

Zouridakis, G. & Tam, D. C. 1997. Multi-unit spike discrimination using wavelet transforms. *Comput Biol Med,* 27, 9-18.

Zugaro, M. B., Berthoz, A. & Wiener, S. I. 2002. Peak firing rates of rat anterodorsal thalamic head direction cells are higher during faster passive rotations. *Hippocampus,* 12, 481-6.

Zugaro, M. B., Tabuchi, E., Fouquier, C., Berthoz, A. & Wiener, S. I. 2001. Active locomotion increases peak firing rates of anterodorsal thalamic head direction cells. *J Neurophysiol,* 86, 692-702.

Zugaro, M. B., Tabuchi, E. & Wiener, S. I. 2000. Influence of conflicting visual, inertial and substratal cues on head direction cell activity. *Exp Brain Res,* 133, 198-208.

Appendix A: List of MATLAB codes

Below is a list of main MATLAB codes used/developed during this PhD:

File name	Description
detailed_analysisV2.m	Extracts basic information about all sorted spikes, and files (*.set) in a specific folder (e.g. Spike width, frequency, height, information content, also plots Autocorrelgram, spike waveform, firing maps, head-direction).
Directional_analysis.m	Provides directional analysis of cells, input a list of cells in a text file. Outputs (direction/location information content, distributive ratio, does MLM correction and plots direction polar plots.
find_burst.m	Outputs burst statics of a cell (number of bursts segments, burst times, number of burst spikes per burst).
firing_extract.m	Gets firing stats of cells (autocorrelgram, average firing).
Get_Firing_Field.m	Finds firing fields of place cells within a firing map.
Get_map_Correlation.m	Calculated correlation between firing maps of two cells.
get_spatial_information_content.m	Calculates spatial information content.
Get_ThetaIndex.m	Calculates theta index from an autocorrelgram (described in chapter 4).
Getspikelocation.m	Outputs the location of the rat when each spike was fired for a specific cell
fuf.m	Finds all files in a specific folder.
k_means.m	*k*-means clustering (described in chapter 2).
k_pbm.m	Calculates PBM index (described in chapter 2).
laplacian_eigen.m	Calculated the laplacian eigenmap (described in chapter 2).
load_axona_file.m	Imports axona files into matlab.
plot_dirs.m	Plots directional polar plots.
plot_field.m	Plots firing maps.
plot_maps_using_breakpoints	Plots firing maps using breakpoint firing rates.
plot_scatterplot_ISI.m	Plots ISI scatter plots (described in Chapter 4)
ratemap.m	Calculates firing map of a cell.
shuffle_HD.m	Shuffles the firing times of a cell to determine if

	head-directionality can appear by chance.
silence_corr.m	Calculates the correlation with pauses of firing pattern of a cells, and a continuous signal (described in Chapter 4)
sniff2phase_peaks.m	Models the sniffing as a series of cosine functions and return the phase of each point.
waveform_extract.m	Outputs information about the amplitude, width, and height of the spikes.
ChopEdges.m	Finds edges of the firing map where errors correspond to camera detection.
EEG_coherence.m	Finds coherence between two LFP signals.
get_pass.m	Finds the time when the rat passed through the place field.
HeadD_theta_analysis.m	Performs batch analysis of HD-by-theta cells.
myspecgram.m	Performs FFT analysis.
MeanShiftCluster.m	Mean shift clustering with flat top kernel.
cluster_ISI.m	Plots ISI scatter plots and finds cluster within the scatter plot.
Overdispersion_analysis.m	Performs over dispersion analysis on place cells.